# Solution properties of polymers in ionic liquids

A DISSERTATION

SUBMITTED TO THE FACULTY OF THE GRADUATE SCHOOL

OF THE UNIVERSITY OF MINNESOTA

BY

Aakriti Kharel

IN PARTIAL FULFILLMENT OF THE REQUIREMENTS

FOR THE DEGREE OF

DOCTOR OF PHILOSOPHY

Advised by:

Timothy P. Lodge

July 2019

# Acknowledgements

In the last five years, I have gained countless valuable experiences because of the help and support of many people. First and foremost, I am extremely grateful to my advisor, Tim, for providing unparalleled guidance and support that has helped me grow as a scientist that I am today. His approach of allowing students to independently direct the project yet steering them in the right direction at necessary times has enabled independent thinking and developed sound scientific judgement within me. I greatly admire his patience and acceptance while I was new to the lab and climbing up the learning curve. He has been very kind to provide suggestions in my best interest and has acted as a source of encouragement during difficult times. Thank you Tim for being the best advisor I could ask for.

My graduate school experience would not have thrived without the mentorship of the following people: Dan Zhao, Sveta Morozova, Soonyong So, Jennifer Laaser, Yaming Jiang, Cecilia Hall, Sujay Chopade, Seyoung Jung, Leo Oquendo, Yuanchi Ma, Yiming Zeng, Matt Irwin, John McAllister, and Akash Arora. I am thankful to them for offering me their expertise in the lab, answering my trivial questions, and helping me figure out my project and career directions. Over the course, I have also built strong friendships with them, which I will forever cherish.

My time in the Smith basement (“The Lodge lodge”) has been very enjoyable because of all the group members: Peter Schmidt, Qile Chen, Ziang Li, Piril Ertem, Claire Seitzinger, Wenjia Zhang, En Wang, Shuyi Xie, Nick Van Zee, Donny Shen, Bo

Zhang, Julia Early, Aaron Lindsay, Emmanuel Onuoha, Sarah Seeger, and McKenzie Coughlin. I have had insightful discussions and conversations over many research topics with them. I will miss sending comics and memes to our Whatsapp group, celebrating birthdays, and chatting over random topics. I have created many good memories with all of you. I am also grateful to my friends, especially Court, Guilhem, Oja and Rohit, for supporting me in every high and low during my graduate school journey. Furthermore, I greatly appreciate the support of the Nepali community in Minnesota, who made me feel that I was close to home.

Finally, I want to acknowledge the most important people in my life, my mom, dad, and my sister for their endless love and encouragement. I am forever indebted to my parents for making sacrifices to build who I am today. I also greatly owe to my sister for being a constant source of motivation, and my moral “guru”. I want to further express my gratitude to my late grandmother, who always showered me with immense love and support. This accomplishment would not have been possible without them.

# Dedication

*For my mom*

# Abstract

Ionic liquids (ILs) are emerging as promising solvents for polymers. They exhibit excellent chemical and thermal stability, favorable ionic conductivity, and negligible vapor pressure, making them attractive alternatives to traditional solvents. Moreover, adding polymers to ILs provides mechanical integrity to these solvents while retaining their transport properties, enabling their use in various applications such as polymer electrolytes, gas separation, and energy storage. However, the use of these materials would benefit from a thorough understanding of the polymer behavior in this relatively new class of solvent. This work focuses on developing a fundamental understanding on solvation behavior of two model polymers in ILs by characterizing their structural, dynamic, and thermodynamic properties.

In the past years, various simulation approaches have reported conflicting conformational characteristics of poly(ethylene oxide) (PEO) in an IL. As much as simulation studies are on-going, experimental work to guide simulation models are lacking. This work focused on assessing the excluded volume exponent, $\nu$, for PEO in an IL by measuring the dependence of PEO coil size on polymer molecular weight. Since this system is not viable in light scattering, small-angle neutron scattering (SANS) was utilized instead. Therefore, a wide range of accessible molecular weights (10 to 250 kg/mol) of perdeuterated polymers (*d*-PEO) were synthesized by anionic polymerization, for enhanced contrast in SANS. The dependence of coil size on polymer molecular weight was assessed to yield $\nu \approx 0.55$ at 80 °C, which indicates that PEO adopts a slightly swollen, flexible coil conformation in the IL. The results clarified the uncertainty surrounding PEO coil dimensions in IL, and also successfully guided the development of new simulation models. This work was further extended to examine the tunability of coil dimensions by varying the ionic liquid components. Altering both the cation and anion of the IL changed the solvent quality, but the anion seemed to exert a more pronounced effect. The temperature dependence of coil dimensions was moderate, however, the coil size varied insignificantly in ternary mixtures of PEO, IL, and a binary salt.

The static and dynamic properties of a range of molecular weights (20 to 160 kg/mol) of poly(benzyl methacrylate) (PBzMA) were assessed in four different ionic liquids over a wide temperature range (27 °C – 155 °C), primarily using light scattering. The relevant structural, dynamic, and thermodynamic parameters were examined as a function of concentration, temperature, and molecular weight. Some interesting observations were revealed. The phase behavior study showed a potential shift of the critical composition to polymer-rich region, as opposed to lower concentrations of polymer commonly observed in polymer solutions. The second-virial coefficient ($A_2$) remains surprisingly positive, even at temperatures close to the phase separation, where $A_2 < 0$ is anticipated. Furthermore, $A_2$ shows a stronger dependence on molecular weight than commonly observed for polymers in good solvents. On the dynamic side, the diffusion virial coefficients remained mostly positive, further corroborating the good solvent behavior of $A_2$. The excluded volume exponents ($\nu \approx 0.52 - 0.55$) obtained from the dependence of hydrodynamic radii on molecular weight also revealed good solvent characteristics of these ILs.

# Table of Contents

# List of Figures

# List of Tables

# Chapter 1 - Introduction

## 1.1 Ionic liquids

In the past two decades, scientific research in ionic liquids has grown rapidly, due to their versatile potential for new chemical technologies.[1–4] Ionic liquids are salts that exist as liquids close to room temperature. This feature is in contrast to many commonly established inorganic salts, such as sodium chloride, that typically have substantially higher melting temperatures. Since ILs are composed of bulky and asymmetrical ions, the crystal packing is disrupted, lowering their melting temperature.[5] There are many fascinating physicochemical properties of ILs that make them unique compared to other solvents in use today. ILs are non-volatile and non-flammable, and are therefore recognized as environmentally friendly alternatives to volatile organic solvents.[2] Furthermore, their non-volatility combined with their chemical and thermal stability enables their use over a wide temperature range. The physicochemical properties of ILs are easily tunable by modifying the size, shape, and functionality of the component cations and anions, due to which they are often labeled as "designer solvents". Moreover, it has been estimated that there are at least a million binary ILs and virtually unlimited number of ternary ILs (compared to only 600 molecular solvents in use today).[6] As molten salts at room temperature, ILs also exhibit good ionic conductivities and wide electrochemical windows, making them suitable candidates for electrochemical applications.

The most commonly reported cations are based on imidazolium, pyridinium, pyrrolidinium, and ammonium. Imidazolium-based ILs are among the most studied due to their stability, ease of synthesis, and low viscosity.[7] On the anion side, tetrafluoroborate ($BF_4^-$), bis(trifluoromethylsulfonylimide) (TFSI), and hexafluoro-phosphate ($PF_6^-$) are widely used. Figure 1.1 shows the structure of some of the cations and anions used in this study. On the cation side, 1-alkyl-3-methylimidazolium cations with ethyl, butyl, or hexyl tails are abbreviated as EMIM, BMIM, and HMIM, respectively, and BMP represents 1-butyl-1-methylpyrrolidinium.

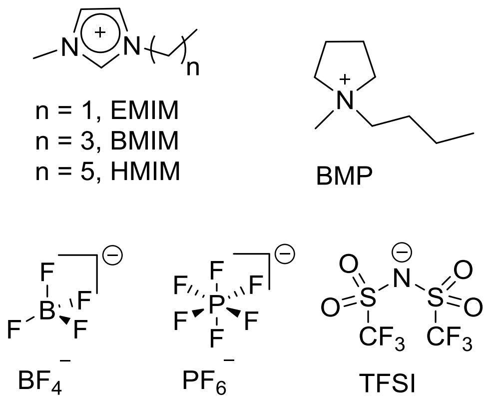

**Figure 1.1:** Structures of cations and anions used in this study.

Despite having all the positive characteristics described above, ILs have a few limitations. It is often difficult to obtain IL free of impurities.[8] Of particular concern is water, which is generally present even in hydrophobic ionic liquids.[9] This has a detrimental effect on the electrochemical properties. For example, it has been shown that the electrochemical window of [BMIM][$BF_4$] decreases by 50% with just 3% water addition.[10] One possible way to overcome this limitation is by drying ILs under vacuum at high temperatures, as they are thermally stable and non-volatile. Besides the presence of water, the high viscosities and larger ion sizes of ionic liquids can also compromise their conductivity compared to traditional aqueous electrolytes.[11,12] Another issue is that the classification of ILs as “green solvents” is questionable. There is very limited information on the toxicity of the ILs, and among the ones that have been studied, many are known to be toxic to the environment.[13,14] The potential toxicity of ILs in combination with their high cost, limits their use in larger scale industrial applications.

ILs can be categorized as a third class of solvents that exhibit characteristics of both aqueous and organic solvents.[15,16] The hydrogen bonding, dipole-dipole, and van der Waals interactions combined with the electrostatic interactions make them miscible with polar molecules. On the other hand, the alkyl chains on the cation and the use of a hydrophobic anion facilitates their compatibility with non-polar groups. For molecular solvents, it is common to determine their polarity based on the dielectric constant. However, in the case of ILs, no single parameter or direct measurement can determine the IL polarity. Crowhurst et al. used an empirical method devised by Kamlet and Taft to estimate the polarity of ILs.[17] The three main Kamlet-Taft parameters are polarizability factor ($\pi^*$), $\alpha$, and $\beta$, listed in Table 1.1 for some common ILs used in this study. Here, $\alpha$ is a measure of the ability of a solvent to donate a proton to a hydrogen bond. $\beta$ is a measure of hydrogen bond basicity, described as the ability of the IL to accept a proton from the hydrogen bond. As seen in Table 1.1, for all the ILs, $\pi^*$ values are similar to water, indicating the high polarity of these solvents. $\alpha$ is almost constant for ILs comprising a BMIM cation, but has a lower value for BMP, reflecting the lack of acidic protons in the BMP cation. On the other hand, $\beta$ is noticeably larger for the case of $BF_4^-$ anion compared to TFSI and $PF_6^-$. Therefore, the parameters $\alpha$ and $\beta$ are determined to be primarily affected by the choice of the cation and the anion, respectively.

**Table 1.1:** Kamlet-Taft parameters for some ILs used in this study*

| **Solvent** | $\pi^*$ | $\alpha$ | $\beta$ |
|---|---|---|---|
| Water | 1.33 | 1.12 | 0.14 |
| [BMIM][$BF_4$] | 1.047 | 0.627 | 0.376 |
| [BMIM][$PF_6$] | 1.032 | 0.634 | 0.207 |
| [BMIM][TFSI] | 0.984 | 0.617 | 0.243 |
| [BMP][TFSI] | 0.954 | 0.427 | 0.252 |

*Obtained from ref. 17

## 1.2 Some applications of ionic liquids in polymer science

In recent years, many developments have been made in the field of polymers incorporating ionic liquids. Their unique properties have enabled the dissolution of polysaccharides, which are known to be insoluble in traditional solvents.[18–21] For example, cellulose was found to dissolve in various polar ILs, in particular, up to 18 wt% in EMIM propionate.[21] The dissolution has been attributed primarily to the IL anions that can disrupt the intra and inter-molecular hydrogen bonding network of cellulose chains. This has provided a platform for cellulose processing and cellulose-based material design such as films, fibers, gels, and composites.[20] In addition to their remarkable capacity to solvate biopolymers, ILs have been investigated as polymerization media, particularly for radical polymerizations due to their ability to enhance the propagation rate constant and decrease the rate of termination.[22–24] For example, the rate of reversible addition−fragmentation chain-transfer (RAFT) polymerization of methyl methacrylate in [BMIM][$PF_6$] was found to be double that in toluene.[25]

Besides their use as media for dissolution, there has been tremendous interest in exploiting polymer and IL composites to make mechanically stable polymer electrolytes.[26] They are considered promising candidates for fuel cells, batteries, gas separation membranes, and many other applications.[27–33] ILs offer good ionic conductivity, making them desirable alternatives to liquid electrolytes, but lack mechanical integrity that can be provided by the addition of a macromolecular architecture. The simplest possible way is to blend homopolymers or copolymers with ionic liquids to form polymer gels (an example of copolymer dissolved in IL is shown in Figure 1.2). Some linear polymers that have been blended with ILs to form materials with "gel-like" consistency are poly(ethylene oxide) (PEO), poly(acrylonitrile) (PAN), poly(vinylalcohol) (PVA), copolymer of vinylidene fluoride and hexafluoropropylene P(VDF-HFP), and poly(methyl methacrylate) (PMMA) in imidazolium and pyrrolidinium based-ILs.[34–39] Another route is to incorporate the IL into the backbone or side groups of the polymers by polymerizing the IL monomers. [29,40–42] A lot of interest has also been diverted towards forming polymeric ion gels by either chemical or physical cross-linking. In the case of chemical crosslinking, monomer and cross-linker are directly dissolved and polymerized in the IL,[43,44] or macromonomers are reacted with multifunctional reactive groups.[45,46] On the other hand, physically crosslinked gels are often achieved by adding a block copolymer architecture that can self-assemble in solution. A versatile way to do this is by allowing self-assembly of ABA triblock copolymers in ILs, where the A block is insoluble but the B block is well-solvated.[47–50] The particular advantage of this approach is that the gels can form with only a few percent polymer, where the network is swollen with ions but the mechanical integrity is not significantly compromised.[51]

**Figure 1.2:** Image of free-standing ion gel of 20% copolymer of vinylidene fluoride and hexafluoropropylene P(VDF-HFP) in [EMIM][TFSI]. Reproduced with permission from ref. 52. Copyright 2012 Wiley.

### 1.3 Solvation of polymers in ionic liquids

As discussed in the previous section, the combination of polymers and ILs provides a platform for designing materials with tunable properties that have a wide range of applications. In order to design these materials intelligently, a thorough understanding of the polymer behavior in ILs is beneficial. In the past two decades, there have been relatively few systematic studies aimed specifically at investigating the general solubility of polymers in ILs. The Watanabe group has studied the solubility of 24 different polymers in four common ILs. They dissolved various acrylate, ether, and amide-based polymers in low concentrations in ILs, and evaluated their mutual miscibility.[15] Snedden et al. also conducted a similar study with acrylate- and pyridine based-homopolymers and copolymers in many ILs.[53] These empirical studies provided a comprehensive list of polymer and IL pairs that are compatible in dilute concentrations. However, these reports pointed out that predicting miscibility is far more complex in ILs than in conventional solvents. For example, Watanabe and coworkers showed that polymers such as poly(acrylic acid) and PVA that are capable of forming strong hydrogen bonds are insoluble in [EMIM][TFSI], whereas PEO is soluble in the same IL.[15] Therefore, the principle of "like dissolves like" might not be applicable in ILs, and the understanding of information on polymer solubility is largely based on trial and error. For the case of molecular solvents, the Hildebrand solubility parameter ($\delta$) can be used to predict the miscibility of the polymer and the solvent. However, even this approach breaks down in the case of ILs.[15] The assumptions of the theory for solubility parameters do not account for strong and directional interactions, such as Coulombic and hydrogen-bonding that are prevalent in ILs. Nevertheless, it is of importance to be able to predict the solubility of polymers in ILs.

The solubility studies discussed above are limited to certain polymer molecular weights and polymer concentrations (often very dilute) investigated at a fixed temperature (generally room temperature). To fully understand the solvation of polymers in solvents, it is desirable to investigate the phase behavior of polymer solutions by determining the dependence of miscibility on composition and temperature. A polymer and solvent pair exhibits upper critical solution temperature (UCST) phase behavior if it is miscible upon heating but phase separates upon cooling. On the other hand, if a polymer system phase separates upon heating but is miscible upon cooling, the system exhibits lower critical solution temperature (LCST) phase behavior. Figure 1.3 represents the critical points in these curves given by the critical temperatures ($T_c$) jointly with the critical compositions ($\phi_c$). A one-phase solution is formed for all compositions at $T > T_c$ for UCST systems, and $T < T_c$ for LCST systems. Using Flory-Huggins theory, $\phi_c$ is predicted to vary as $\phi_c \approx 1/\sqrt{N}$, where $N$ is the degree of polymerization in units of solvent molar volume.[54] Therefore, it is common to observe $\phi_c$ skewed towards low polymer concentrations.

For polymer and organic solvent mixtures, UCST behavior is frequently observed, where the entropy of mixing is positive ($\Delta S_{mix} > 0$).[55,56] However, there are a few cases where a LCST is also observed.[57,58] LCST phase behavior mainly results from strong and directional interactions of the solvent and the polymer that lowers the entropy of mixing ($\Delta S_{mix} < 0$). Therefore, polymers in aqueous systems generally exhibit an LCST due to the existence of strong hydrogen bonding interactions, which result in the formation of cage-like ordered structures of water molecules.[56,59,60]

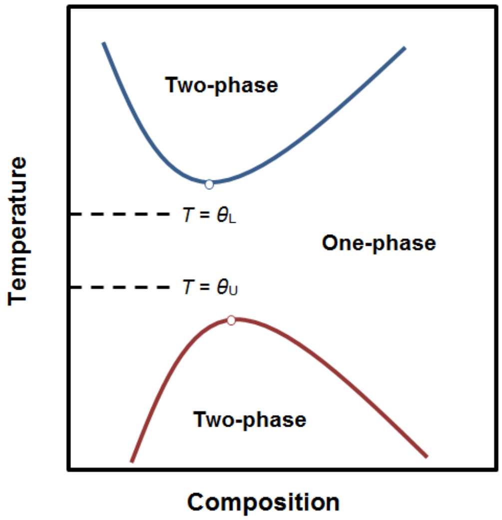

**Figure 1.3:** Cartoon illustration of polymer/solvent mixture phase diagram, showing LCST (blue) and UCST (red) behavior. The open

circles in the curves are the critical points.

Interestingly, both LCST and UCST behavior is observed for polymer/IL systems. For a UCST, the first report was shown by Watanabe and Ueki for poly(N-isopropylacrylamide) (PNIPAm) in [EMIM][TFSI].[61] It is interesting to note that PNIPAm in this IL exhibits completely opposite phase transitions to its well-known LCST behavior in aqueous solutions.[62] Certain methacrylates having long alkyl chains such as poly(octadecyl methacrylates) are also known to exhibit UCST phase transitions in ILs.[63] However, as compared to UCST reports, more polymers in ILs investigated to date have shown LCST behavior.

Polyethers such as PEO[64–66] and poly(ethyl glycidyl ether) (PEGE)[67] show LCST behavior in imidazolium-based ILs, attributed to the strong hydrogen bonding capacity of these polymers with the cation.[68] Lee and Lodge have constructed a full phase diagram (shown in Figure 1.4a) of PEO in [EMIM][$BF_4$] and [BMIM][$BF_4$], showing an unusual characteristic of this system, where the phase diagrams were relatively symmetric ($\phi_c$ ~ 50 wt%) or asymmetric shifted to high PEO composition ($\phi_c$ ~ 80 wt%).[65,66] On the contrary, a PEO derivative, PEGE, in [EMIM][TFSI] has an asymmetric phase diagram shifted towards polymer-poor region with $\phi_c < 10$ wt%.[67] LCST behavior has also been observed in many poly(methacrylate) polymers in ILs[68] such as poly(benzyl methacrylate)[69,70] and poly(n-butylmethacrylate)[71,72] in [EMIM][TFSI]. The origin of negative entropy of mixing is different in both cases. For PBzMA in ILs, it is speculated that the cation interacts with the aromatic side chain of the polymer via cation-π interactions, forming a liquid clathrate.[69,70,73–77] For PnBMA, the alkyl tails in ILs form oriented solvation around the n-butyl groups of the polymer.[71,72,78] It is also worth noting that PnBMA in [BMIM][TFSI] show a strongly asymmetric phase diagram with $\phi_c$ shifted to low concentrations of PnBMA (< 5 wt%), as also seen for PEGE in IL.

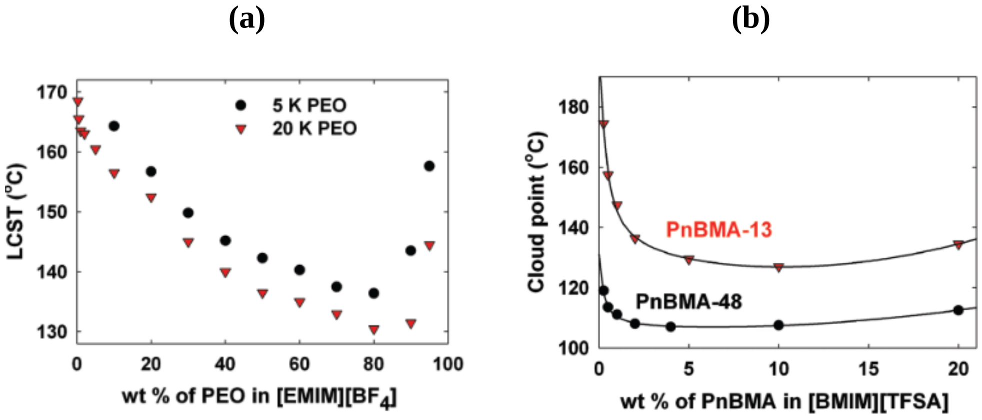

**Figure 1.4:** LCST phase diagrams of polymers in ILs (a) Unusual phase behavior of PEO in [EMIM][BF$_4$], where the $\phi_c$ is shifted to polymer-rich region. (b) PnBMA in [BMIM][TFSI] showing asymmetric phase diagram shifted towards lower composition of polymers. Figures adapted with permission from ref. 66 (Copyright 2010 American Chemical Society) and ref. 71 (Copyright 2011 American Chemical Society) .

One common observation in all the LCST and UCST systems in ILs is that the phase separation temperatures vary strongly depending on the choice of cations and anions of the ILs, and the polymer structure. An example can be seen in Figure 1.5, where the phase separation (cloud point) temperature ($T_{cp}$) for PnBMA in [BMIM][TFSI] increases by 140 °C by incorporating 80 wt% of [HMIM][TFSI]. This characteristic offers the potential to readily tune the solvation of polymers to meet specific application requirements. Indeed, the phase transitions of polymers in ILs and their tunability have been exploited to design complex thermoresponsive materials.[63,71,79–83] For example, a thermoreversible ion gel was prepared by He and Lodge by incorporating PNIPAm as the thermosensitive block in an ABA type block copolymer.[48] Because of the UCST phase behavior, PNIPAm can undergo low-temperature-gel to high-temperature-sol transitions. Furthermore, optically switchable ion gels, in which gel formation is achieved under UV-visible light have also been reported.[84–86] With all these applications in mind, it is crucial to understand the mutual miscibility of polymers and ionic liquids to effectively design materials for these stimuli-responsive materials.

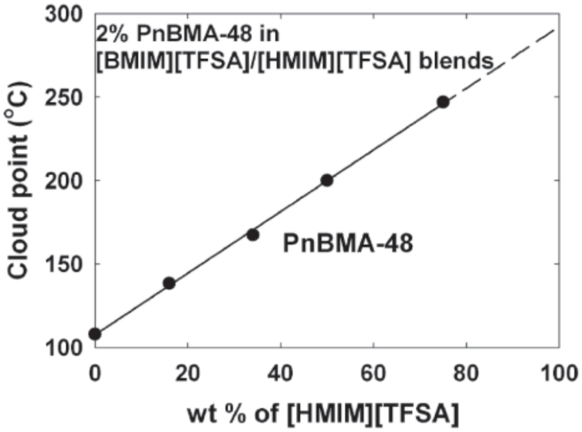

**Figure 1.5:** The phase separation temperature of a 2 wt% PnBMA in [BMIM][TFSI] changes almost linearly from 108 °C to 247 °C with the incorporation of [HMIM][TFSI]. Figure adapted from ref. 71 with permission. Copyright 2011 American Chemical Society.

Most of the publications discussed earlier have verified the existence of either LCST or UCST of polymers in ILs, but only limited reports have investigated the relevant thermodynamic parameters. Some important parameters include the second virial coefficient, $A_{2,}$ and the interaction parameter, $\chi$. $A_2$ is a measurable quantity that is model-independent, and can be obtained directly using experimental techniques such as scattering. On the other hand, $\chi$ is a quantity incorporated in the Flory-Huggins lattice model of binary polymer solutions. When $\chi < 1/2$, $A_2$ is positive and mixing of polymer and solvent are favorable, implying good solvent conditions. On the other hand, when $\chi > 1/2$, $A_2$ is negative and there are unfavorable interactions resulting in a poor solvent condition. Finally, when $\chi = 1/2$, $A_2$ is zero and this condition is defined as the theta condition, achieved at the theta temperature ($T_\Theta$) for a chosen solvent. Therefore, both $A_2$ and $\chi$ give information on the solvent quality. A quick way to estimate $\chi$ is using solubility parameter ($\delta$) approach, where polymers and solvents with similar $\delta$ generally have good miscibility. However, this approach is not reliable in the case of predicting the miscibility of polymers and ILs. As discussed previously, the presence of strong directional interactions in ILs results in oriented solvation that is not accounted for in the pure combinatorial entropy of Flory-Huggins theory.

To the best of our knowledge, parameters such as $\chi$, $A_2$, and $T_\Theta$, have only been evaluated for a few polymers in ILs.[72,76,87] Hoarfrost et al. reported the first detailed investigation of polymer solution thermodynamics in ILs.[72] They used a combination of techniques–turbidimetry, static light scattering, and small-angle neutron scattering (SANS) –to assess $A_2$ at various temperatures for PnBMA in mixtures of [EMIM][TFSI] and [BMIM][TFSI].[72] The values of the effective interaction parameter ($\chi_{\mathrm{eff}}$) were evaluated from $A_2$ in the dilute regime, and from random-phase approximation (RPA) fits of SANS data in the concentrated regime. Furthermore, the theta temperature was located by establishing the temperature dependence of $A_2$, and from the extrapolation of critical temperature to infinite molecular weight. They report that the values of $T_\Theta$ obtained from two techniques are in reasonable agreement with each other. The major conclusion of this work was that all the thermodynamic parameters are readily tunable with varying ratio of the two ILs used. In particular, the incorporation of [BMIM][TFSI] improved PnBMA solubility, reflected on the larger values of $A_2$ and $T_\Theta$. Watanabe and coworkers also used SANS to measure $A_2$ and evaluate $\chi_{\mathrm{eff}}$ as a function of temperature for PNIPAm and poly(2-phenylethyl methacrylate) (PPhEtMA) in [EMIM][TFSI].[76,87] The theta temperatures are found to be 45 °C and 28 °C for PNIPAm and PPhEtMA, respectively, where $A_2 = 0$ is obtained.

Although progress has been made in studying the phase behavior of polymers and ILs, studies related to dynamics of polymers in ILs remain largely unexplored. Some effort has been put on measuring the diffusion of the ionic components in the polymer/IL matrix, since the transport of ions in mixtures of polymers and ILs are significant for electrochemical applications.[44] On the other hand, the dynamic behavior of polymers in these ionic solvents still remains an open question. The few papers published so far have only evaluated the trend in apparent hydrodynamic radii near the phase separation temperature for PBzMA, PPhEtMA, and PNIPAm using dynamic light scattering.[68,76,87,88] These studies reveal that two populations (free polymer chains and aggregates) appear near $T_{\mathrm{cp}}$. However, many questions regarding the diffusion coefficients of polymers, their dependence on concentration, polymer molecular weight, and temperature are yet to be investigated.

Light scattering is an accessible and powerful tool in elucidating the structure, dynamics, and thermodynamics of polymer solutions. It is quite surprising that there are not many light scattering studies (in particular static light scattering) in the literature for polymers and ILs solutions. In addition to the PnBMA/IL system studied by Hoarfrost et al. (discussed above),[72] we are aware of only one study that assessed solution properties of linear polymers in ILs using both static and dynamic light scattering.[89] Chen et al. studied polyvinyl alcohol (PVA), polysulfonamide (PSA), and cellulose in 1-allyl-3-methylimidazolium chloride ([AMIM][Cl]) and BMIM formate ([BMIM][COOH]), and reported several interesting observations.[89] They report that one of the ILs, [BMIM][COOH], has large density fluctuations, and hence, exhibits an angular dependence. This observation is very surprising as no angular dependence is seen in similar ILs, such as [BMIM][TFSI]. Moreover, the angular dependence of [BMIM][COOH] is in contrast to conventional solvents, such as toluene, where scattering intensity is not a function of angle. Using DLS, the authors observe that PSA in [BMIM][COOH] aggregates at 50 °C, but PVA in the same IL shows no evidence of aggregation. They attribute the aggregation of the polymer to the spatial heterogeneity of the ILs, but give no explanation on how the solvent induces aggregation of the polymer. Furthermore, the authors provide no information on whether this system is a UCST or LCST, and if the experimental temperature is close to the phase separation temperature. Another surprising observation is that the relaxation mode of cellulose in [AMIM][Cl] was found to be non-diffusive. They speculated that the relaxation of cellulose couples with that of ILs, and the polymer undergoes an extra motion caused by solvent molecules. This type of observation is unusual and needs further investigation.

The assessment of structural properties such as chain dimensions of polymers in ILs has also raised many questions in the past few years. It is often desirable to measure the dependence of radius of gyration ($R_g$) on polymer molecular weight to evaluate the scaling exponent, $\nu$, which is a measure of the solvent quality. The value of $\nu$ is 0.6 for a good solvent, 0.5 for a theta solvent, and 0.33 for a poor solvent. Yethiraj and coworkers have reported conflicting conformational characteristics of PEO in [BMIM][$BF_4$], using various simulation methodologies.[90–92] Fully atomistic simulations for modest degrees of polymerization, *N*, indicated that PEO is an extended chain at room temperature ($\nu \approx 0.9$) but adopts a random coil conformation ($\nu \approx 0.5$) when the temperature is increased closer to its LCST (400 K).[90,92] In contrast, when coarse-grained models were employed at similar temperatures, PEO chains were found to be collapsed ($\nu \approx 0.3$).[91] The inconsistency in the conformation of a neutral polymer chain (PEO) in an IL solvent by these models suggests a remarkable sensitivity of structural properties to the simulation parameters. These studies therefore emphasize the need for relevant experiments to elucidate the actual conformations of PEO chains in [BMIM][$BF_4$]. In particular, experiments that obtain conformations for a range of polymer molecular weights are desirable so that $\nu$ can be obtained. Scattering methods can be used to directly measure $R_g$ in dilute polymer solutions. However, any scattering technique mandates substantial scattering intensity to accurately obtain information on the $R_g$ of polymer chains. The similarity in the refractive indices of PEO and [BMIM][$BF_4$] makes it difficult to obtain $R_g$ using established light scattering procedures. However, such difficulty can be circumvented by SANS.

Previously, SANS has been used to measure the radius of gyration for one lower molecular weight PEO (*ca*. 30 kg/mol) in different ILs including [BMIM][$BF_4$].[93–98] Triolo et al. measured apparent $R_g$ of dilute solutions of a perdeuterated PEO (*d*-PEO, 27 kg mol) in [BMIM][$BF_4$].[93] They report a scaling of apparent $R_g$ with concentration as $R_g \sim c^{-0.25}$, and point out the deviation from the scaling law ($R_g \sim c^{-0.125}$) proposed for

Gaussian chains. However, there are two major shortcomings of such comparison. First, the scaling relationship $R_g \sim c^{-0.125}$ is only valid in the semi-dilute regime, and cannot be applied for dilute solutions.[99] Second, the scaling law applies only for single chain $R_g$, and not apparent $R_g$ evaluated in this study. This work also reported a positive value of $A_2$ at room temperature from SANS Zimm plots. Based on this observation, [BMIM][$BF_4$] is concluded to be a good solvent for PEO. However, PEO is reported to crystallize in [BMIM][$BF_4$] at room temperature (which will be discussed in detail in Chapter 2), even for moderate molecular weights.[100] Therefore, the room temperature measurement of apparent $R_g$ and $A_2$ for PEO in [BMIM][$BF_4$] is also questionable.

Werzer et al. assessed $R_g$ of *d*-PEO (38 kg/mol) in ethylammonium nitrate (EAN) in dilute and semi-dilute regime using SANS.[94] They obtain an infinite dilution radius of gyration ($R_{g,0}$) of 81 Å, which is slightly larger than $R_g$ obtained in theta-condition. Hence, they conclude that EAN is a moderately good solvent for *d*-PEO. They also obtain a scaling of $R_g \sim c^{-0.25}$ for dilute solutions, similar to that reported by Triolo (discussed above), and attribute this behavior to steric interactions between neighboring coils. However, this conclusion is again questionable, as these scaling relationships are not valid in the dilute regime. Another shortcoming of this study is that the authors evaluate $R_g$ in semi-dilute regime without contrast-matching, where the inter-chain polymer interactions are prevalent. Hence, the $R_g$ values obtained in the semi-dilute regime are quantitatively unreliable. The lack of relevant experiments combined with the contradictory simulation predictions, underscores the need to measure $R_g$ for a range of PEO molecular weights to evaluate the scaling exponent. However, to the best of our knowledge, there have been no reports that describe the scaling relationship between $R_g$ and $M_w$ for any polymers in ionic liquids.

In addition to the direct dependence of $R_g$ on $M$, evaluation of intrinsic viscosity ($[\eta]$) can also yield the values of $\nu$, given as $[\eta] = KM^a$. The Mark-Houwink parameter, $a$, relates to $\nu$ as $a = 3\nu - 1$, and $K$ is a constant. There are many studies that have measured $[\eta]$ of synthetic and bio-polymers in ILs,[101–106] but limited number studies have evaluated $\nu$ from the molecular weight dependence of $[\eta]$.[100,107] The study of cellulose in EMIM acetate revealed Mark-Houwink exponents between 0.4 and 0.6, indicating a theta-like solvent. The authors point out that one of the difficulties in measuring viscosities of these solutions is the significant uptake of water by the IL. Within 30 mins, the viscosity of pure EMIM acetate decreased by 22%. Another study by Liu et al. conducted intrinsic viscosity measurements on PEO in [BMIM][$BF_4$] (the same system studied by simulation studies discussed above).[100] They report that [BMIM][$BF_4$] is actually a moderately poor solvent ($\nu = 0.48$, $M$ ranging from $10^5$–$10^7$ g/mol) for PEO at 80 °C. This result is surprising, as PEO is known to be miscible in [BMIM][$BF_4$] up to high temperatures (*e.g.*, a 2 wt% solution of 20 kg/mol PEO in [BMIM][$BF_4$] has a lower critical temperature of 209 °C). Therefore, both simulation and experimental results present conflicting findings on evaluating solvent quality of [BMIM][$BF_4$].

## 1.4 Thesis overview

The fundamental properties of polymer solutions heavily influence the design, structures and processing of polymers in solvents. A straightforward way of obtaining mixtures of polymers and solvents would be to dissolve a polymer in the desired solvent.

However, dissolution studies only give information on the formation of a homogenous solution. It is essential to know the limits of complete miscibility as a function of temperature and composition to control many polymer processes such as polymerization and extrusion. Similarly, mixing of polymer in a solvent is governed by the diffusion of chains in the respective solvent media. Moreover, electrochemical applications require detailed knowledge about the transport properties of polymers that bind to the migrant ions. Interestingly, both thermodynamic and dynamic properties frequently exhibit a dependence on polymer molecular weight, which in turn is also related to the spatial extent or the chain dimensions of the polymer. In fact, coil dimensions of polymers affect significant properties such as mechanical strength and processing behavior, making polymer chain dimensions an important area of study. The interdependence of these properties emphasizes that in order to fully understand the solvation of polymers in ionic liquids, it is important to characterize structural, dynamic, and thermodynamic properties of these mixtures.

The subject of a number of studies in the literature has been to assess the dissolution of polymers and ionic liquids based on solubility trends and phase behavior.[15,16,53,108] However, many other solution properties such as chain dimensions and dynamics of polymer/ILs remain incompletely characterized or understood. This thesis aims on providing more detailed information on polymer solvation in ILs by investigating the solution properties of two technologically relevant polymers, PEO and PBzMA, in varying ionic liquid components.

The early motivation for this project originated from the need to experimentally measure the molecular weight dependence of the chain dimensions of PEO in

$[BMIM][BF_4]$, due to the contradictory behavior reported by simulations (discussed above). Therefore, Chapter 2 focuses on using small-angle neutron scattering to experimentally determine the scaling relationship of $R_g$ and $M$ ($R_g \sim M^{\nu}$) for PEO in $[BMIM][BF_4]$. Chapter 3 extends the previous work by determining the dependence of $\nu$ and coil size on IL choice, temperature, and LiTFSI incorporation. The results will be discussed in terms of the relative interactions among PEO, the cation, and the anion. Chapter 4 will assess the thermodynamic, dynamic, and structural properties of a range of molecular weights of PBzMA in four different ILs. On the thermodynamic side, the phase transition temperatures of PBzMA and IL mixtures are evaluated using turbidimetry. Using static light scattering, the temperature and molecular weight dependence of second virial coefficients are determined. Dynamic light scattering is used to measure the diffusion coefficients and hydrodynamic radii as a function of concentration, temperature, and molecular weight. Additional relevant parameters such as diffusion virial coefficients and frictional coefficients are determined at several temperatures and molecular weights. The key parameters of interest that describe the behavior of dilute solutions of PBzMA in all ILs are summarized and discussed. Finally, in Chapter 5, a summary of the dissertation is given, with possible future directions.

# Chapter 2 -Coil Dimensions of Poly(ethylene oxide) in an Ionic Liquid*

## 2.1 Introduction

Chain dimension is a key macromolecular feature of a polymer coil that directly governs the unique and versatile properties of polymers.[109,110,111] The spatial extent of the polymer affects significant properties such as mechanical strength and processing behavior, making polymer chain dimensions an important area of study. The chain dimensions of polymers can be assessed by measuring the radius of gyration ($R_g$), which essentially describes the size of a polymer chain.

Solvents for polymers are generally categorized into good, poor, and theta ($\theta$) depending on the interactions between the polymer and the solvent.[111,112] In a good solvent, favorable interactions occur between monomer and solvent, which results in swelling of the polymer chains. In other words, the excluded volume interactions between the polymer segments expand the chain dimensions. On the other hand, in the case of a poor solvent, the unfavorable interactions between the polymer and the solvent cause the chains to collapse and contract into a collapsed globule. In the third case, i.e., the theta solvent, the excluded volume effects cancel the unfavorable polymer-solvent interactions.

---

*Reprinted with permission from Kharel, A.; Lodge, T. P. Coil Dimensions of Poly(ethylene oxide) in an Ionic Liquid by Small-Angle Neutron Scattering. *Macromolecules* **2017**, *50*, 8739–8744. Copyright 2017 American Chemical Society.

As a result, the polymer chain in theta solvent behaves like an ideal chain following Gaussian statistics. This behavior is represented in one of the classic scaling laws developed by Flory, [111,113]

$$R_g = bN^{\nu} \qquad (2.1)$$

where $b$ is a pre-factor and $\nu$ is the excluded volume exponent. $\nu$ is a universal property that is same for all the coils in a given class, while the pre-factor is a local property, dependent on the monomer and the choice of the solvent. The value of $\nu$ is 0.6 for a good solvent (0.588 as predicted by the renormalization group theory[114]), 0.5 for a theta solvent, and 0.33 for a poor solvent (all illustrated in Figure 2.1). In general, as the solvent quality improves, the coil size has a stronger dependence on the chain length. For a polyelectrolyte chain in low salt concentration, $\nu$ can even take the value of 1, and adopt an extended chain conformation.[99,115] In addition to the direct dependence of $R_g$ on $N$, evaluation of intrinsic viscosity ($[\eta]$) can also yield the values of $\nu$, given as $[\eta] = KM^{a}$. The Mark-Houwink parameter, $a$, relates to $\nu$ as $a = 3\nu - 1$, and $K$ is a constant.

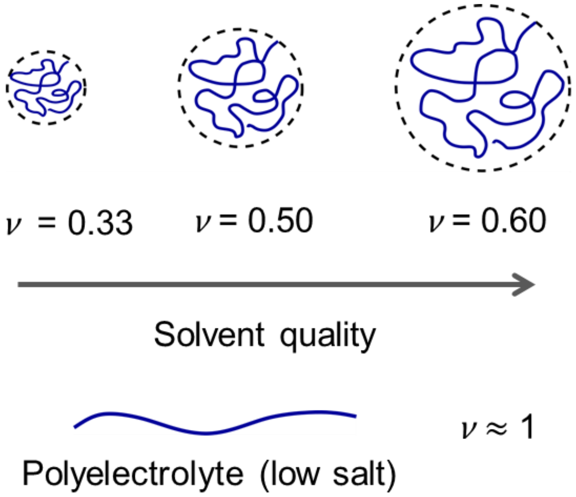

**Figure 2.1:** Cartoon illustrating the chain conformations of polymer in solvents. As the solvent quality gets better, the value of $\nu$ increases expanding the polymer coil. A polyelectrolyte chain dissolved in low salt concentration adopts an extended chain like conformation, where $\nu \approx 1$. Figure not drawn to scale.

The chain dimensions of polymers in molecular solvents have been long-established in the literature.[116–122] However, in the past decade, ionic liquids (ILs) have gained considerable attention as promising alternative solvents for polymers. As pointed out in the previous chapter, ILs offer many unique characteristics over conventional solvents, making them an attractive solvent class of interest. This underscores the need to assess the chain dimensions of polymers in ILs.

Among numerous combinations of polymers and ILs, poly(ethylene oxide) (PEO) is particularly attractive from both fundamental and technological perspectives. For example, polymer gel electrolytes based on PEO and ILs are being investigated as replacements for current battery technologies that otherwise employ flammable and volatile organic solvents.[123–128] Moreover, ABA triblock copolymers using PEO as the solvophilic block B in alkyl-imidazolium ($C_n$mim)-based ILs have been utilized in preparing temperature sensitive ion gels with high ion conductivity.[49] Despite the increasing significance of these mixtures, only a few experimental and theoretical studies have been conducted for PEO in these ILs; in particular, PEO in 1-butyl-3-methylimidazolium tetrafluoroborate ([BMIM][$BF_4$]) is reported to have interesting structural and thermodynamic properties. Lee and Lodge[66,65] described the existence of unusual lower critical solution temperature (LCST) phase behavior of PEO in [BMIM][$BF_4$], where the critical composition ($\phi_c$) is shifted to unusually high polymer volume fractions. Such behavior contrasts with typical polymer/IL and other polymer/solvent mixtures, where $\phi_c$ is generally low. On the computational side, Yethiraj and coworkers have reported conflicting conformational characteristics of PEO in [BMIM][$BF_4$], using various simulation methodologies. Fully atomistic simulations for modest degrees of polymerization, $N$, indicated that PEO is an extended chain at room temperature[90] ($\nu \approx 0.9$) but adopts a random coil conformation ($\nu \approx 0.5$) when the temperature is increased closer to its LCST (400 K).[92] In contrast, when coarse-grained models were employed at similar temperatures, PEO chains were found to be collapsed ($\nu \approx 0.3$).[91] The inconsistency in the conformation of a neutral polymer chain (PEO) in an IL solvent by these models suggests a remarkable sensitivity of structural properties to the simulation parameters.

These studies therefore emphasize the need for relevant experiments to elucidate the actual conformations of PEO chains in [BMIM][$BF_4$]. In particular, experiments that obtain conformations for a range of polymer molecular weights are desirable so that $\nu$ can be obtained. We are aware of only one such experimental work, using intrinsic viscosity measurements, which concluded that [BMIM][$BF_4$] is actually a moderately poor solvent ($\nu = 0.48$, $M$ ranging from $10^5$–$10^7$ g/mol).[100] This result is also surprising, as PEO is known to be miscible in [BMIM][$BF_4$] up to high temperatures (*e.g.*, a 2 wt% solution of 20 kg/mol PEO in [BMIM][$BF_4$] has a lower critical temperature of 209 °C),[66] and thus underscores the need for direct measurements of chain conformations using, *e.g.*, scattering techniques.

Scattering methods can be used to directly measure $R_g$ in dilute polymer solutions. However, any scattering technique mandates substantial scattering intensity to accurately obtain information on the radius of gyration of polymer chains. The intensity of scattering is directly proportional to the contrast, and the origin of contrast is dependent on the type of scattering.[129] In the case of light scattering, the contrast arises from concentration fluctuations proportional to the refractive index increment ($dn/dc$). In order to realize if a system is viable in light scattering, it is common to seek polymer/solvent pairs which have substantial differences in refractive index ($n_D$). In the case of PEO and [BMIM][$BF_4$], the $n_D$ values are given as 1.454 and 1.422, respectively.[130,131] The similarity in the refractive indices of PEO and [BMIM][$BF_4$] makes it difficult to obtain $R_g$ using established light scattering procedures. However, such difficulty can be circumvented by small-angle neutron scattering.

Small-angle neutron scattering involves the interaction of neutrons with nuclei, and the coherent scattering length ($b_i$) depends on the type of target atom, not the fluctuations in refractive index. The contrast in SANS stems from the difference in $b_i$ of atoms, generally between hydrogen ($b_H = -0.37 \times 10^{-12}$ cm) and deuterium ($b_D = 0.67 \times 10^{-12}$ cm).[132] This can be utilized to increase the scattering intensity by deuterating the sample of interest. One can calculate the contrast between two species, such as a polymer and a solvent, by using the following equation

$$\text{Contrast} = V_{\text{ref}}\left[\left(\frac{b}{V}\right)_1 - \left(\frac{b}{V}\right)_2\right]^2 \tag{2.2}$$

where $V_{\text{ref}}$ is the reference volume and $V$ is the specific monomer volume. The term ($b/V$) is known as scattering length density ($\rho$), which is simply the ability of a sample to scatter neutrons coherently per unit volume. It should be noted that $b$ in the equation represents $\sum_{\text{i}} b_{\text{i}}$ in the volume element $V$, which means that it is a sum of coherent scattering lengths for all $i$ atoms in the monomer or the solvent. This is a very important characteristic of neutron scattering compared to light scattering, as adequate contrast can be obtained for almost any polymer-solvent pair by deuterating either the polymer or the solvent.

Previously, small-angle neutron scattering (SANS) has been used to measure the infinite dilution radius of gyration ($R_{\text{g},0}$) for one lower molecular weight PEO (*ca*. 30 kg/mol) in different ILs[93–98,133] including [BMIM][BF$_4$], but to the best of our knowledge, there have been no reports that describe the scaling relationship between $R_{\text{g},0}$ and polymer molecular weight ($M$) for PEO in ILs. Here, we report the chain dimensions from dilute solutions of five different molecular weights of perdeuterated PEO (*d*-PEO) in [BMIM][BF$_4$] by SANS. By extrapolating to zero concentration for each molecular weight, we obtained the weight-average molecular weight ($M_{\text{w}}$) dependence of $R_{\text{g},0}$, which is found to follow $R_{\text{g},0} \sim M_{\text{w}}^{0.55\pm0.02}$ at 80 ºC. Thus, these results suggest that [BMIM][BF$_4$] is of moderately good quality and PEO chains behave as flexible coils in this ionic liquid.

## 2.2 Experimental

### 2.2.1 Selection of a deuterated system

For PEO/[BMIM][$BF_4$], the contrast was calculated for different combinations of perdeuterated polymer and hydrogenated IL and vice versa, as given in Table 2.1. The maximum contrast is attained by *d*-PEO/[BMIM][$BF_4$] or PEO/$d_{15}$-[BMIM][$BF_4$] systems. However, synthesis of large quantity ( ~ 50 g) of fully deuterated [BMIM][$BF_4$] is significantly expensive compared to the synthesis of *d*-PEO. First, the multi-step synthesis of $d_{15}$-[BMIM][$BF_4$] is inefficient as the overall yield drops with each reaction step. On the other hand, very small amounts of *d*-PEO (< 0.05 g) are required due to the use of dilute solutions. Second, if *d*-PEO is synthesized, the scope of this study can be expanded to additional ILs that are also nearly isorefractive with PEO. Therefore, to study the conformational properties, perdeuterated PEOs were synthesized.

**Table 2.1:** Contrast Calculation for PEO/[BMIM][$BF_4$]

| **Polymer** | **Ionic liquid** | $\rho_{\mathbf{PEO}}$ ($10^{10}$ cm$^{-2}$) | $\rho_{\mathbf{IL}}$ ($10^{10}$ cm$^{-2}$) | $(\rho_{\mathbf{PEO}} - \rho_{\mathbf{IL}})^2$ ($10^{20}$ cm$^{-2}$) |
|---|---|---|---|---|
| PEO | $d_3$-[BMIM][$BF_4$] | 0.64 | 2.38 | 3.0 |
|  | $d_6$-[BMIM][$BF_4$] | 0.64 | 3.95 | 7.3 |
|  | $d_{12}$-[BMIM][$BF_4$] | 0.64 | 5.16 | 20 |
|  | $d_{15}$-[BMIM][$BF_4$] | 0.64 | 6.04 | 29 |
| *d*-PEO | [BMIM][$BF_4$] | 6.88 | 1.41 | 30 |

### 2.2.2 Synthesis of perdeuterated poly(ethylene oxide)

*Living polymerization*

Living polymerization is a chain growth process free of irreversible chain termination and chain transfer steps, which can result in controlled molecular weight and narrow molecular weight distribution of the synthesized polymers.[134] The key advantage of living polymerization is to be able to predict the molecular weight solely on the basis of monomer to initiator ratio (assuming 100% initiation efficiency). Therefore, the degree of polymerization ($N$) is reduced to

$$N = \frac{[\mathrm{M}]_0}{[\mathrm{I}]_0} \tag{2.3}$$

where $[\mathrm{M}]_0$ and $[\mathrm{I}]_0$ are the initial concentrations of monomer and initiator, respectively. In order to estimate the reaction times for allowing almost 100% conversion ($p \rightarrow 1$) of monomer, the following form is used

$$t = \frac{\ln(1-p)}{-k_\mathrm{p}[\mathrm{I}]_0} \tag{2.4}$$

where $p$ is the extent of the reaction, $k_\mathrm{p}$ is the rate of propagation, and $[\mathrm{I}]_0$ is the initiator concentration. For synthesizing high molecular weight polymers, it is desirable to increase the initiator concentration to attain high percent conversion in reasonable period of time.

Poly(ethylene oxide) can be synthesized by the living anionic polymerization of ethylene oxide as shown in Figure 2.2. A general reaction involves initiation by an alkoxide and propagation of the anionic species by ring opening of more monomer to form long chains. For initiators, ion-pairs of $K^+$ and alkoxides are preferred due to their ability to form loose ion-pairs, compared to tight ion-pairs with smaller cations, such as $Li^+$.[134] The alkoxide acts as a nucleophile by attacking EO; this is highly favorable due to the release of ring strain present in the three-membered epoxide. However, due to the high reactivity of the propagating chains, any impurities capable of deactivating the initiators or the growing alkoxide chains must be excluded. Therefore, the synthesis must be performed under dry and oxygen-free conditions by incorporating high vacuum and inert atmospheres. In the particular case of EO polymerization, additional technical challenges arise due to the gaseous and highly reactive nature of EO (b.p. 10 °C). Since EO is both volatile and toxic, it is important to safely handle all the reagents and glassware in the procedure.

### *Purification of ethylene oxide*

Ethylene oxide (99%) was purchased from Sigma-Aldrich. In each of two glass 500 mL round bottom flasks, ~ 5 mL of n-butyl lithium (1.6 M in hexanes, Sigma-Aldrich) is added under inert atmosphere (inside a glovebox) and sealed with Teflon stopcocks. Outside the glovebox, these flasks were connected to vacuum to evacuate hexanes to obtain dry n-butyllithium. In order to purify EO, several steps were taken. First, EO (3–5g) was transferred from the cylinder to a sealed 500 mL round bottom flask and degassed by three freeze-pump-thaw cycles. Then, the monomer was distilled twice into two dried n-butylllithium flasks, and stirred for 30 mins in each flask under salt-water ice bath (<0 °C).  The purified EO was finally transferred to a glass burette (sealed with Teflon stopcock) by vacuum distillation and left under an ice bath. In the need for overnight storage, EO in the burette was stored in a mixture of dry ice and isopropanol (~ –70 °C).

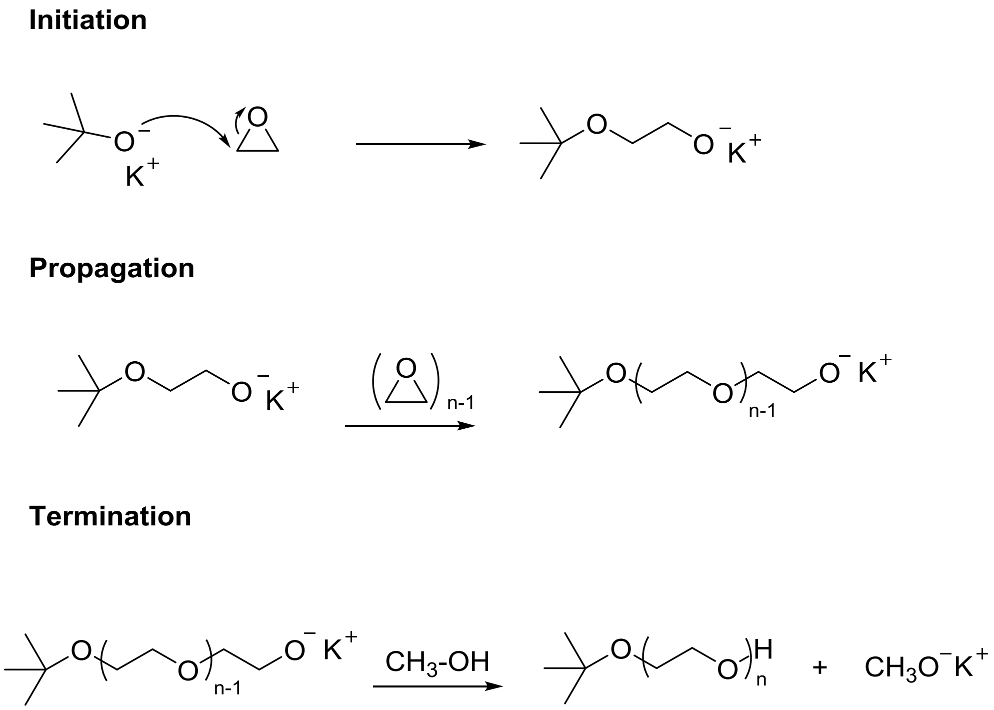

**Figure 2.2:** Reaction scheme of living anionic polymerization of ethylene oxide with initiation, propagation, and termination steps.

### *Incorporation of crown ether*

Several works have shown that the addition of crown ethers or cryptands accelerate the polymerization rate and lower the molecular weight distribution of synthesized PEO.[135–138] The propagating carbanion ($CH_2O^-$) can strongly bind with the counterion ($K^+$), decreasing the reactivity of the growing chains as shown in Figure 2.3a. Therefore, adding crown ether or cryptand can convert the tight ion-pairs into loose-ion pairs by complexing the $K^+$ counterion (shown in Figure 2.3b), and hence enhancing the rate of propagation. Therefore, 18-crown-6 or Kryptofix 222 was freeze dried from a solution in benzene in a 500 mL round bottom flask with a Teflon seal. A typical ratio of 1.1:1 of crown ether to initiator was used.

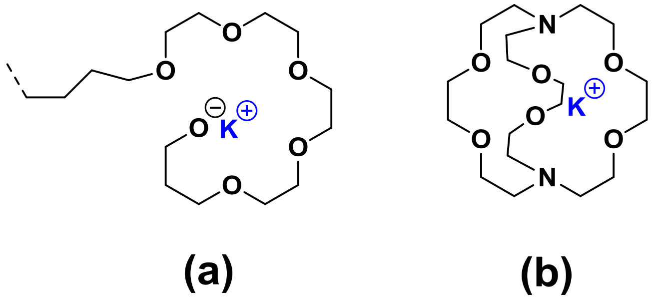

**Figure 2.3:** Complexation of $K^+$ by propagating chain and cryptand (a) The propagating chain with alkoxide ends tend to complex with the counterion (b) Cryptand coordinates with $K^+$ increasing the proportion of free propagating chains.

*Solvent purification*

For synthesizing low molecular weights PEO (< 50 kg/mol), the flask containing the crown ether was filled with tetrahydrofuran obtained directly from the purification column (purging with argon and passing through activated alumina under inert atmosphere). However, an additional purification step was required for synthesizing higher molecular weights PEO (> 100 kg/mol). The amount of initiator incorporated was generally in the order of $10^{-3}$ L and $10^{-5}$ L for low and high molecular weights PEO, respectively. As a result, any trace levels of impurities that are ineffective at high initiator concentration (low molecular weight synthesis) can “kill” the reaction at low initiator concentration (high molecular weight synthesis). As more than 90% of the reaction volume is solvent, it is important to keep the solvent free of impurities, moisture, oxygen, etc. Therefore, THF collected from the column was purified additionally by transferring and stirring it in a benzophenone-sodium still. Once ready to use in the reactor, THF was vacuum distilled into another solvent flask (containing cryptand) and sealed under Ar. For low molecular weight synthesis, around 300 mL of solvent was collected while for very high molecular weight PEO, solvent volume was limited to 50 mL to increase the initiator concentration and enhance reaction kinetics.

### *Reaction*

A glass covered magnetic stir bar was inserted into a 1 L glass reactor with 5 threaded ports incorporated with the solvent flask, reaction manifold, airlock, temperature seal, and glass seal. The purified solvent was first introduced in the reaction flask and stirred at 45 °C. A glass syringe was used to draw the desired amount of initiator, potassium tert-butoxide (1.0 M, purchased from Sigma-Aldrich), in glovebox and protected using a rubber septum. The syringe needle was inserted through the manifold to add initiator to the solvent. Then the purified EO was slowly added from the burette to the reactor, carefully monitoring the reactor pressure (< 8 psi). The reaction time was estimated by using eqn 2.4, assuming 99% conversion, using $k_\mathrm{p}$ of 0.035 $\mathrm{L.mol^{-1}.s^{-1}}$, and the given initiator concentration.[139] The reaction was terminated by addition of degassed methanol via cannula transfer, and stirring for 30 mins. The reaction mixture was dried under a rotovap to obtain PEO in solid state, which was further dissolved in dichloromethane, and precipitated twice in cold hexanes. The complex of $K^+$/crown ether or $K^+$/kryptand is known to dissolve in hexane, assuring that no salt residue remains after precipitation.[135] The solid PEO after purification was dried under dynamic vacuum (100 mTorr) for 48 h and massed. The percent yield in all cases was > 85%.

Four deuterated versions of PEO were synthesized using the identical procedures described above assuming no change in kinetics and reactivity. *d*-EO (98% D) was purchased from Sigma Aldrich. A further *d*-PEO ($M_\mathrm{w}$ = 54 kg/mol) was purchased from Polymer Source. The final product was characterized by $^1$HNMR, $^2$H NMR, size-exclusion chromatography (SEC) and matrix assisted laser desorption/ionization time of flight (MALDI-TOF) mass spectrometry.

### 2.2.3 Characterization of perdeuterated poly(ethylene oxide)

*Size-exclusion Chromatography*

The weight-average molecular weights ($M_\mathrm{w}$) and dispersities ($Đ$) of the synthesized and commercial polymers (Table 2.2) were determined by size-exclusion chromatography (SEC) performed in THF at 25 °C on an Agilent 1260 Infinity system. The eluents were monitored by a Wyatt Optilab T-rEX refractive index detector, and the corresponding molecular weights and distributions were determined by using Zimm plots obtained from a Wyatt Dawn Heleos II multiangle laser light scattering (MALS) detector. The SEC traces for all the synthesized *d*-PEOs are shown in Figure 2.4. A Wyatt Optilab T-rEX refractive index detector with 637 nm wavelength was used to measure the differential refractive index of 6 concentrations (well below the overlap concentration) of *d*-PEO in THF. The d*n*/d*c* of a high molecular weight *d*-PEO (120 kg/mol) was obtained from the slope of *d*RI vs. *c* plot (shown in Figure 2.5) as 0.0568 mL/g. However, the refractive index increment (d*n*/d*c*) is known to have a dependence on molecular weight given as

$$\frac{\mathrm{d}n}{\mathrm{d}c} = \left(\frac{\mathrm{d}n}{\mathrm{d}c}\right)_\infty + \frac{K}{M_\mathrm{n}} \qquad (2.5)$$

where $K$ is a chemical composition dependent factor, and $(\mathrm{d}n/\mathrm{d}c)_\infty$ is the d*n*/d*c* at infinite molecular weight. [140] In general, d*n*/d*c* approaches an asymptotic value approximately for

$M$ > 20 kg/mol. Therefore, d$n$/d$c$ is additionally measured for a low molecular weight *d*-PEO (10 kg/mol) given as 0.0528 mL/g. The deuterated polymers are denoted as *d*-PEO-*x,* where *x* represents the $M_w$ of the respective polymer.

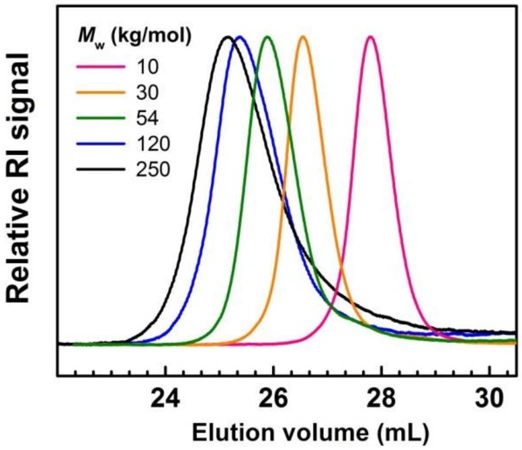

**Figure 2.4:** SEC traces of synthesized *d*-PEO of different molecular weights in THF

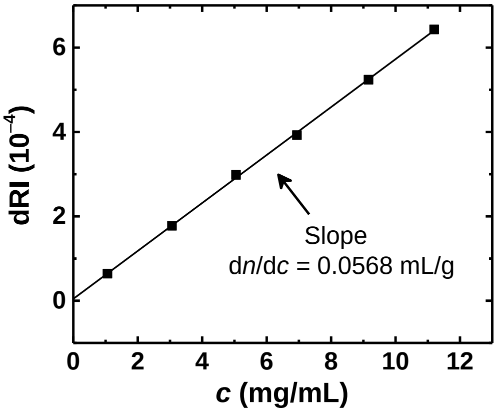

**Figure 2.5:** Differential refractive index versus concentration for *d*-PEO-120 at 25 °C. The slope yields the d$n$/d$c$ as 0.0568 mL/g.

**Table 2.2:** Molecular weights of synthesized *d*-PEO

| $M_w$ (kg/mol) ($\pm$10%) | *Đ* |
|---|---|
| 10 | 1.01 |
| 30 | 1.01 |
| 54[a] | 1.06 |
| 120 | 1.04 |
| 250 | 1.10 |

[a]Purchased from Polymer Source

*MALDI-TOF*

MALDI-TOF can be used to characterize relatively low molecular weight polymers and therefore, only *d*-PEO-10 could be analyzed accurately. A typical MALDI mass spectrum consists of Intensity plotted as a function of mass to charge ratio (m/z) that yields the molecular weight distribution of the polymer (shown in Figure 2.6a and b). The experiment was performed using established procedures described elsewhere.[65] A typical recipe comprised of matrix (dithranol, 20 mg/mL), cationizing agent (silver trifluoroacetate, 2 mg/mL), and *d*-PEO (10 mg/mL). The values of $M_w$ and *Đ* obtained are 9 kg/mol and 1.01, respectively. The $M_w$ value obtained from MALDI is close to the value obtained from SEC. MALDI-TOF was also attempted for *d*-PEO-30 but the resolution diminishes at this molecular weight as shown in Figure 2.6c. Regardless, the obtained $M_w$ and *Đ* values of 30 kg/mol and 1.01 for *d*-PEO-30 are in excellent agreement with those obtained from SEC.

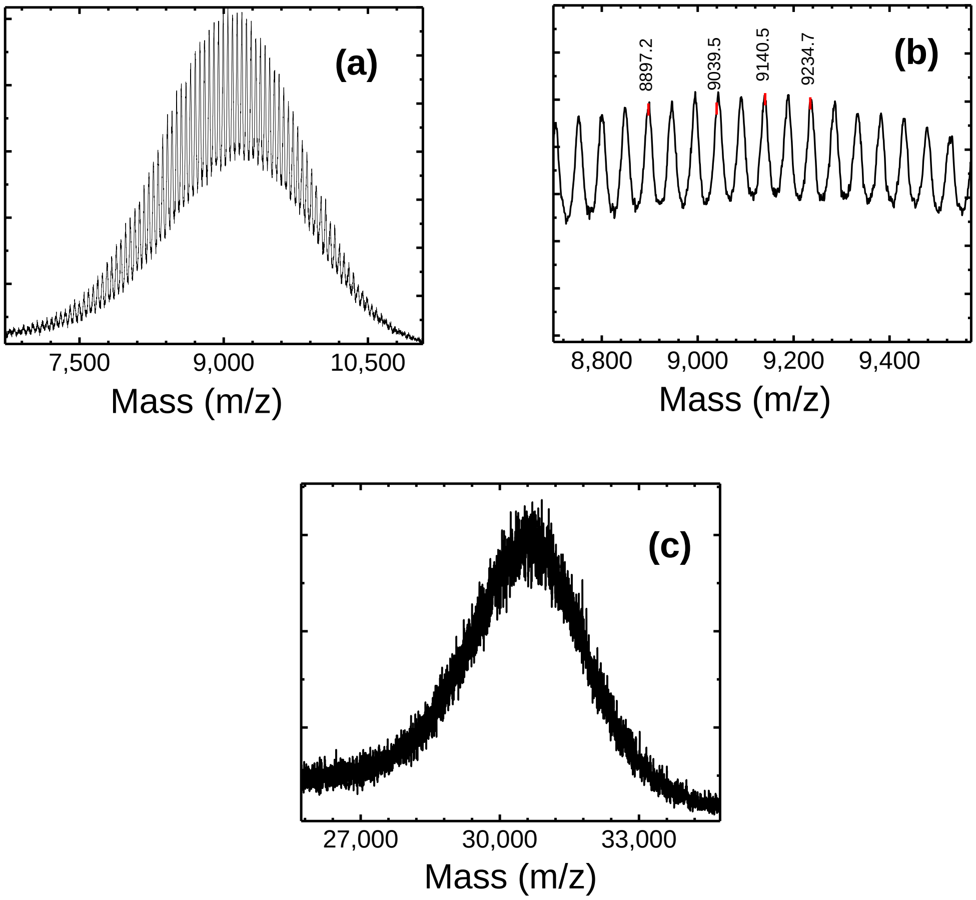

**Figure 2.6 :** MALDI spectra of *d*-PEO (a) MALDI spectra of *d*-PEO-10 (b) Zoomed-in view of the MALDI spectra of *d*-PEO-10 showing the corresponding imers (b) MALDI spectra of *d*-PEO-30 with considerably diminished resolution.

### *$^{1}$H and $^{2}$H NMR*

All the synthesized polymers were characterized using $^{1}$H and $^{2}$H NMR in deuterated and hydrogenated chloroform, respectively. The NMR traces are shown in Figure 2.7 and Figure 2.8.

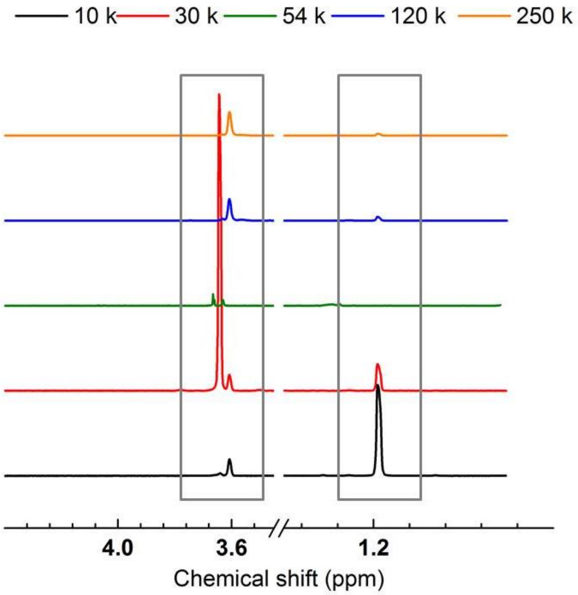

**Figure 2.7**: $^1$H NMR spectra of *d*-PEOs in deuterated chloroform. The peaks at chemical shifts around 1.2 ppm indicate the *tert*-butoxide end group, which is absent for the hydroxyl terminated commercial *d*-PEO (54 k). The peaks at around 3.6 ppm correspond to the repeat unit structure with one or more protons.

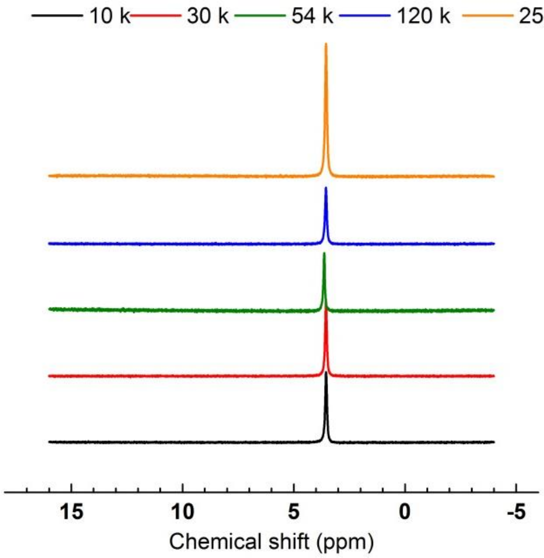

**Figure 2.8:** $^2$H NMR spectra of *d*-PEOs in chloroform. The single peak at 3.6 ppm corresponds to equivalent deuterons in the repeat unit structure.

### 2.2.4 Sample preparation

The IL [BMIM][$BF_4$] was purchased from Sigma-Aldrich, diluted in dichloromethane (DCM) and washed with distilled water until no precipitate was observed using a silver nitrate test. The mixture was stirred with activated charcoal for 24 h and then run through a neutral alumina column to remove impurities. Finally, [BMIM][$BF_4$] was dried under vacuum (<100 mtorr) for 72 h at 70 °C. The dried product was characterized using $^1$H, $^{19}$F and $^{13}$C NMR spectroscopy as shown in Figure 2.9 and Figure 2.10. The overlap concentrations ($c$*) of *d*-PEO (listed in Table 2.4) were estimated using the following equation,

$$c^* = 3M/(4\pi R_{g,0}^3 N_A) \tag{2.6}$$

where $N_A$ is Avogadro's number. The value of $R_{g,0}$ under theta conditions was estimated using

$$R_{g,0}^2 = Nb^2/6 \tag{2.7}$$

where $b$ is the statistical segment length, taken as 6 Å for PEO in the melt state.[141] The $R_{g,0}$ values obtained for *d*-PEO 10, 30, 54, 120, 250 kg/mol are 36, 60, 80, 120, 168 Å, respectively. In order to remain in the dilute limit, all solutions were prepared with polymer concentrations below 0.5$c$*. The polymer/IL solutions were prepared using co-solvent evaporation where *d*-PEO and [BMIM][$BF_4$] were added by weight in the desired ratio followed by the addition of dichloromethane (DCM) to facilitate dissolution. DCM was then evaporated under stirring using a nitrogen purge overnight, and the mixtures were further dried under vacuum (< 100 mtorr) for 46 h at 50 °C. Despite the fact that the solutions were carefully dried prior to the SANS measurements, uptake of trace amounts of water cannot be excluded. However, for the purpose of studying coil dimensions, trace amounts of water, another good solvent for PEO, should not affect the values of $R_g$ within the uncertainty.

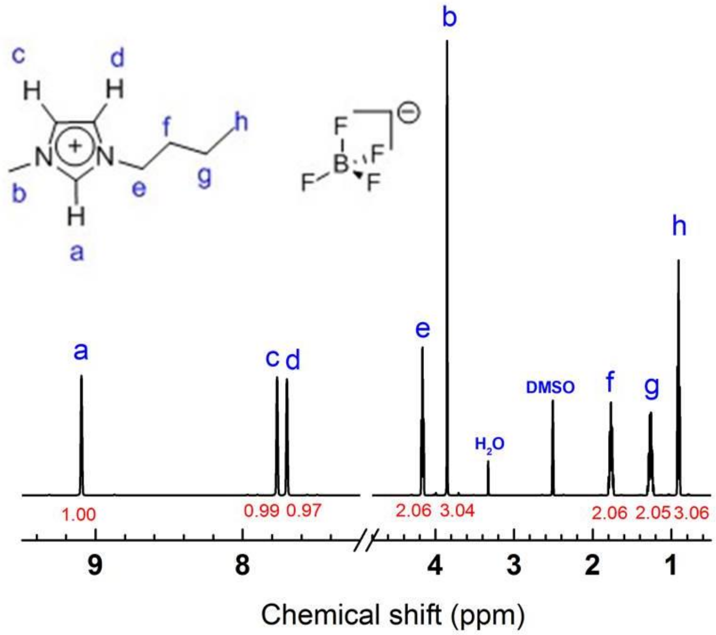

**Figure 2.9:** $^1$H NMR spectrum of [BMIM][$BF_4$] in deuterated dimethyl sulfoxide (DMSO).

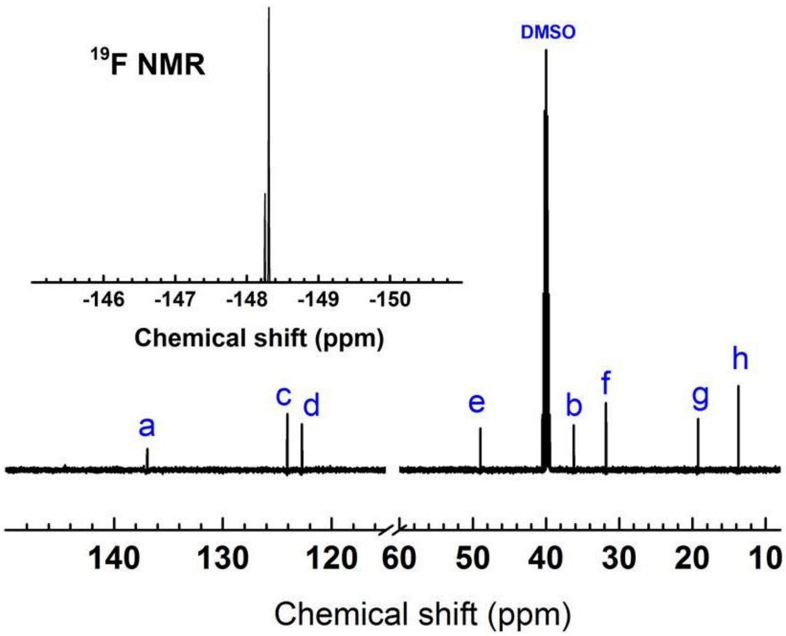

**Figure 2.10:** $^{13}$C NMR spectrum of [BMIM][BF$_4$] in deuterated dimethyl sulfoxide (DMSO). The inset shows the $^{19}$F NMR spectrum indicating the fluorine atoms in the anion.

*Crystallization of PEO in [BMIM][BF$_4$]*

Simulation studies reported conflicting conformations of PEO (extended chain) at room temperature.[90] However, experiments could not be performed at room temperature due to the crystallization of PEO in [BMIM][BF$_4$]. Our observation of PEO crystallization in [BMIM][BF$_4$] is consistent with the report by Liu and coworkers.[100] *d*-PEO-30 (1.5 to 2 wt%) was dissolved in various imidazolium-based ILs as shown in Figure 2.11. The ILs used are [EMIM][BF$_4$], 1-propyl-3-methylimidazolium tetrafluoroborate ([MPIM][BF$_4$]), [BMIM][BF$_4$] , [HMIM][BF$_4$], and BMIM][TFSI]. Even at such low concentration and molecular weight, *d*-PEO crystallizes in [EMIM][BF$_4$], [MPIM][BF$_4$], and [BMIM][BF$_4$]. However, no crystallization was observed in [HMIM][BF$_4$] and [BMIM][TFSI] solutions.

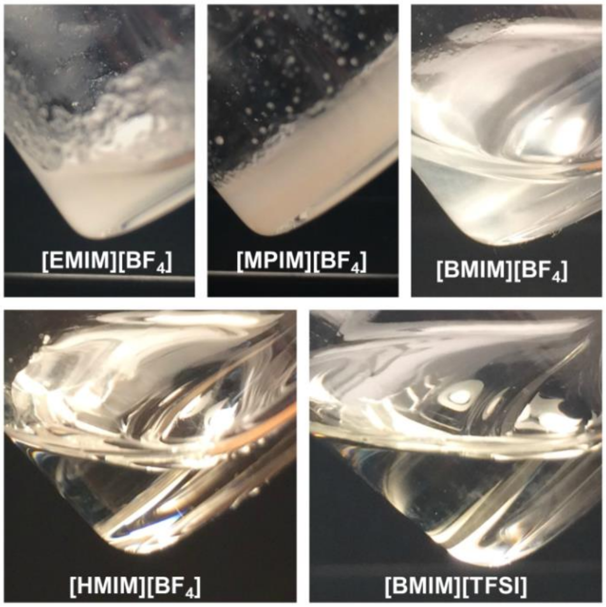

**Figure 2.11:** *d*-PEO-30 dissolved in various ILs in concentration range of 1.5 to 2 wt%.

More reliable experimental techniques are required to further investigate the crystallization behavior of PEO in ILs. Nevertheless, the crystallization of PEO in the IL of interest is evident and therefore, SANS experiments were conducted at 80 °C, which is above the crystallization temperature of PEO (~65 °C).

### 2.2.5 Small-angle neutron scattering

In a scattering experiment, the magnitude of moment transfer vector is given by

$$q = \frac{4\pi}{\lambda}\sin\left(\frac{\theta}{2}\right) \qquad (2.8)$$

where $\lambda$ is the wavelength in the material and $\theta$ is the scattering angle. $q$ has units of inverse length and $1/q$ determines the length scale of interest. Therefore, a scattering technique with large $q$ value is required to probe structures at a smaller length scale. One of the advantages of using SANS is that it spans relevant size scales for polymer system, as $q$ typically ranges from 0.001 to 0.1 Å$^{-1}$.[129]

The intensity of scattering as a function of $q$ for dilute polymer solutions is represented in a general form

$$I(q) = (\text{contrast})cMP(q) \tag{2.9}$$

where $c$ is the concentration and $M$ is the molecular weight of the polymer, and $P(q)$ is the single particle form factor that contains information about $R_g$, as will be discussed in detail later. [132,142]

SANS utilizes a neutron beam as the radiation that is produced by either reactor-based or spallation-based sources. Throughout this thesis work, only reactor-based source at National Institute of Standards and Technology (NIST) Center for Neutron Research and High Flux Isotope Reactor (HFIR) facility of the Oak Ridge National Laboratory (ORNL) was used. The SANS instrument setup and experimental procedure are described in detail elsewhere.[143] In short, reactor-based sources release "thermal" neutrons that are guided towards the sample cell, and finally scattered onto a 2D detector. The obtained 2D scattering SANS data need to undergo various correction procedures described in the well-established reduction protocol.[144] Briefly, the sample data is corrected for background, empty cell scattering, sample transmission, and detector efficiency, and converted to an absolute intensity scale. The corrected data is reduced to 1D $I(q)$ vs. $q$ format by azimuthal integration. In all the following SANS plots, the $I(q)$ is the absolutely calibrated intensity in the units of cm$^{-1}$ .

In our experiments, SANS was performed on the NG-7 30 m and NG-B 30 m instruments at the National Institute of Standards and Technology (NIST) Center for Neutron Research. Three sample-to-detector distances (SDD) of 13, 4 and 1 m, two mean neutron wavelengths ($\lambda$) of 6 and 8 Å, with wavelength spreads ($\Delta\lambda/\lambda$) of 0.125 and 0.115, respectively, were used to access a $q$ range of approximately 0.004 – 0.443 $\text{Å}^{-1}$. The solutions were injected into 1 mm thick demountable cells and placed in a heating block equilibrated at 80 °C.

*SANS model fits in conformational studies*

A Guinier plot is one of the most commonly used methods provide the value of $R_g$ irrespective of the structure.[132] The logarithm form is represented as

$$\ln I(q) = \ln(I_0) - \frac{q^2 R_g{}^2}{3}, P(q) \approx \exp\left[1 - \frac{q^2 R_g{}^2}{3}\right] \tag{2.10}$$

where $\ln(I_0)$ is the y-intercept, $P(q)$ is the appropriate form factor, and $I(q)$ is the background subtracted absolute intensity. Guinier analysis, however, is valid only in the limit of $qR_g \ll 1$, known as the Guinier regime (low $q$ region). When the Guinier regime cannot be probed, Debye fit[145] can be used, given by

$$I(q) = \frac{2A}{x^2}(e^{-x} - 1 + x) + B, \qquad x = q^2 R_g{}^2 \tag{2.11}$$

where $A$, $B$ and $R_g$ are used as fitting parameters. Although this function is strictly applicable to Gaussian chains, the use of a Debye fit for polymer coils that may deviate from Gaussian statistics has been previously justified in the literature by both experiment and theory.[146,147] The $R_g$ values obtained from Debye plots are apparent $R_g$, owing to the inter-chain contributions. Therefore, $R_g$ values measured at finite concentrations need to be extrapolated to the limit of infinite dilution to determine the infinite dilution chain size of the polymer chain.

*Small-angle neutron scattering of neat ionic liquid*

One unique feature of SANS is the presence of incoherent scattering. Coherent scattering depends on $q$ and contains information about the size of the scattering particles, while incoherent scattering is independent of the scattering angle and holds no information of interest. Systems comprising many $^1$H atoms have significant incoherent scattering, which must be subtracted from the scattering signal. For dilute polymer solutions, the scattering from the solvent can be measured independently and subtracted as the background incoherent scattering.

In Figure 2.12a, the scattering curve of neat [BMIM][BF$_4$] shows an upturn above $q \approx 0.1$ Å$^{-1}$, indicating the existence of relatively long-ranged local structure within the solvent. Mid-angle X-ray scattering (MAXS) was subsequently utilized to probe this structure at higher $q$ (Figure 2.12b). MAXS data were collected at the DND-CAT 5-ID-D beamline at the Advanced Photon Source, Argonne National Laboratory. A wavelength $\lambda = 0.73$ Å and SDD of 1 m was used to obtain a $q$ range of approximately 0.13 – 0.86 Å$^{-1}$. The samples were contained in 1.5 mm diameter quartz capillaries, and the experiments were conducted at room temperature. The measured isotropic two-dimensional scattering patterns were converted to one-dimensional plots of $I(q)$ (in arbitrary units) vs. $q$. The MAXS profile of [BMIM][BF$_4$] suggests the presence of spatial correlations on the nm length-scale, and these correlations become more prominent when the alkyl chain length in the imidazolium cation is increased to six carbons (hexyl). The existence of such spatial correlations in imidazolium-based ILs, and the strong dependence of ordering on alkyl chain length, was previously identified by Triolo and coworkers.[148–150]

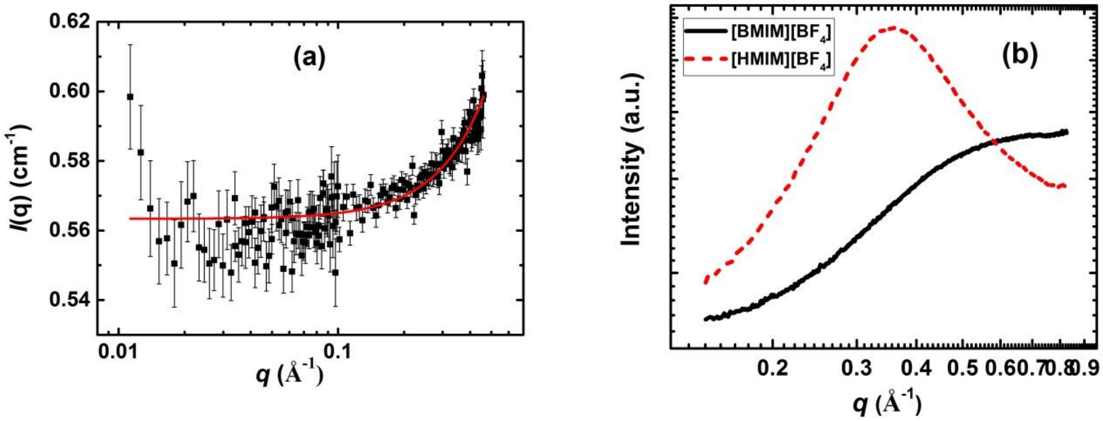

**Figure 2.12:** Solvent scattering profiles of as-prepared ILs at room temperature. (a) SANS scattering profile (symbols) of [BMIM][$BF_4$] fit to a quadratic equation (represented by solid curve). A sharp upturn at $q \geq 0.1$ Å$^{-1}$ can be observed. (b) MAXS patterns of [BMIM][$BF_4$] and 1-hexyl-3-methylimidazolium ([HMIM])[$BF_4$] at room temperature, emphasizing the existence of spatial correlations within the ionic liquid.

## 2.3 Results and Discussion

### 2.3.1 Background subtraction

The PEO/[BMIM][$BF_4$] system characteristically suffers from low signal-to-noise ratio for the following reasons. First, the use of dilute solutions significantly lowers the scattering intensity. Second, the hydrogen content of [BMIM][$BF_4$] leads to a substantial incoherent background (shown in Figure 2.13), that results in inevitable uncertainty in background subtraction. Third, despite maximizing the contrast of the polymer with the solvent, the presence of strong neutron absorbing atoms such as boron in [BMIM][$BF_4$], significantly reduce scattering intensity even at long collection times. As a result, the transmission factors were roughly 0.20 for all solutions, even at a sample thickness of 1 mm. Therefore, to minimize uncertainty in the background subtraction for the polymer/IL solutions, the solvent SANS data were fit to a quadratic form $I_{\text{solvent}} = C + Dq^2$, where $C$ and $D$ are fitting constants. The incoherent background weighted by the solvent volume fraction was then subtracted from the polymer/IL scattering data. The background-subtracted SANS profiles of several dilute solutions of *d*-PEO measured at 80 °C are shown in Figure 2.14. As expected, the absolute scattering intensity increases with increasing polymer concentration.

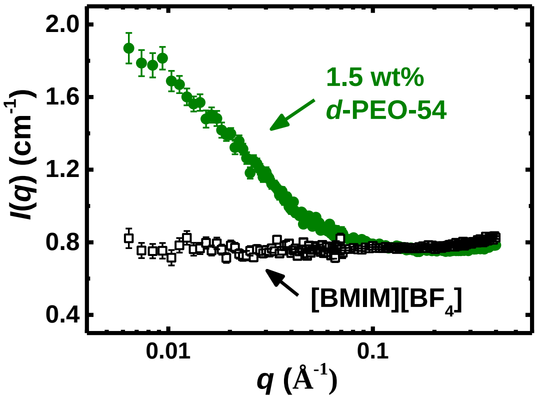

**Figure 2.13:** Scattering profiles of 1.5 wt% *d*-PEO-54 and the solvent, [BMIM][BF$_4$]. The solvent scattering is in the same order of magnitude as the solution scattering.

### 2.3.2 Debye fits

As previously mentioned, Guinier analysis is typically preferred for $R_g$ determination, as prior assumptions about the chain conformation are not necessary. In this case, however, due to low signal-to-noise ratio, significant incoherent scattering, and insufficient usable data points in the Guinier regime ($qR_g < 1$), this fitting approach was not used. Instead, the background-subtracted profiles were fit to the Debye function (eqn 2.11),[145] where *B* was left as a floating parameter. For all molecular weights, the residual incoherent scattering (*B*) values obtained from the fits were roughly 1 to 10% of the corresponding *I*(0). The Debye function fits are depicted by solid lines in Figure 2.14 and are in good agreement with the observed scattering profiles. For each molecular weight, measurements were performed for four concentrations in the estimated dilute regime.

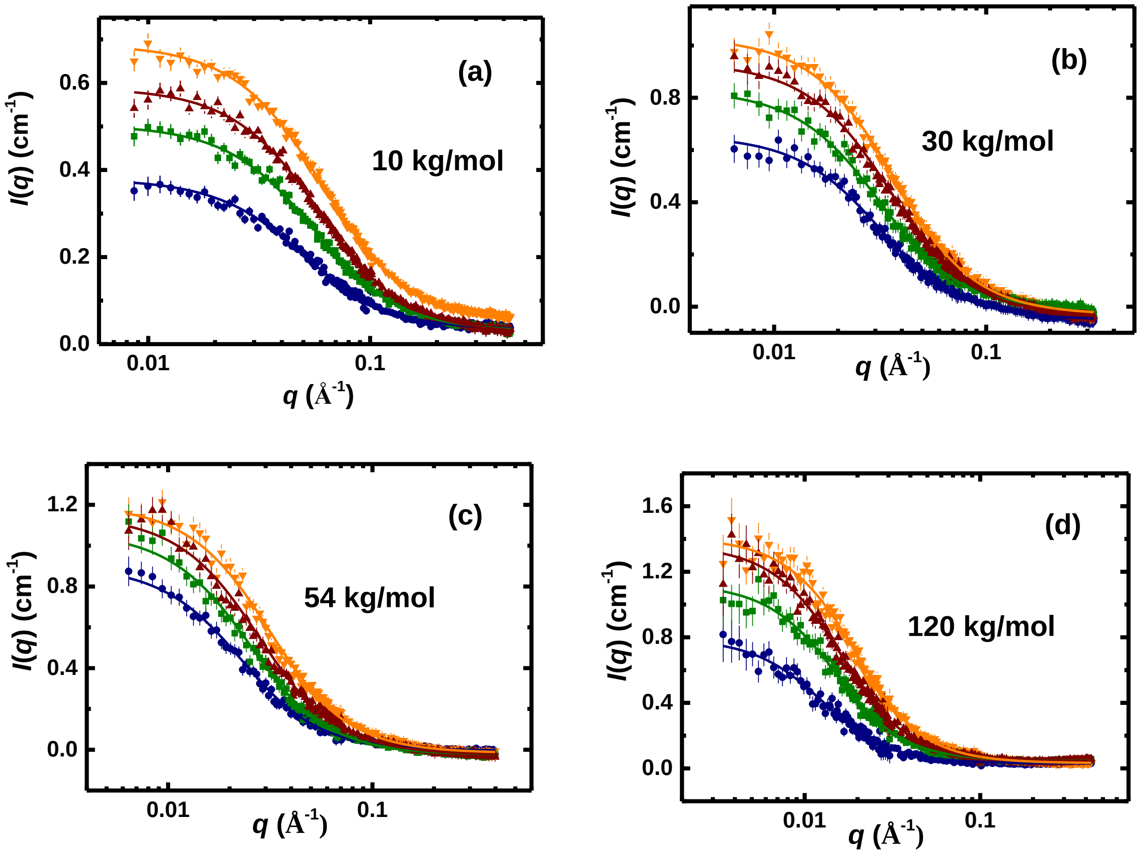

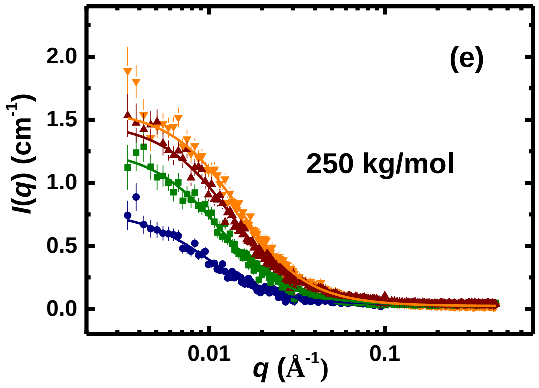

**Figure 2.14:** Background subtracted SANS scattering profiles (symbols) for the *d*-PEOs in [BMIM][BF$_4$] with the corresponding Debye function fits (eqn 2.11) represented by solid curves. The colors blue, green, red and orange represent 0.2, 0.3, 0.4 and 0.5 *c** for (a), (b) and (c), and 0.1, 0.2, 0.3, 0.4 c* for (d) and (e), respectively. The overlap concentrations (*c**) are listed in Table 2.4 and the respective concentrations are listed in Table 2.3.

**Table 2.3**: List of Debye function (eqn 2.11) fitting parameters for background subtracted SANS scattering profiles.

| $M_w$ (kg/mol) | *c* (wt%) | *A* | *B* | Apparent $R_g$ (Å) |
|---|---|---|---|---|
| 10 | 1.47 | 0.34 | 0.03 | 31.7 |
| | 2.20 | 0.48 | 0.03 | 28.9 |
| | 2.95 | 0.57 | 0.02 | 27.2 |
| | 3.69 | 0.63 | 0.05 | 26.5 |
| 30 | 0.87 | 0.71 | -0.05 | 51.2 |
| | 1.29 | 0.84 | -0.01 | 51.5 |
| | 1.74 | 0.97 | -0.04 | 45.8 |
| | 2.15 | 1.06 | -0.03 | 43.9 |
| 54 | 0.78 | 0.91 | -0.005 | 71.0 |
| | 1.11 | 1.09 | -0.03 | 64.3 |
| | 1.46 | 1.17 | -0.02 | 58.2 |
| | 1.93 | 1.22 | -0.02 | 51.6 |
| 120 | 0.22 | 0.76 | 0.03 | 128 |

| | | | | |
|---|---|---|---|---|
| | 0.43 | 1.08 | 0.05 | 107 |
| | 0.65 | 1.32 | 0.04 | 100 |
| | 0.84 | 1.38 | 0.03 | 83.0 |
| 250 | 0.16 | 0.74 | 0.04 | 168 |
| | 0.31 | 1.24 | 0.03 | 142 |
| | 0.47 | 1.44 | 0.04 | 122 |
| | 0.64 | 1.56 | 0.02 | 109 |

### 2.3.3 Evaluation of Flory exponent

The apparent $R_g$ determined for various concentrations are plotted in Figure 2.15 and listed on Table 2.3, where the error bars represent the uncertainty in the non-linear fits. The y-intercepts of $R_g$ ($c$) vs. $c$ plots provide the infinite dilution radii of gyration, $R_{g,0,}$ which are listed in Table 2.4 along with the errors represented by the estimated uncertainty from the linear fits.

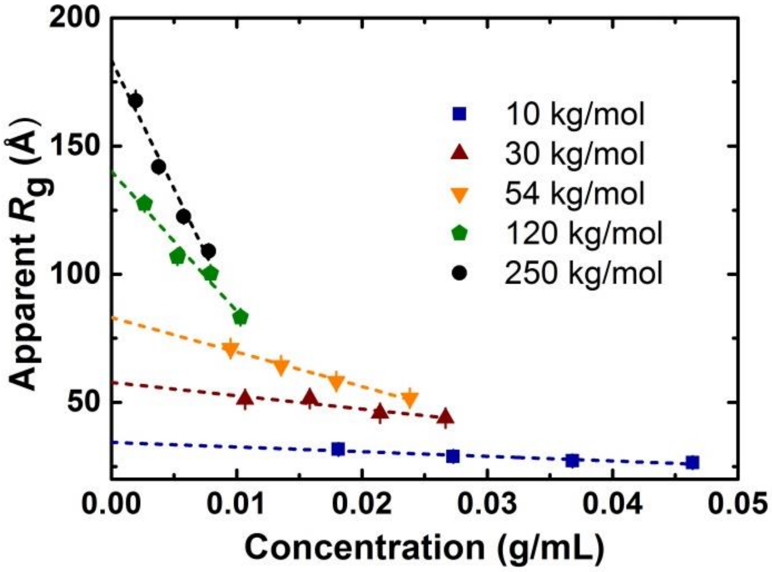

**Figure 2.15:** Apparent $R_g$ as a function of concentration extrapolated to infinite dilution

for various molecular weights of *d*-PEO in [BMIM][$BF_4$] at 80 °C.

The infinite dilution radii are plotted versus molecular weight in Figure 2.16 in double logarithmic form to evaluate the excluded volume exponent from the slope of a linear fit. The errors in $M_w$ are approximated by the accuracy in determination of molecular weights by SEC, which is roughly ± 10%. [111] The dependence of $R_{g,0}$ on $M_w$ was found to be

$$R_{g,0} = (0.22 \pm 0.05)\, M_w^{(0.55 \pm 0.02)}\ (\text{Å}) \tag{2.12}$$

where the uncertainty in the exponent and the pre-factor are obtained from the errors in the slope and intercept of the linear fit, respectively.

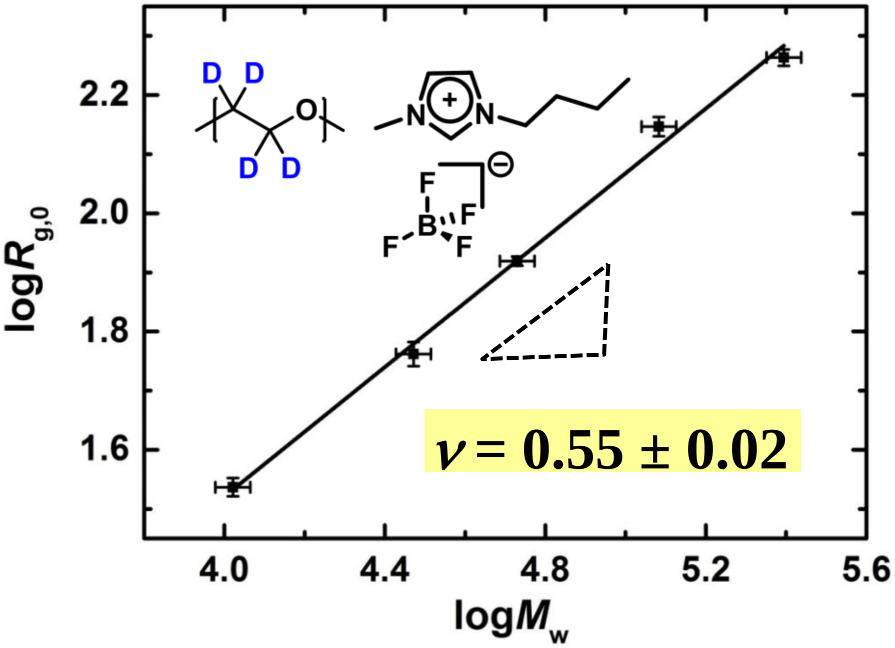

**Figure 2.16:** Double-logarithmic plot of $R_{g,0}$ vs. $M_w$ for *d*-PEO in [BMIM][$BF_4$] at 80 °C.

The slope gives $\nu = 0.55$, indicating that [BMIM][BF$_4$] lies in the intermediate regime between a theta and a very good solvent.

**Table 2.4:** Polymer Characteristics for *d*-PEO in [BMIM][BF$_4$] at 80 °C.

| $M_w$ **(kg/mol) (±10%)** | $Đ$ | $c^*$ **(wt%)** | $R_{g,0}$ **(Å)** $\theta$ **condition**[a] | $R_{g,0}$ **(Å) SANS** |
|---|---|---|---|---|
| 10 | 1.01 | 7.3 | 36 | 34 ± 1 |
| 30 | 1.01 | 4.3 | 60 | 58 ± 3 |
| 54 | 1.06 | 3.3 | 80 | 83 ± 2 |
| 120 | 1.04 | 2.2 | 120 | 140 ± 5 |
| 250 | 1.10 | 1.6 | 168 | 183 ± 6 |

[a] Estimated using eqn 2.7

The exponent of 0.55 ± 0.02 suggests that [BMIM][BF$_4$] is a moderately good solvent for PEO. Since the effect of excluded volume is dependent on both the chain length (range of $M$) and the experimental temperature, it is common to obtain scaling exponents between 0.5 and 0.6.[111] Table 2.4 contains the estimated (melt) unperturbed dimensions for each molecular weight of PEO used here. By comparing the obtained $R_{g,0}$ values for PEO in [BMIM][BF$_4$] and in the melt, it is apparent that the lowest three molecular weights exhibit dimensions close to the theta condition. On the other hand, excluded volume influences the dimensions of the two highest molecular weights as the coil expands more than the unperturbed state. Such behavior is consistent with the fact that excluded volume effects do not strongly influence the chain dimensions until relatively large values of $M$ are reached.[151] The measured $R_{g,0}$ for the highest molecular weight PEO used (250 kg/mol) increases by roughly 10% of its $R_{g,0}$ estimated at theta conditions. In comparison, a PEO chain of the same length expands by almost a factor of 2 in water and methanol at room temperature, both of which are reported to be good solvents on the basis of light scattering[121,152] and intrinsic viscosity.[153,154] This relatively modest expansion of PEO chains in [BMIM][$BF_4$] relative to their substantial expansion in good solvents suggests that the IL is of intermediate quality at 80 °C. We note that the presence of deuterons rather than protons on the backbone of the PEO may also have some modest influence on the values of $R_g$ and the exponent obtained. Indeed, it has been reported that the deuteration of [BMIM][$BF_4$] lowered the miscibility of PEO slightly (*i.e.*, decreased the lower critical solution transition by a few degrees).[65] It is possible that the coil dimensions would be slightly larger if hydrogenated PEO were used instead.

Nonetheless, these results provide strong evidence that PEO adopts a flexible random coil-like conformation in [BMIM][$BF_4$], which deviates substantially from the conclusions drawn from some of the simulations mentioned previously.[90,91] However, more recent atomistic simulations employed a polarizable force field approach that predicted theta-like behavior for PEO in [BMIM][$BF_4$] at 127 °C, which is closer to our experimental results. On the basis of this agreement, it appears that polarizable force fields better depict the polymer/IL interactions, but the use of very short chains ($N = 9$ to 40) and a different temperature compromise exact comparison of theory and experiment. However, it is clear that the results of simulations studies are very sensitive to the parameterization of the interaction between polymers and ILs, and thus this experimental study can help to benchmark better simulation models to accurately predict polymer conformations in ILs.

Triolo *et al*. previously conducted a room temperature SANS study of *d*-PEO (27 kg/mol) in [BMIM][BF$_4$] and reported $R_{g,0} \approx 65$ Å, which is not far from our interpolated $R_{g,0}$ of 57 Å for the same chain length.[93] The discrepancy can be attributed to a combination of the differences in temperature, concentration range, polymer end groups, and uncertainty in molecular weight. However, it seems that the radii at infinite dilution ($M_w$ = 38 kg/mol) are considerably smaller in [BMIM][BF$_4$] (69 Å) than in ethylammonium nitrate (EAN) (81 Å)[94] and lithium tetraglyme bis(trifluoromethanesulfonyl)imide ([Li(G4)][TFSI]) (86 Å).[97] The reported radii in these two ILs are almost 15 Å larger than in [BMIM][BF$_4$], suggesting that they are better solvents, but it would be helpful to confirm this hypothesis by determining $\nu$ for these ILs for larger values of $N$.

Intrinsic viscosity ([$\eta$]) measurements made by Liu *et al*. for PEO in [BMIM][BF$_4$] at 80 °C suggest different solvent characteristics than our SANS study.[100] A Mark-Houwink exponent ($a$) of 0.44 ($\nu$ = 0.48, where $a = 3\nu - 1$) was obtained, suggesting poor solvent behavior. Although the source of this discrepancy is not immediately clear, there are a few factors to consider. First, these scaling exponents ($a$ and $\nu$) are sensitive to the range of molecular weights used. Our SANS experiment probes a different range of molecular weights ($10^3 < M_w < 10^5$ g/mol) than the intrinsic viscosity study ($10^5 < M_w < 10^7$ g/mol). Second, the polymers used in intrinsic viscosity are broadly distributed ($1.2 < Đ < 1.6$), with $Đ$ varying significantly with $M_w$, compared to those used in SANS ($1.01 < Đ < 1.10$). Since both $R_{g,0}$ and [$\eta$] are a measure of the average properties of the all the polymer chains in the sample, nearly monodisperse polymer samples are preferred. Although the Mark-Houwink expression is assumed to be independent of dispersity, using polymers that are heterogeneous, with dispersities varying with $M$, can affect the values of the exponent.[155] Some reports have emphasized the importance of using narrowly distributed polymers in order to accurately establish the $[\eta]$-$M_w$ relationships.[156,157] Third, the equilibrium property, $R_g$, more directly reflects solvent quality than the dynamic properties $[\eta]$ and hydrodynamic radius ($R_h$). This has been attributed to the weaker dependence of $R_h$ on $M$ as compared to that of $R_{g,,}$ which also reduces the dependence of $[\eta]$ on $M$ due to the proportionality $[\eta] \sim R_h R_g^2/M$. [158,159] Therefore, it is conceivable that intrinsic viscosity would yield a smaller exponent than scattering studies, but it is still surprising that the exponent would be as low as 0.48. Another major consideration is that based on phase separation studies, PEO is well-soluble in [BMIM][$BF_4$] at temperatures below 200 °C. Cloud point measurements showed that 2 wt% PEO (20 kg/mol) in [BMIM][$BF_4$] phase separates at approximately 209 °C, and that the critical temperature ($T_c$) is not a strong function of PEO molecular weight.[65,66] Therefore, assuming the $T_c$ does not change significantly across the molecular weight range used, all PEO coils of different chain lengths should be well miscible in [BMIM][$BF_4$] at 80 °C (below the LCST), which is not consistent with the intrinsic viscosity results.

## 2.4 Conclusion

The study of polymer conformations in ionic liquids is of great interest from a fundamental standpoint. The dimensions of *d*-PEO chains of accessible molecular weights (10 to 250 kg/mol) in [BMIM][$BF_4$] is evaluated using small-angle neutron scattering. We find an excluded volume exponent of 0.55 at 80 ºC, which strongly suggests that PEO adopts a slightly swollen, flexible coil conformation in [BMIM][$BF_4$]. The infinite dilution radii for lower molecular weights are similar to the unperturbed radii in the melt state, indicating theta-like behavior. On the other hand, the coils expand relatively more for larger molecular weights *d*-PEO, revealing the onset of excluded volume effects. However, compared to good solvents for PEO such as water and methanol, the expansion of PEO of the same chain length in [BMIM][$BF_4$] is more modest. Therefore, this study reveals that [BMIM][$BF_4$] is a moderately good solvent for PEO at 80 °C. Moreover, these results clarify the discrepancies among simulation studies of PEO chain dimensions in [BMIM][$BF_4$], hence, emphasizing the need for models that account for the complexity of intermolecular interactions in ionic liquids that eventually affect the solvation of polymer chains.

## Acknowledgement

This work was supported by the National Science Foundation (DMR-1707578). Portions of this work were performed at the DuPont-Northwestern-Dow Collaborative Access Team (DND-CAT) located at Sector 5 of the Advanced Photon Source (APS). DND-CAT is supported by Northwestern University, E.I. DuPont de Nemours & Co., and The Dow Chemical Company. This research used resources of the Advanced Photon Source, a U.S. Department of Energy (DOE) Office of Science User Facility operated for the DOE Office of Science by Argonne National Laboratory under Contract No. DE-AC02-06CH11357. Data was collected using an instrument funded by the National Science Foundation under Award Number 0960140. SANS experiments were conducted on NG-7 30 m and NG-B 30 m SANS instruments in National Institute of Standards and Technology (NIST) Center for Neutron Research (NCNR). We would like to specifically thank Dr. Yimin Mao and Dr. Paul Butler for their assistance in SANS measurements and data analysis. We also acknowledge the help of Dr. Dan Zhao for insightful discussions and Peter Schmidt for taking the MAXS measurements.

# Chapter 3 - Effect of Ionic Liquid Components on the Coil Dimensions of Poly(ethylene oxide)*

## 3.1 Introduction

One of the advantages of using ionic liquids (ILs) as solvents for polymers is that they offer a wide range of solvation properties. As discussed in Chapter 1, they are often labeled as "designer solvents" since slight modifications to the cation or the anion structure can significantly vary the physicochemical properties of ILs. Therefore, ILs can be exploited to provide varying solvation environments for polymers. As chain dimensions are dictated primarily by polymer-solvent interactions, the interactions can be readily tuned by altering the cation or anion of the ILs. For example, the mixing behavior of polymers in ILs varies significantly with the ion identity in many cases.[15,16] The LCST of PEO in [BMIM][$BF_4$] with a butyl chain at the imidazolium cation is 45 °C higher than its ethyl counterpart, [EMIM][$BF_4$].[65,66] An even more pronounced effect is observed when the anion [$BF_4$]$^-$ is replaced by bis(trifluoromethylsulfonyl)imide ([TFSI]) or hexafluorophosphate ([$PF_6$]$^-$), as no phase separation has been observed in the experimental temperature window (up to 200 °C) for PEO in these ILs.[65,66] It is now well

---

*Reprinted with permission from Kharel, A.; Lodge, T. P. Effect of Ionic Liquid Components on the Coil Dimensions of PEO. *Macromolecules* **2019**, *52*, 3123–3130. Copyright 2019 American Chemical Society established that polymer miscibility in an IL is affected by ion identity, but the dependence of polymer coil dimensions and excluded volume exponent on IL is yet to be investigated.

The previous chapter discussed the evaluation of coil dimensions of perdeuterated poly(ethylene oxide) in [BMIM][BF$_4$] at 80 °C by evaluating the molecular weight dependence of $R_{\mathrm{g},0}$. It is well established that a flexible chain in solution changes its conformation with temperature as the increase or decrease of coil size is governed by solution thermodynamics.[111,160,161] As noted in Chapter 1, a polymer and a solvent system can either phase separate upon heating or cooling, exhibiting UCST or LCST behavior, respectively. Depending on whether a system is LCST or UCST, the increase in temperature can enhance or worsen the solvent quality, affecting the radius of gyration. Therefore, the solvent quality can be altered by changing the temperature, which in turn affects the dimensions of polymer chains. In the case of polymers and ILs, the temperature dependence of $R_{\mathrm{g},0}$ has not been experimentally established.

Another route to alter the solvation of polymers in solutions is by adding salt. In the particular case of PEO and ILs, adding lithium-based salts to PEO/IL mixtures is of great interest in the area of solid polymer electrolytes.[33,162] For example, ternary blends of PEO/IL/LiTFSI have been shown to increase both conductivity and stability of the electrolytes compared to binary blends of PEO and $\mathrm{Li}^+$ salt.[39] Although previous studies, have investigated the physical properties of these ternary blends, [33,39,126,162] the underlying PEO coil dimensions remain unexplored. Some prior works assessed the coil dimensions of PEO in the melt with added $\mathrm{Li}^+$ salts, and found a modest reduction of coil size in the presence of $\mathrm{Li}^+$ salts.[163,164] On the other hand, our work has shown that PEO coil expands moderately in IL compared to its melt state.[165] Therefore, the evaluation of PEO coil dimensions in the presence of both $Li^+$ salt and IL is also of interest.

This work explores the coil dimensions of PEO in imidazolium-based ILs by (1) evaluating $\nu$ in ILs comprising different cations and anions, (2) establishing the temperature dependence of $R_{g,0}$ in one IL, and (3) assessing any changes in $R_{g,0}$ in presence of LiTFSI. As PEO is nearly isorefractive with [EMIM][$BF_4$], [HMIM][$BF_4$], [BMIM][TFSI], and [BMIM][$PF_6$], it is very difficult to measure coil dimensions using light scattering. Therefore, we utilize SANS instead, using *d*-PEO for enhanced contrast. For all the ILs studied at 80 °C, $0.58 \leq \nu \leq 0.60$, indicating good solvent behavior compared to *d*-PEO in [BMIM][$BF_4$] investigated in the previous chapter ($\nu = 0.55$). In general, greater expansion of *d*-PEO coils is observed in ILs with cations with longer alkyl chains and with less basic anions; interestingly, variation of the anion has a stronger effect. We also demonstrate that $R_{g,0}$ of *d*-PEO has a moderate dependence on temperature, and no significant variation of $R_{g,0}$ was observed in ternary mixtures containing up to 10 wt% LiTFSI.

## 3.2 Experimental

### *Materials and Methods*

Four perdeuterated PEO homopolymers were synthesized by anionic polymerization, and an additional *d*-PEO (54 kg/mol) was purchased from Polymer Source. Detailed information on the *d*-PEO synthesis and characterization, and estimation of the overlap concentration ($c^*$) and $R_{g,0}$ under $\theta$ conditions, can be found in Chapter 2. The ILs [EMIM][$BF_4$], [BMIM][TFSI], [BMIM][$PF_6$], and [HMIM][$BF_4$] were purchased from

Iolitec and dried under dynamic vacuum (<100 mTorr) for 48 h at 60 °C. LiTFSI was purchased from 3M, vacuum dried at 100 °C for 96 h, and stored in an argon-filled glovebox.

All dilute *d*-PEO/IL solutions were prepared using a co-solvent evaporation method, as described in Chapter 2. In order to study the effect of added lithium salt, stock solutions of LiTFSI/[BMIM][TFSI] were prepared by adding desired amounts of LiTFSI to [BMIM][TFSI] under inert atmosphere in glovebox. A small volume of DCM was added to the solutions, which were stirred until complete dissolution was obtained. The stock solutions were then dried under dynamic vacuum (< 100 mTorr) at 75 °C for 40 h and stored in a glovebox. The salt concentration in [BMIM][TFSI] was varied up to 10 wt%. The polymer volume fraction was kept almost constant for all salt concentrations, as summarized in Table 3.1.

**Table 3.1:** Volume Fractions of *d*-PEO-30 in LiTFSI/[BMIM][TFSI] Solutions

| | **Volume fraction of *d*-PEO-30 ($\varphi$)** | | | |
|---|---|---|---|---|
| **LiTFSI (wt%)** | **0.7 wt%** | **1.3 wt%** | **1.9 wt%** | **2.5 wt%** |
| 0 | 0.009 | 0.016 | 0.023 | 0.030 |
| 1 | 0.008 | 0.016 | 0.023 | 0.030 |
| 5 | 0.009 | 0.016 | 0.023 | 0.031 |
| 10 | 0.009 | 0.016 | 0.024 | 0.031 |

Estimated using density of LiTFSI ($\rho_{\mathrm{LiTFSI}}$) = 2.023 g/mL[166]

*Small-angle Neutron Scattering*

SANS experiments were performed in part on the CG-2 instrument at the High Flux Isotope Reactor (HFIR) facility of the Oak Ridge National Laboratory (ORNL). Three sample-to-detector distances (SDD) of 19.2, 8.8, and 1.8 m, with a mean wavelength of 4.75 Å and a wavelength spread ($\Delta\lambda/\lambda$) of 0.13 were used to access a $q$ range of approximately 0.003 – 0.464 Å$^{-1.}$ SANS measurements were also performed on the NG-B 30 m instrument at the National Institute of Standards and Technology (NIST) Center for Neutron Research. [143] Two sample-to-detector distances (SDD) of 6 and 1 m, with a mean neutron wavelength of 6 Å and $\Delta\lambda/\lambda = 0.125$ were used; the $q$-range of this configuration is approximately 0.006 – 0.445 Å$^{-1}$. The samples were contained in 1 mm thick banjo or demountable cells, and placed in heating blocks pre-equilibrated at the desired temperature. Due to the crystalline nature of PEO and previous indications of crystallization of PEO in [BMIM][BF$_4$], the measurements were carried out at temperatures ($T$) ≥ 80 °C. For $d$-PEO/[EMIM][BF$_4$] and $d$-PEO/(LiTFSI/[BMIM][TFSI]), the samples were kept under N$_2$ atmosphere throughout the measurements to minimize moisture absorption by the hygroscopic LiTFSI, and to avoid degradation of $d$-PEO at even higher temperatures.

The measured isotropic two-dimensional scattering patterns were azimuthally integrated to produce one-dimensional $I(q)$ versus $q$ plots, using Igor SANS reduction software provided by NIST. [144] The reduction protocol corrected for sample transmission, detector efficiency, scattering from the empty cell and calibration to absolute intensity.

### *Mid-angle X-ray scattering (MAXS) measurements*

MAXS data were collected at the DND-CAT 5-ID-D beamline at the Advanced Photon Source, Argonne National laboratory. A wavelength $\lambda = 0.73$ Å and SDD of 1 m was used to obtain a $q$ range of approximately 0.13 – 0.86 Å$^{-1}$. The samples were contained in 1.5 mm diameter quartz capillaries, and the experiments were conducted at room temperature. The measured isotropic two-dimensional scattering patterns were converted to one-dimensional plots of $I\ (q)$ (in arbitrary units) vs. $q$.

*Scattering from neat ionic liquids*

In Chapter 2, we discussed the existence of structural heterogeneity in the neat IL, [BMIM][BF$_4$]. In this study, we use neat imidazolium-based ILs with moderate length alkyl chains that also exhibit some local ordering as evidenced from the SANS scattering profiles, which exhibit a slight upturn at $q \geq 0.1$ Å$^{-1}$ , as shown in Figure 3.1a for a representative IL. The scattering profiles of neat ILs were also probed at higher $q$ using MAXS, which further confirmed the existence of mesoscopic structure, as shown in Figure 3.1b. Therefore, the solvent scattering was first fit to the quadratic form $C + Dq^2$, where $C$ and $D$ are fitting constants, and weighted by the solvent volume fraction to subtract from each solution scattering curve.

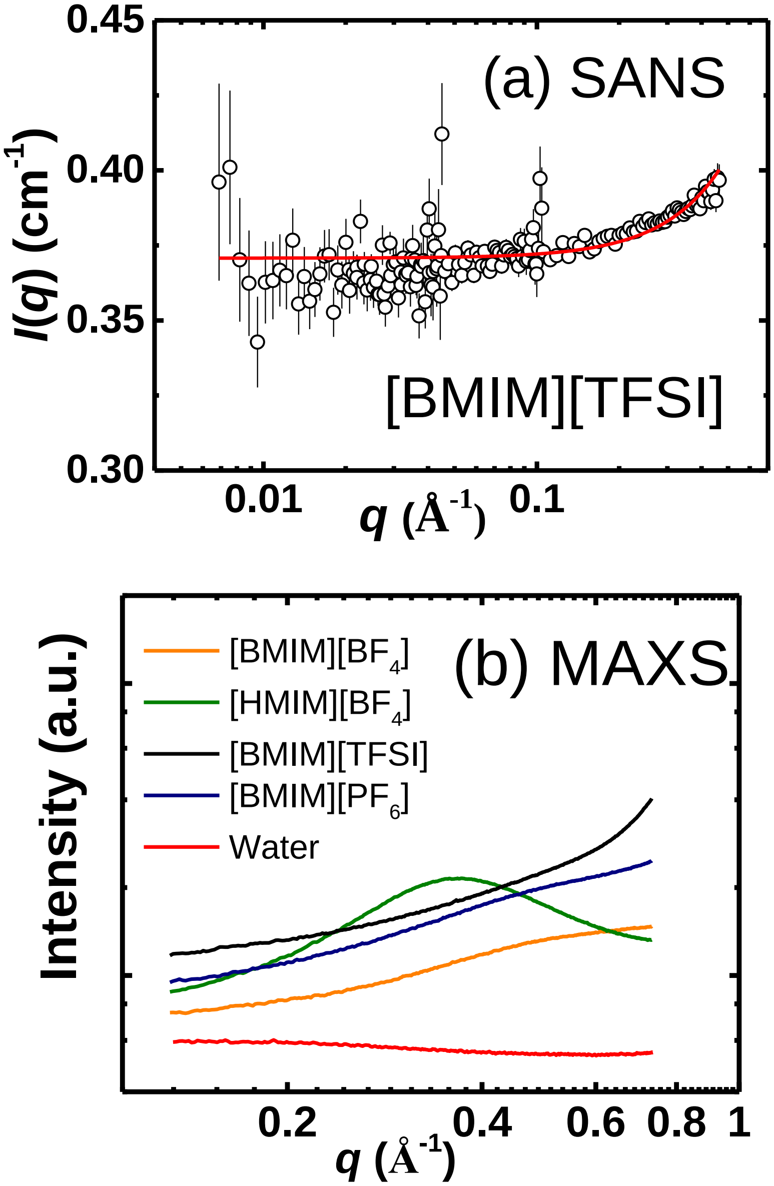

**Figure 3.1:** Solvent scattering profiles of ILs (a) SANS scattering profile (shown in symbols) of a representative IL, [BMIM][TFSI], fit to a quadratic equation (solid curve) to account for the upturn at higher $q$. (b) MAXS scattering patterns from different solvents. All imidazolium-based ILs show an upturn at higher $q$ compared to flat scattering from water. For IL cation with hexyl side chain, [HMIM][BF$_4$], a distinct maximum is observed, indicative of pronounced spatial correlation for longer alkyl tails.

### 3.3 Results and Discussion

The data were analyzed using similar procedures to those described in Chapter 2. The inevitable uncertainty in PEO/IL systems limits the use of Guinier plots as previously discussed in Chapter 2. Therefore, we used Debye function (Chapter 2, eqn 2.11) that enables us to exploit data over the full $q$-range. The successful fit of this function to the background-subtracted scattering profiles can be seen in Figure 3.2 for one representative system (*d*-PEO-30 in [BMIM][TFSI]), and in Appendix A for all other systems. The values of the residual baseline, $B$, mostly ranged between 0 to 10% of the intensity scaling factor, $A$. For each sample and solvent pair, the apparent $R_g$ was extracted for four different concentrations in the dilute regime. The apparent $R_g$ values were plotted against polymer concentration to obtain the infinite dilution radii, $R_{g,0}$, from the linear extrapolation, as shown in Figure 3.3. For each *d*-PEO and solvent pair, the resulting values of infinite dilution radii are summarized in Table 3.2. The Flory exponent is determined from the

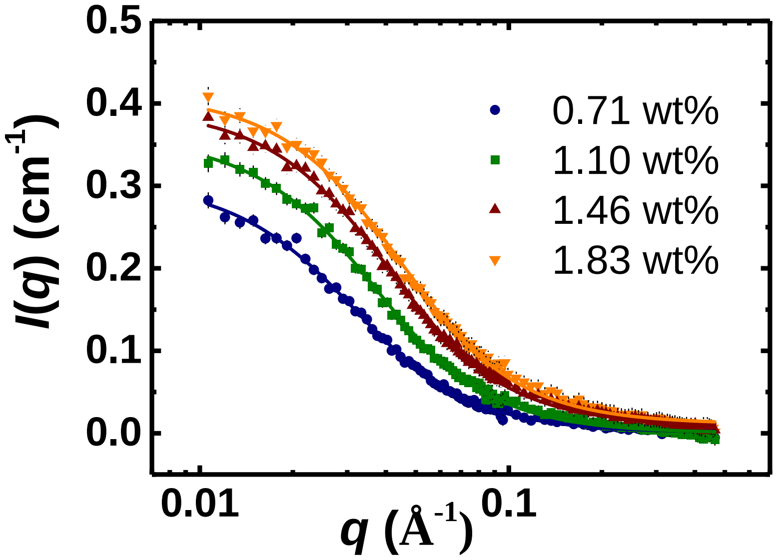

**Figure 3.2:** Representative background subtracted scattering curve for four different concentrations of *d*-PEO-30 in [BMIM][TFSI] at 80 °C. The solid lines denote the best-fit Debye function (Chapter 2, eqn 2.11).

slope of a logarithmic plot of log $R_{g,0}$ vs. log $M_w$ as shown in Figure 3.4. The dependence of $R_{g,0}$ on $M_w$ is represented as

$$R_{g,0} = a\, M_w^{\nu}\ (\text{Å}) \tag{3.1}$$

where $a$ is the pre-factor. The values of $\nu$ and pre-factors for *d*-PEO in ILs are listed in Table 3.3.

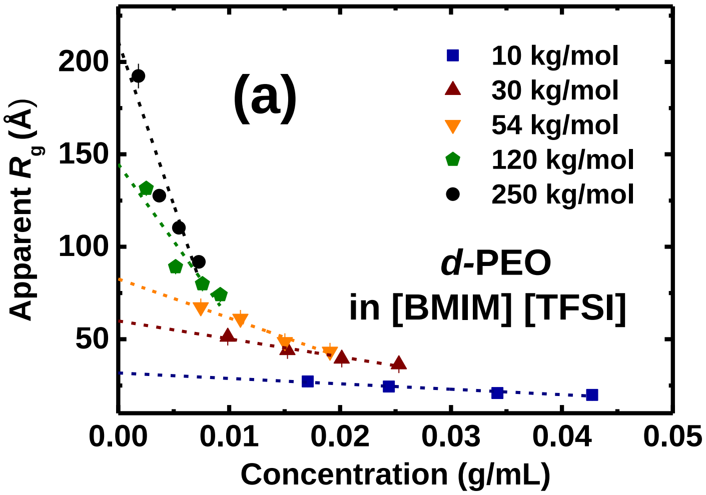

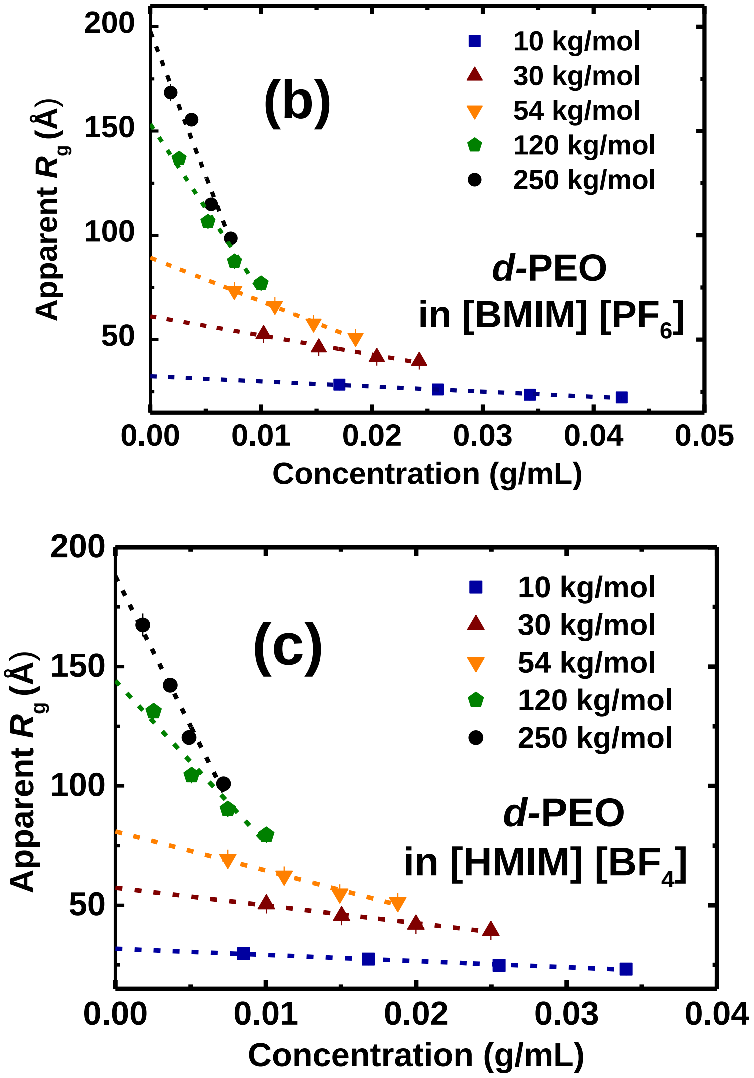

**Figure 3.3:** Extrapolation of apparent radii of gyration to infinite dilution for *d*-PEO in [BMIM][TFSI], [BMIM][PF$_6$], and [HMIM][BF$_4$] represented in parts a, b and c, respectively.

### 3.3.1 Interpretation of Flory exponent

The exponent reflects the quality of the solvent, with $\nu = 0.5$ for theta solvents and $\nu = 0.6$ for good solvents.[99,112] The values of $\nu$ for *d*-PEO in 3 different imidazolium-based ILs studied (as shown in Table 3.3 and Figure 3.5a) lie between 0.58 and 0.6, indicating that all these solvents are good at 80 °C. Moreover, compared to the previously studied system ($d$-PEO in [BMIM][BF$_4$], where $\nu = 0.55$), all the ILs in this work exhibit better solvent quality.

It is quite common to observe a broad crossover regime between unperturbed and swollen chain behavior for many polymers and solvent pairs, as anticipated in the original Flory-Krigbaum theory.[151,167] It is also tempting to draw a strong conclusion on solvent quality solely based on the exponent; however, it should be noted that these exponents should be viewed with caution. First, the values can be dependent on the range of molecular weights used, and the range used in this study might not reflect the infinitely long chain behavior. Second, minor changes in $R_g$ values can affect these exponents significantly, particularly considering the substantial errors in $R_g$ values for the longest chains. Third, the value of the pre-factor in eqn 3.1 should also be considered, as its value can differ slightly between two solvents with equivalent exponents. Therefore, in order to compare various ILs in terms of solvent quality, in addition to the $\nu$ values, attention should be given to the magnitude of individual infinite dilution radius. For example, the value of $\nu$ = 0.58 (Table 3.3) is identical for PEO in two different solvents, water and [HMIM][BF$_4$], but due to the pre-factor, PEO chains are significantly larger in water compared to [HMIM][BF$_4$]. The longest $d$-PEO used here has $R_{g,0} \approx 188$ Å in [HMIM][BF$_4$], but for the same chain length, $R_{g,0}$ is calculated to be 300 Å in water.

**Table 3.2:** $d$-PEO Coil Size in Imidazolium Based Ionic Liquids at 80 °C

| **$M_w$ (kg/mol) (±10%)** | **$R_{g,0}$ (Å) $\theta$ condition** | **$R_{g,0}$ (Å) Water[a]** | **$R_{g,0}$ (Å)** | | | |
|---|---|---|---|---|---|---|
| | | | [BMIM][BF$_4$] [b] | [HMIM][BF$_4$] | [BMIM][PF$_6$] | [BMIM][TFSI] |
| 10 | 36 | 48 | 34 ± 1 | 32 ± 0 | 32 ± 1 | 32 ± 1 |

| | | | | | | |
|---|---|---|---|---|---|---|
| 30 | 60 | 87 | 58 ± 3 | 57 ± 1 | 61 ± 2 | 60 ± 2 |
| 54 | 80 | 123 | 83 ± 2 | 81 ± 2 | 89 ± 1 | 84 ± 4 |
| 120 | 120 | 198 | 140 ± 5 | 144 ± 7 | 153 ± 8 | 145 ± 15 |
| 250 | 168 | 300 | 183 ± 6 | 188 ± 6 | 198 ± 11 | 211 ± 21 |

[a] Calculated from $R_{g,0} = 0.22\, M_w^{0.58}$ using Ref. 121, [b] Reported in Ref. [165]

As seen in Table 3.2, for shorter *d*-PEO chains in all ILs, infinite dilution radii are closer to the coil size in the melt, indicative of theta-like behavior. As the chain length increases, the radii are significantly larger in the ILs relative to theta-condition. We can see this trend clearly in graphical format; the radii of gyration plotted in Figure 3.4 show that up to *d*-PEO-54, the points lie close to the theta solvent line but for the two highest molecular weights, the radii lie between the lines corresponding to theta and good solvent. This type of behavior is not surprising as it is well-known that excluded volume interactions are more pronounced for long polymer chains, and for solvents with smaller molar volumes. [151] Much higher molecular weights would be required to observe substantial swelling. Unfortunately, large coil sizes can only be probed at much lower $q$ than accessible in SANS. For our systems that are intrinsically weak scatterers, the issue of low signal-to-noise ratio becomes more pronounced at lower $q$. Nevertheless, it is clear from Table 3.2 that longer *d*-PEO chains expand moderately in all the ILs studied. In particular, *d*-PEO-250 in [BMIM][$BF_4$], [HMIM][$BF_4$], [BMIM][$PF_6$], and [BMIM][TFSI] swells by 9, 12, 18, and 26 % compared to its theta state, respectively.

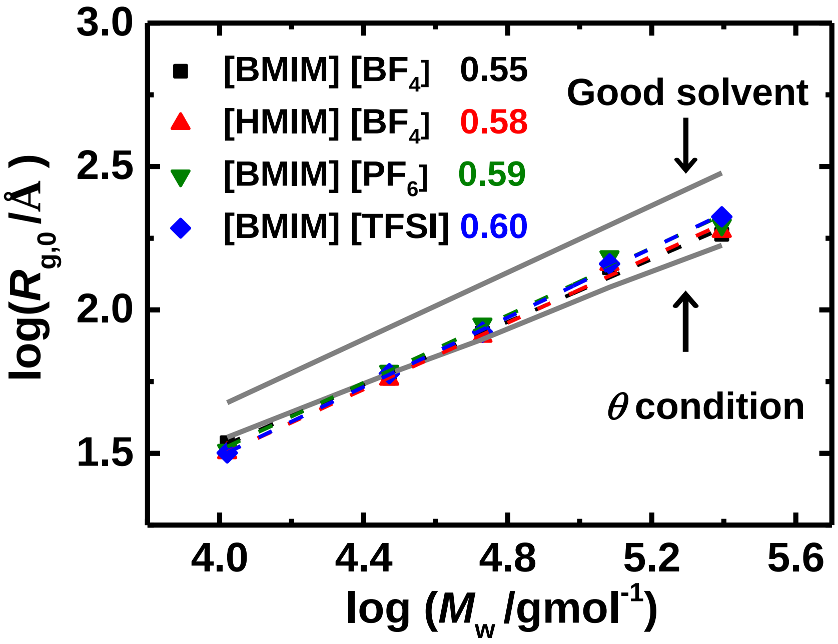

**Figure 3.4:** Double logarithmic plots of $R_{g,0}$ versus $M_w$ for *d*-PEO in 4 different imidazolium-based ILs varying in cation and anion identity at 80 °C. Data points are denoted in colored symbols and the linear fits are represented by dashed colored lines. The slopes of the fits give the values of $\nu$ for *d*-PEO in [BMIM][BF$_4$], [HMIM][BF$_4$], [BMIM][PF6], [BMIM][TFSI] as 0.55, 0.58, 0.59, and 0.60, respectively. The gray solid lines correspond to radii for *d*-PEO in a representative good solvent (water, upper line)[121] and under $\theta$ conditions (melt state values from Table 3.2, lower line). The values for *d*-PEO in [BMIM][BF$_4$] were reported in Ref. [165].

**Table 3.3:** Values of Flory Exponent and Pre-factor ($a$) for *d*-PEO in Various Solvents

| **Solvent** | $\nu$ | $a$ (Å) |
|---|---|---|
| Water[121] | 0.58 ± 0.03 | 0.22 |
| [BMIM][BF$_4$][165] | 0.55 ± 0.02 | 0.22 ± 0.05 |
| [HMIM][BF$_4$] | 0.58 ± 0.03 | 0.15 ± 0.04 |
| [BMIM][PF$_6$] | 0.59 ± 0.03 | 0.14 ± 0.05 |
| [BMIM][TFSI] | 0.60 ± 0.01 | 0.12 ± 0.01 |

As noted above, irrespective of the solvent quality, the volume of the solvent also affects the swelling behavior of a polymer coil. As pointed out by Flory and Krigbaum,[151] the extent of swelling is inversely related to the molar volume ($V_m$) of the solvent. Therefore, it can be expected that a given polymer chain will expand more in a smaller solvent as compared to solvent with larger molar volume. As seen in Table 3.4, the values of $V_m$ rank in the following order: Water < [BMIM][$BF_4$] < [BMIM][$PF_6$] < [HMIM][$BF_4$] < [BMIM][TFSI]. The $V_m$ of ILs are an order of magnitude larger than water, which can at least partly explain the significant coil expansion in water compared to all the ILs (Table 3.4). However, among the ILs, no clear trend can be observed between the degree of swelling of PEO and the $V_m$ of the IL, partly due to the smaller variation in $V_m$ across the ILs. Besides the differences in solvent volume, the details of how a solvent solvates the chain can also affect the conformational statistics (e.g., distribution of trans and gauche conformers), to some degree, independent of the solvent quality.

**Table 3.4:** Molar volume ($V_m$) of solvents, $\nu$, and % expansion of *d*-PEO

| **Solvent** | $V_m$ **(cm$^3$/mol)** | $\nu$ | **% expansion**[a] |
|---|---|---|---|
| [BMIM][$BF_4$] | 194 | 0.55 | 9 |
| [BMIM][$PF_6$] | 215 | 0.59 | 18 |
| [HMIM][$BF_4$] | 230 | 0.58 | 12 |
| [BMIM][TFSI] | 302 | 0.60 | 26 |
| Water | 18 | 0.58 | 79 |

---

[a] % expansion is calculated for *d*-PEO-250 using ($R_{g,0}$ –$R_{g,0,\theta}$ )/ $R_{g,0,\theta}$

### 3.3.2 Effect of cation chain length

From Table 3.3 and Figure 3.5a, $\nu$ increases from 0.55 to 0.58 as the alkyl chain length of the cation is changed from butyl ([BMIM]) to hexyl ([HMIM]). It is fair to conclude that the increase in alkyl chain length of the imidazolium cation leads to a better solvent. However, the infinite dilution radii for larger molecular weights of *d*-PEO (as listed in Table 3.2 and shown in Figure 3.5b) are not significantly different in [HMIM][$BF_4$] as compared to in [BMIM][$BF_4$]. Therefore [HMIM][$BF_4$] is only slightly a better solvent than [BMIM][$BF_4$], leading to modest expansion of the coil (seen in Figure 3.6). A SANS study by Chen et al. evaluated $R_{g,0}$ of a moderate molecular weight *d*-PEO (36 kg/mol) in alkylammonium bromide with glycerol in a 1:2 molar ratio.[168] In contrast to our results, they found that as the cation alkyl chain length increased in the ammonium cation from ethyl to butyl, $R_{g,0}$ of *d*-PEO decreases from 97 Å to 91 Å. The contraction was attributed to the decrease in average hydrogen bond density with bulkier alkyl tails. However, it must be emphasized that these conclusions are based on a single molecular weight of *d*-PEO with moderate chain length. The evaluation of $\nu$ and $R_{g,0}$ for longer *d*-PEO chains in alkylammonium bromide might be more revealing.

Our results are consistent with the phase behavior studies of PEO in [EMIM][$BF_4$] and [BMIM][$BF_4$] reported by Lee et al.[65,66] The LCST of PEO was higher in [BMIM][$BF_4$] than [EMIM][$BF_4$], emphasizing that better miscibility is obtained by increasing the alkyl chain of the cation. In addition to PEO, other polymers and ILs systems also exhibit a similar trend in LCST behavior, where the LCST increases when cations with longer alkyl tails are incorporated.[72,73,169]

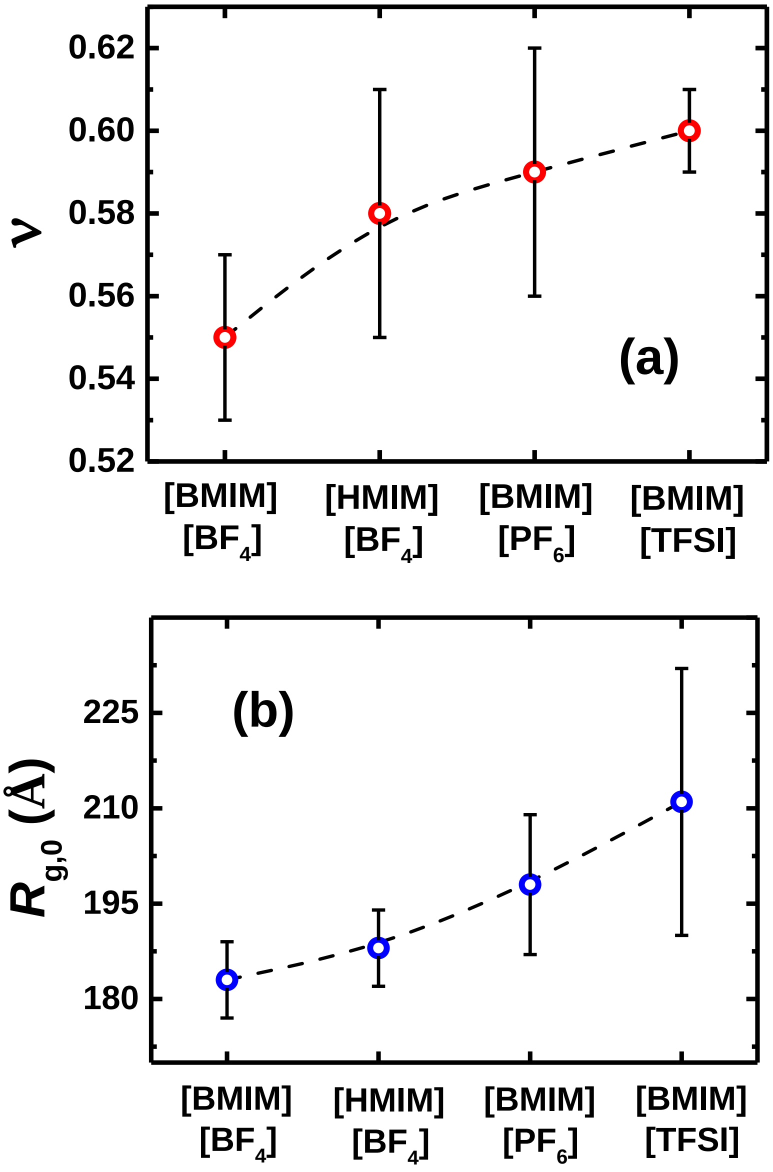

**Figure 3.5:** Variation of solvent quality and coil dimensions for *d*-PEO in imidazolium-based ILs (a) The value of $\nu$ subtly increases as the cation chain length is increased from butyl to hexyl in [BMIM][$BF_4$] and [HMIM][$BF_4$], respectively. As the anion structure is changed from [$BF_4$]$^-$ to [$PF_6$]$^-$ and [TFSI] with a fixed cation ([BMIM]), a slight increase in the value of $\nu$ can be observed. (b) The infinite dilution coil size of longest *d*-PEO chain (250 kg/mol) in the ILs studied also displays a similar trend as the order in which the coil size increase is consistent with increasing $\nu$ values. The dashed lines are intended as guides for the eye.

### 3.3.3 Effect of anion identity

In contrast to the slight expansion of *d*-PEO coil in ILs with longer cation alkyl chains, a more significant change in coil size occurs when the anion is altered (shown in Figure 3.6). As seen in Table 3.3 and Figure 3.5a, the scaling exponents for [BMIM][$BF_4$], [BMIM][$PF_6$], and [BMIM][TFSI] are 0.55, 0.59, and 0.60, respectively. By merely changing the anion, ILs vary from moderately good to very good solvent for *d*-PEO. The increase of $\nu$ is further confirmed by the substantial increase in the infinite dilution radii of the longer *d*-PEO chains. For example, $R_{g,0}$ increases from 182 Å for *d*-PEO-250 in [BMIM][$BF_4$] to 198 Å and 211 Å in [BMIM][$PF_6$] and [BMIM][TFSI], respectively. It might be desirable to compare the phase separation temperatures of PEO in the aforementioned ILs to confirm the trend in the solvation behavior of these solvents. However, to the best of our knowledge, the phase separation of PEO in imidazolium-based ILs with [TFSI] and [$PF_6$]$^-$ anions have not been reported to date; any LCST is assumed to be above the experimental window. Regardless, a clear conclusion is inferable, i.e., PEO remains miscible in [TFSI] and [$PF_6$]$^-$-based ILs, whereas phase separation occurs if the $[BF_4]^-$ anion is used. Therefore, [TFSI] and $[PF_6]^-$-based ILs are better solvents than $[BF_4]^-$ based ILs, consistent with our experimental results.

It has been proposed that the interaction between PEO and the IL is influenced by the hydrogen bonding between the acidic proton of the cation ([BMIM]) and the ether oxygen of PEO. [65,66,170] Now, the question arises; why does the anion have a larger effect on solvation than the cation? The phase behavior of a PEO derivative, poly(ethyl glycidyl ether) (PEGE), was evaluated in a series of ILs with varying combinations of cations and anions.[169] It was shown that the solubility of PEGE depends more strongly on the structure and basicity of the anions, with improved miscibility obtained for weakly basic anions. In our case, the imidazolium cation ([BMIM]) is the hydrogen bond donor, while PEO and the anions ($[PF_6]^-$, $[BF_4]^-$, [TFSI]) are all hydrogen bond acceptors. In PEO/IL mixtures, PEO and the anions compete for hydrogen bonding with the cation.[169] Strongly basic anions tend to associate tightly with the cation, hence disrupting the hydrogen bonding between PEO and the cation. The strength of the hydrogen bonding interaction between cations and anions can be correlated with established Kamlet-Taft parameters that quantify hydrogen bond basicity ($\beta$).[171] It has been reported that $[BF_4]^-$ has a larger hydrogen bond accepting capacity ($\beta = 0.38$) than the other anions [TFSI] ($\beta = 0.24$) and $[PF_6]^-$ ($\beta = 0.21$).[17] Another relevant computational study using *ab initio* molecular orbital calculations also supports this explanation. The magnitude of intermolecular interaction energies of $[BF_4]^-$with imidazolium cation was shown to be the highest, while that of [TFSI] and $[PF_6]^-$ with the same cation are much smaller.[172] The conclusion is that $[BF_4]^-$-based ILs have stronger complexation of the cation and anion as compared to

[TFSI] and $[PF_6]^-$, resulting in the decrease in PEO coil size. As a result, [BMIM][TFSI] and $[BMIM][PF_6]$ are both better solvents than $[BMIM][BF_4]$.

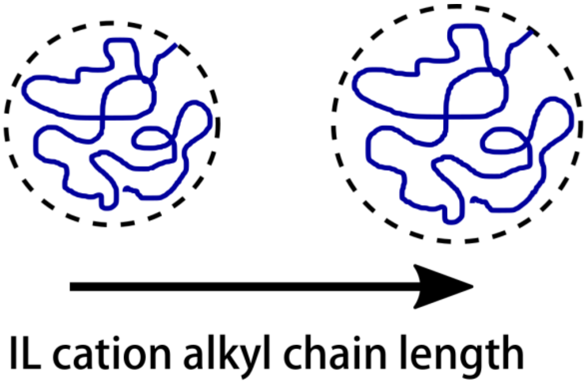

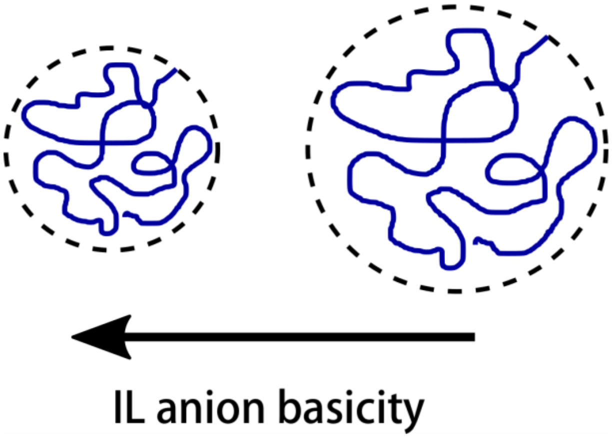

**Figure 3.6:** Cartoon illustrating the change in *d*-PEO coil size with changing ion identity of the IL solvent. As the cation chain length is increased from butyl ([BMIM]) to hexyl ([HMIM]), *d*-PEO is slightly swollen. The anion basicity has a more pronounced effect on coil size with coil size decreasing upon increasing anion basicity in the order [TFSI] ~[$PF_6$] < [$BF_4$]. The coils are not drawn to scale.

### 3.3.4 Effect of temperature

The dependence of apparent $R_g$ on polymer concentration for *d*-PEO-54 in [EMIM][$BF_4$] at four different temperatures is shown in Figure 3.7a. The slope of apparent $R_g$ vs. $c$ decreases upon increasing the temperature, due to the decrease in the second virial coefficient, as anticipated for an LCST system.  The extrapolated infinite dilution radii at 80 °C, 120 °C, 129 °C, and 135 °C are 91 ± 1 Å, 86 ± 1 Å, 82 ± 1 Å, 83 ± 2Å, respectively (Figure 3.7b). As the temperature is increased from 80 °C to 135 °C, a distinct decrease in $R_{g,0}$ is seen as the coil shrinks by 9% for $N \approx 1100$. This size reduction with increasing temperature is expected in an LCST system. In the future, it will be interesting to evaluate the dependence of $\nu$ on temperature that reveal two interesting phenomena that haven't been explored in polymer/IL systems; the coil-to-globule transition[160,173] and the evaluation of $\nu$ at the theta temperature.[122]

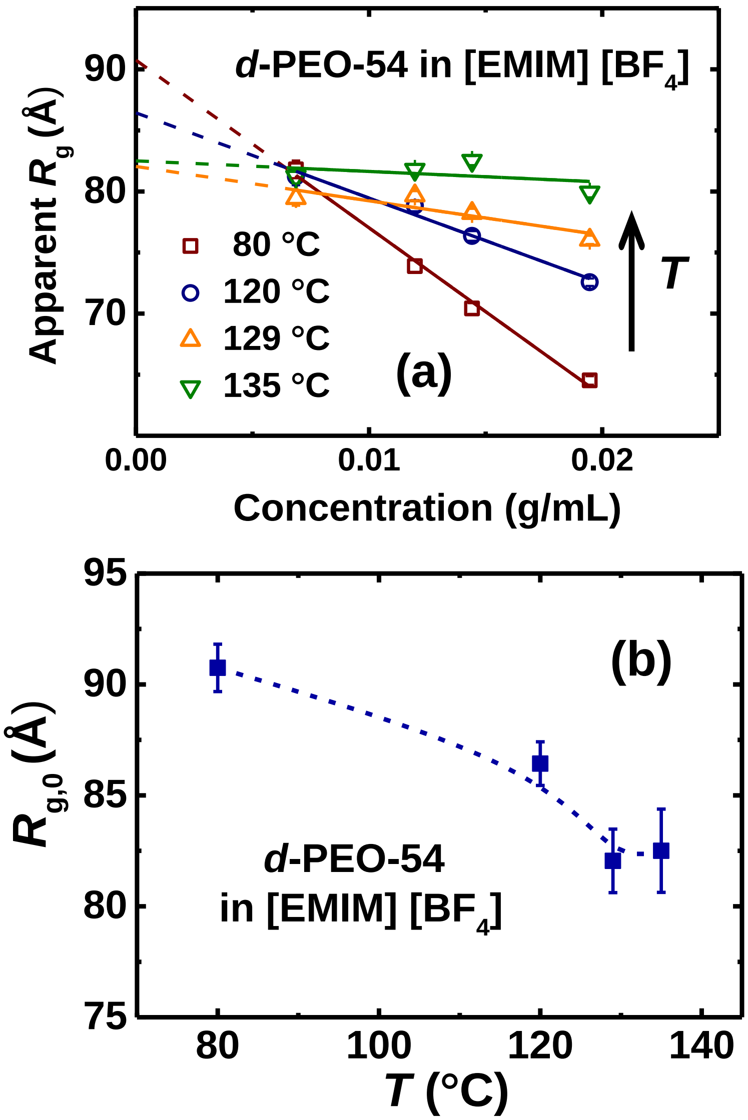

**Figure 3.7:** Temperature dependence of coil dimensions of *d*-PEO-54 in [EMIM][BF$_4$] (a) $R_g$ vs. $c$ plots at various temperatures. The values of infinite dilution radii are determined from the y-intercepts of the linear fits (solid lines). (b) Infinite dilution radii as a function of temperature. The dashed line is intended as a guide for the eye.

### 3.3.5 Effect of LiTFSI

Figure 3.8a shows the $R_g$ ($c$) vs. $c$ plot for *d*-PEO-30 in mixtures of LiTFSI and [BMIM][TFSI]. The apparent $R_g$ values remain fairly constant as the salt concentration increases from 0 to 10 wt%; any variation is within 10%, and close to the experimental uncertainty. A similar trend can be seen in Figure 3.8b, where $R_{g,0}$ within the error (Table 3.5) varies insignificantly with salt concentration. This result is possibly surprising, as PEO in the melt state has been shown to shrink in size by 10–15% with relatively modest concentrations of added LiI ($[Li^+]:[EO] = 0.07$).[164] The authors speculated that the EO units in PEO wrap around the $Li^+$ cations, resulting in a slight contraction of the chain. Although it is not yet clear on why *d*-PEO coil size in [BMIM][TFSI] has a more modest effect upon adding LiTFSI, the explanation presumably reflects a modest difference in interactions between PEO and the $Li^+$ and BMIM cations.

**Table 3.5:** Infinite Dilution $R_{g,0}$ Dependence on LiTFSI Concentration

*d*-PEO-30 in LiTFSI/[BMIM][TFSI]

| **LiTFSI (wt%)** | **$[Li^+]/[EO]$[a]** | **$R_{g,0}$ (Å)** |
|---|---|---|
| 0 | 0 | $60 \pm 3$ |
| 1 | 0.24 | $56 \pm 2$ |
| 5 | 1.08 | $57 \pm 2$ |
| 10 | 2.17 | $65 \pm 6$ |

[a] Calculated for the lowest concentration of *d*-PEO-30

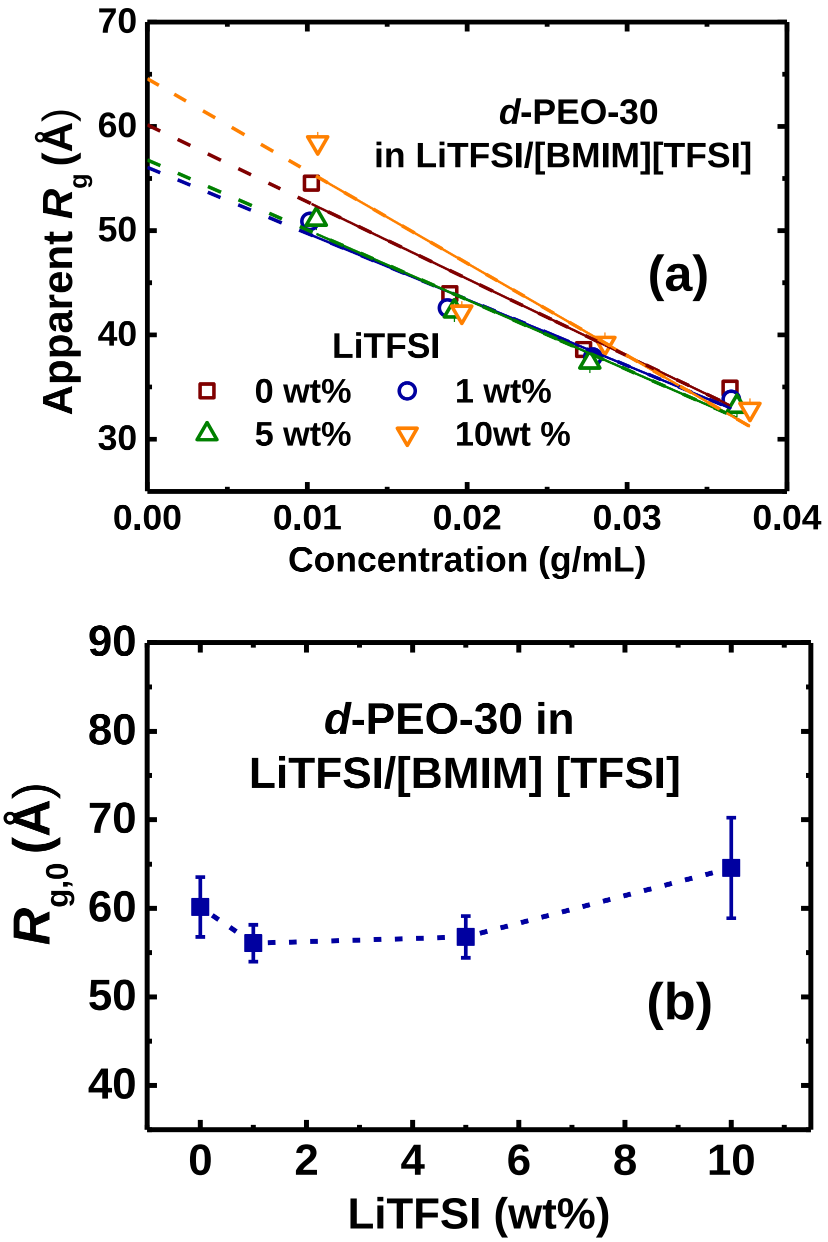

**Figure 3.8:** Coil dimensions *d*-PEO-30 in LiTFSI/[BMIM][TFSI] (a) Apparent $R_g$ vs. $c$ (b) $R_{g,0}$ as a function of [LiTFSI]. The dashed line is intended as a guide for the eye.

### 3.4 Summary

The solvation of PEO in ILs is an interesting topic from both fundamental and technological perspectives. We previously used SANS to determine the Flory exponent for *d*-PEO in [BMIM][$BF_4$] ($\nu$ = 0.55), establishing that this IL is a moderately good solvent for PEO. Here, we expand on our previous work to examine the change in coil dimensions upon varying the cation and anion structure of the ILs, and also probing the influences of temperature and added salt. The principal conclusions are as follows:

1. The Flory exponent for *d*-PEO in all three ILs [BMIM][TFSI], [BMIM][$PF_6$], and [HMIM][$BF_4$] lies between 0.58 to 0.60, indicating that these ILs are all better solvents for *d*-PEO than [BMIM][$BF_4$] ($\nu$ = 0.55).

2. Increasing the cation alkyl chain length from butyl ([BMIM]) to hexyl ([HMIM]) slightly enhances the solvent quality, as evidenced by the increase in $\nu$ from 0.55 to 0.58. However, the absolute coil size in these two ILs is similar for the longest *d*-PEO coil. The influence of IL cation chain length on *d*-PEO coil dimensions is therefore relatively weak, and [HMIM][$BF_4$] is only slightly better than [BMIM][$BF_4$].

3. On the other hand, the values of $\nu$ were found to be 0.59 and 0.60 for *d*-PEO in [BMIM][$PF_6$] and [BMIM][TFSI], respectively. The infinite dilution radii for the longest *d*-PEO chains also expanded significantly in both [BMIM][$PF_6$] and [BMIM][TFSI] compared to [BMIM][$BF_4$]. We can thus conclude that [BMIM][$PF_6$] and [BMIM][TFSI] are significantly better solvents than [BMIM][$BF_4$]. Moreover, the anion identity of the IL exerts a more pronounced effect on the coil dimensions of *d*-PEO than the cation, in agreement with previous studies of phase behavior.

4. The infinite dilution coil size of a moderate molecular weight *d*-PEO-54 in [EMIM][$BF_4$] decreased moderately with increasing temperature from 80 °C to 135 ºC.

4. The addition of LiTFSI salt in concentrations from 1 to 10 wt% in *d*-PEO-30/[BMIM][TFSI] solutions exerted a negligible effect on the infinite dilution radii, within the uncertainty.

## Acknowledgements

This work was supported by the National Science Foundation (DMR-1707578). Portions of this work were performed at the DuPont-Northwestern-Dow Collaborative Access Team (DND-CAT) located at Sector 5 of the Advanced Photon Source (APS). DND-CAT is supported by Northwestern University, E.I. DuPont de Nemours & Co., and The Dow Chemical Company. This research used resources of the Advanced Photon Source, a U.S. Department of Energy (DOE) Office of Science User Facility operated for the DOE Office of Science by Argonne National Laboratory under Contract No. DE-AC02-06CH11357. Data was collected using an instrument funded by the National Science Foundation under Award Number 0960140. SANS experiments were conducted on the NG-B 30 m SANS instrument at the National Institute of Standards and Technology (NIST) Center for Neutron Research (NCNR), U.S. Department of Commerce and the High Flux Isotope Reactor in Oak Ridge National Laboratory, which is sponsored by the Scientific User Facilities Division, Office of Basic Energy Sciences, U.S. Department of Energy. We would like to specifically thank Dr. Yimin Mao (NIST), Dr. Paul Butler (NIST), and Dr. Lilin He (ORNL) for their assistance in SANS measurements and data analysis. We also acknowledge Shuyi Xie for helping during the measurements, Julia Early for taking the MAXS measurements, and Dr. Svetlana Morozova for helpful discussions.

# Chapter 4 - Dilute Solution Properties of Poly(benzyl methacrylate) in Ionic Liquids*

## 4.1 Introduction

The previous chapters have focused on the solvation behavior of poly(ethylene oxide), in particular, the assessment of PEO coil dimensions in ILs. In this system, the IL of interest is isorefractive with PEO, limiting the use of light scattering. Fortunately, the remarkable contrast between $^{1}$H and $^{2}$H for neutrons allowed the measurement of $R_\mathrm{g}$. However, SANS is relatively inaccessible, with only few sites around the world, limiting the number of systems we can study in a given amount of time. Moreover, our system characteristically suffers from low signal-to-noise ratio, requiring unusually long collection times to obtain the information of interest. In order to study several relevant structural, dynamic, and thermodynamic parameters as a function of concentration and temperature, it is desirable to employ a more accessible technique, such as light scattering.

For a system to be viable in light scattering, the polymer and the solvent should provide considerable contrast determined by the refractive index increment. One such polymer is poly(benzyl methacrylate) (PBzMA) in imidazolium, pyrrolidinium, and glyme-based ILs. In the recent years, Watanabe and coworkers have studied the phase behavior and microscopic solvation structure of PBzMA in various ILs.[69,73,76,88,174] Of particular interest is the lower-critical solution temperature (LCST) phase behavior of

---

*In collaboration with Cecilia Hall

PBzMA in ILs that originates primarily from the negative entropy of mixing ( $\Delta S_{mix} < 0$).

It has been speculated that the cation–$\pi$ interactions between the imidazolium cations and the aromatic rings in the PBzMA side chain result in a structurally ordered solvation shell and, hence lower the entropy of mixing. Watanabe and coworkers have reported the phase transition (cloud point) temperatures ($T_{cp}$) of a fixed concentration of dilute PBzMA solution in a number of ILs.[73] Interestingly, the values of $T_{cp}$ were found to be tunable with the IL cation and anion identity, an observation similar to the polymers and ILs systems discussed in previous chapters.[15,16,65,66,72,169] The $T_{cp}$ increased with increasing cation chain length for imidazolium cations ($C_n$mim, where n = 1 to 8) spanning a temperature window of almost 200 °C. On the other hand, the change in cation structure from imidazolium to pyrrolidinium also increased the $T_{cp}$, despite the absence of an aromatic ring in the pyrrolidinium cation. The miscibility was reported to be remarkably sensitive to the anions, as PBzMA only dissolved in TFSI-based and a few $PF_6$-based ILs. This interesting LCST-type phase behavior motivates the study of temperature dependent static and dynamic properties of PBzMA in ILs.

The investigation of fundamental properties of PBzMA in ILs is also advantageous from the application standpoint. In the past decade, many advances have been made in utilizing PBzMA and ILs composites in thermosensitive applications.[63,77,80,86,175] One such example is a thermoreversible ion gel that can be obtained by the self-assembly of an ABA triblock, with solvaphilic block A and solvaphobic block B.[77] PBzMA is generally used as the A block, resulting in an ion gel that forms on heating as the polymer becomes incompatible with the IL at higher temperature due to its LCST behavior.

In the past years, light and neutron scattering have been used to characterize the solvation behavior of a handful number of polymers, poly(N-isopropyl acrylamide), poly(2-phenylethyl methacrylate), and poly(n-butyl methacrylate), in ILs.[72,76,87,174] For PBzMA in IL, however, we are aware of only one work that has evaluated the apparent $R_g$ and hydrodynamic radius ($R_h$) change with temperature near the phase separation temperature.[88] This study reveals that two populations (free polymer chains and aggregates) appear near $T_{cp}$. The effective interaction parameter ($\chi_{eff}$) was also assessed for a fixed concentration of PBzMA using SANS model fits. The authors report $\chi_{eff} < 0.5$, indicating that [EMIM][TFSI] is a good solvent for PBzMA. However, the diffusion coefficients, second-virial coefficients, and hydrodynamic radii, and their dependence on concentration, polymer molecular weight, and temperature are yet to be investigated. Therefore, there is a renewed interest in fully exploring the solution properties of PBzMA in ILs that reveal a detail picture of solvation behavior.

This chapter will discuss the assessment of thermodynamic, dynamic, and structural properties of a range of molecular weights of PBzMA (20–160 kg/mol) in three different imidazolium-based ILs and one pyrrolidinium-based IL. On the thermodynamic side, the phase transition (cloud point) temperature ($T_{cp}$) is evaluated by turbidimetry experiments to determine the concentration dependence of $T_{cp}$. Furthermore, $T_{cp}$ is measured as a function of cation chain length and cation identity. Static light scattering (SLS) is employed to evaluate the second-virial coefficients ($A_2$) for PBzMA in all the ILs, hence establishing the molecular weight dependence of $A_2$ for these systems. For the longest PBzMA chain, the temperature dependence of $A_2$ is additionally examined over the range of 27 °C – 155 °C. Dynamic light scattering (DLS) is used to measure the diffusion coefficients and hydrodynamic radii as a function of concentration and temperature (27 °C – 155 °C) to evaluate the infinite dilution translation diffusion coefficient ($D_0$) and the infinite dilution hydrodynamic radii ($R_{h,0}$). Flory exponents ($\nu$) are determined from the molecular weight dependence of both of these experimental quantities ($R_{h,0}$ and $D_0$). Additional relevant parameters such as the diffusion virial coefficient ($k_d$) and frictional coefficient ($k_f$) are determined from the concentration dependence of the mutual diffusion coefficient, $D_{m,}$ at several temperatures. Overall, the key parameters of interest ($T_{cp}$, $A_2$, $D_0$, $R_{h,0}$, $\nu$, $k_d$, $k_f$) that describe the behavior of dilute solutions of PBzMA in all ILs are summarized and discussed.

## 4.2 Experimental

### 4.2.1 Materials

Various molecular weights of poly(benzyl methacrylate) (PBzMA) were kindly provided by Dr. Cecilia Hall (previous graduate student in the Lodge group, University of Minnesota) who prepared the polymers by atom-transfer radical polymerization and characterized them using $^1$H NMR spectroscopy. The weight-average molecular weights ($M_w$) and dispersities ($Đ$) of the synthesized polymers (listed in Table 4.1) were also determined by size-exclusion chromatography (SEC) performed in THF at 25 °C on an Agilent 1260 Infinity system. The eluents were monitored by a Wyatt Optilab T-rEX refractive index detector (shown in Figure 4.1), and the corresponding molecular weights and distributions were determined using Zimm plots obtained from a Wyatt Dawn Heleos II multiangle laser light scattering (MALS) detector, using a d$n$/d$c$ of 0.144 mL/g in THF.[176] The polymers are denoted as PBzMA-x, where x denotes the weight average molecular weight of PBzMA, represented as PBzMA-20, PBzMA-40, PBzMA-70, and PBzMA-160 for 21, 41, 70, 156 kg/mol, respectively.

**Table 4.1:** Characteristics of PBzMA

| $M_{\mathrm{w}}$ (kg/mol) (±10%)[a] | $Đ$[a] | $N$[b] | $c^*$ (g/mL)[c] |
|---|---|---|---|
| 21 | 1.12 | 106 | 0.13 |
| 41 | 1.11 | 208 | 0.08 |
| 70 | 1.15 | 335 | 0.05 |
| 156 | 1.16 | 757 | 0.03 |

[a] Obtained from SEC (refractive index and light scattering detector) using THF as a mobile phase

[b] Calculated using $M_{\mathrm{n}}/M_{\mathrm{o}}$, where $M_{\mathrm{o}}$ is the mass of repeat unit taken as 178 g/mol

[c] Estimated using $R_{\mathrm{g}} = 0.011\ M_{\mathrm{w}}^{0.588}$ (nm) for PBzMA in methyl ethyl ketone[177]

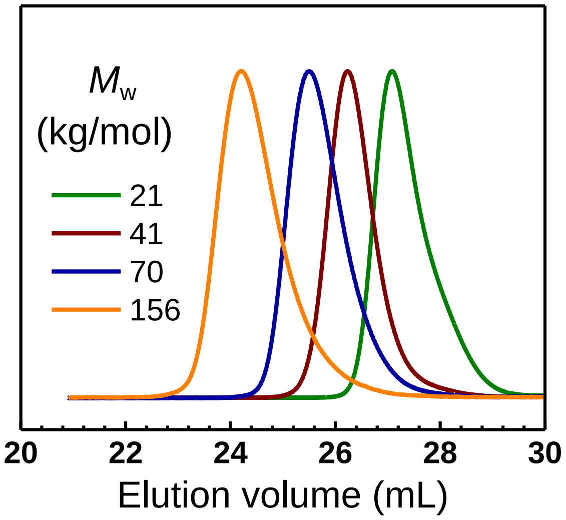

**Figure 4.1:** SEC traces of different molecular weights of PBzMA in THF.

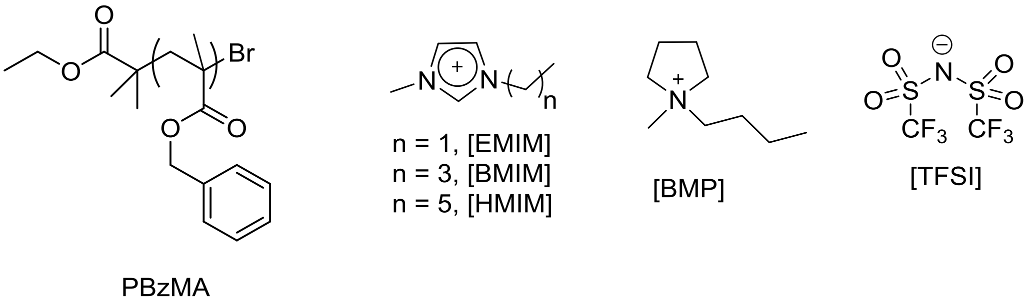

**Figure 4.2:** The structures of cations and anion of the ILs and PBzMA used in this study.

*Sample preparation*

The ILs [EMIM][TFSI], [BMIM][TFSI], [HMIM][TFSI], and [BMP][TFSI] were purchased from Iolitec and dried under dynamic vacuum (<100 mTorr) for 48 h at 60 °C. The overlap concentrations ($c$*) of PBzMA were estimated from eqn 2.6 in Chapter 2 using the relationship $R_g = 0.011\ M_w^{\ 0.588}$ (nm) for PBzMA in methyl ethyl ketone (good solvent).[177] The values of $c$* are listed in Table 4.1. In order to remain in the dilute limit, all solutions were prepared with polymer concentrations below $c$*. The polymer/IL solutions were prepared using co-solvent evaporation as described in Chapter 2. PBzMA and the IL were added by weight in the desired ratio followed by the addition of tetrahydrofuran (THF) to facilitate dissolution.[73] THF was then evaporated under stirring using a nitrogen purge overnight, and the mixtures were further dried under vacuum (< 100 mTorr) for 48 h at 60 °C. The solutions were carefully filtered using a 0.45 $\mu$m PTFE syringe filter into the sample cell for scattering measurements. The concentrations in wt% were converted into g/mL by using the appropriate density (assuming no change in volume upon mixing) of the IL at each temperature reported in the literature.[178–180] The temperature dependence of density ($\rho$) is established as $\rho = b - aT$, where $a$ and $b$ are the fitting parameters listed in Table 4.2 for all the ILs.

**Table 4.2:** Fitting parameters of the equation $\rho = b - aT$

| IL | $a$ ($10^{-4}$ gmL$^{-1}$K$^{-1}$) | $b$ (g/mL) |
|---|---|---|
| [EMIM][TFSI][178] | 1.00 | 1.82 |
| [BMIM][TFSI][178] | 0.94 | 1.72 |
| [HMIM][TFSI][178] | 1.02 | 1.67 |
| [BMP][TFSI][180] | 0.91 | 1.67 |

### 4.2.2 Static light Scattering

A dilute polymer solution scatters light due to concentration fluctuations.[181,182] The intensity of excess scattered light ($I_{\text{ex}}$) is calculated by measuring the difference in scattering intensity of the solution ($I_{\text{soln}}$) and the solvent ($I_{\text{solv}}$). The Rayleigh ratio ($R_\theta$) is obtained by normalizing $I_{\text{ex}}$ by the incident laser intensity $I_{\text{o}}$, and correcting for the distance between sample and the detector ($r$).

$$R_\theta = \frac{I_{\text{soln}} - I_{\text{solv}}}{I_{\text{o}}} r^2 \tag{4.1}$$

The dependence of $R_\theta$ on the concentration of the polymer solution ($c$) and $q$ is reduced to a widely used form known as the Zimm equation,

$$\frac{Kc}{R_\theta} = \frac{1}{M_W}\left(1 + \frac{q^2}{3}R_g{}^2 + \ldots\right) + 2A_2c + \ldots \quad K = \frac{4\pi^2 n^2}{\lambda_o{}^4 N_A}\left(\frac{\mathrm{d}n}{\mathrm{d}c}\right)^2 \tag{4.2}$$

where $n$ is the solvent refractive index, $N_A$ is Avogadro's number, and $\lambda_o$ is the wavelength of the light in vacuum.[111] $M_w$ is determined from intercepts obtained from the plots of $Kc/R_\theta$ vs. $q^2$ and $Kc/R_\theta$ vs. $c$ in the dual limits of $c = 0$ and $q = 0$. For a particle that is in the Guinier regime ($qR_g < 1$) and large enough to exhibit a $q$ dependence, the $R_g$ value can be obtained from the slope of the Zimm extrapolation to $c = 0$. However, for small particles that do not have dependence on $q$, scattering from the solution is dominated by Rayleigh scattering ($qR_g \ll 1$). Therefore, eqn 4.2 reduces to

$$\frac{Kc}{R_\theta} = \frac{1}{M_W} + 2A_2c + \ldots \tag{4.3}$$

Irrespective of the size of the particle, the slope of the linear fit (eqn 4.3) extrapolated to $q = 0$ yields $A_2$. Positive values of $A_2$ indicate a good solvent, whereas negative values of $A_2$ indicate a poor solvent. When $A_2 = 0$, the solvent is in the theta condition.

SLS measurements were performed in the Institute of Macromolecular Chemistry, Prague, CZ. Five different dilute solutions for four molecular weights of PBzMA in four different ILs were prepared, resulting in a total of 80 samples. The corresponding solutions (~ 1 mL) were filtered into 12 mm glass ampoules and flame sealed under Ar. SLS measurements were performed on an ALV/CGS-8F goniometer with a laser wavelength of 633 nm. The angular range was 40° to 120° in increments of 10°, corresponding to a $q$ range of $9.42\times10^{-3}$ – $2.44\times10^{-2}$ nm$^{-1}$. The measurements were performed over a temperature range of 27 °C to 155 °C, maintained at ± 0.5 °C. The samples were placed in a pre-heated sealed oven at the desired temperature before placing in the instrument for faster temperature equilibration. In the instrument, the ampoules containing the samples were held for 5–10 mins prior to the measurement. For $T$ range of 27 °C to 130 °C, $R_\theta$ of the sample was calibrated using an ultrapure toluene standard. For $T > 130$ °C (above the boiling temperature of toluene in a sealed ampoule), $R_\theta$ was extrapolated from the linear dependence of $R_\theta$ on $T$ (plot shown in Appendix B). The values of the refractive index ($n$) of the ILs at each temperature were obtained from the literature using the relation $n = n_0 T + n_1$, where $n_0$ and $n_1$ are the fitting parameters, listed in Table 4.3.[183,184]

**Table 4.3:** Fitting parameters of $n = n_0 T + n_1$

| IL | $n_0$ $(10^{-4}\,\mathrm{K}^{-1})$ | $n_1$ |
|---|---|---|
| [EMIM][TFSI][183] | –2.50 | 1.497 |
| [BMIM][TFSI][183] | –3.09 | 1.517 |
| [HMIM][TFSI][183] | –2.61 | 1.508 |
| [BMP][TFSI][184] | –2.80 | 1.507 |

For some systems at 27 °C, SLS measurements were performed additionally in the UMN facility. SLS data was collected on a Brookhaven BI-200SM research goniometer and laser light scattering system, version 2.0, with a laser wavelength of 637 nm. Scattering angles between 40° to 110° were used with 5° increments, corresponding to a $q$ range of approximately $9.62\times10^{-3}$ – $2.30\times10^{-2}$ $\mathrm{nm}^{-1}$. The Rayleigh ratio of the sample was calibrated using an ultrapure toluene standard at 27 °C. PBzMA and ILs solutions (~

1mL) were filtered into 13 mm glass tubes using 0.45 um PTFE filters and covered with parafilm. The samples were equilibrated for 10 mins at 27 °C prior to the measurement.

d*n*/d*c measurement*

The refractive index increment d*n*/d*c* was measured by Abbé refractometry. Five different solutions of PBzMA-40 were prepared in each IL ranging in approximate concentration of 11 to 90 mg/mL. The temperature in the refractometer was controlled by circulating water at 27 °C, and 70:30 ethylene glycol:water bath at 45 °C and 60 °C. The refractive index ($n_D$) of neat IL and five solutions were measured using a red light source to mimic the wavelength of the laser in the light scattering instrument. Ideally, a wide temperature window is desired for accurate extrapolation of d*n*/d*c* versus *T*, but at higher temperatures, the measurement in $n_D$ is unstable. Furthermore, d*n*/d*c* is very sensitive to slight changes in $n_D$, which makes the error in measuring d*n*/d*c* larger than the dependence of d*n*/d*c* on *T*. Therefore, measurements were limited to 60 °C. The d*n*/d*c* was evaluated as the slope of $n_D$ versus *c*.

### 4.2.3 Dynamic light Scattering

The scattered intensity, $I_s$, is measured as a function of time (*t*), and a time autocorrelation function is computed, which can be normalized to yield the normalized autocorrelation function ($g^{(2)}(t)$) and converted to $g^{(1)}(t)$ by the Siegert relation[185]

$$g^{(2)}(t) = 1 + \beta \left| g^{(1)}(t) \right|^2 \tag{4.4}$$

where $\beta$ is an instrumental constant between 0 and 1. For dilute monodisperse polymer solutions, eqn 4.4 reduces to

$$g^{(2)}(t) = 1 + \beta \exp\left(-2\Gamma t\right) \tag{4.5}$$

where Γ is the decay rate.[186] For dilute polymer solutions with a monomodal distribution, the decay rate can be obtained by using the cumulant fitting of $\left|g^{(1)}\right|^2$ given as

$$\left|g^{(1)}\right|^2 = Ae^{-2\Gamma\tau}\left(1 + \frac{\mu_2}{2!}\tau^2 - \frac{\mu_3}{3!}\tau^3\right)^2 + B \tag{4.6}$$

where $A$, Γ, $\mu_2$, $\mu_3$, and $B$ are floating variables, and $\mu_2$ and $\mu_3$ are related to the dispersity and the skewness of the Γ distribution. The parameter $B$ should be theoretically zero. The distribution of Γ can be obtained by performing the regularized positive exponential sum (REPES) inversion on the auto correlation function.[187] For a particle in the Guinier regime ($qR_g < 1$), Γ depends linearly on $q^2$ with zero intercept, and an average value of $D_m$ can be obtained from the slope given as

$$D_m = \frac{\Gamma}{q^2} \tag{4.7}$$

The concentration dependence of the mutual diffusion coefficient in dilute solutions is represented by

$$D_m = D_0(1 + k_d c + ...) \tag{4.8}$$

where $D_0$ is the infinite dilution translational diffusion coefficient of the polymer, $c$ is the concentration of polymer molecules, and the constant $k_\mathrm{d}$ is known as the diffusion virial coefficient.[121] $k_\mathrm{d}$ is given as

$$k_\mathrm{d} = 2A_2M - k_\mathrm{f} - V_\mathrm{p} \tag{4.9}$$

where $k_\mathrm{f}$ is the linear term in the concentration expansion for the frictional coefficient, and $V_\mathrm{p}$ is the partial specific volume of the polymer. [188,189] The relations shown in equations (4.8 and 4.9) reveal both thermodynamic and dynamic information of dilute polymer solutions. The coefficient $k_\mathrm{d}$ is determined by the thermodynamic driving force ($2A_2M$) and an opposing frictional resistance, $k_\mathrm{f}$ (the contribution of the term term, $V_\mathrm{p}$, is usually negligible). Positive values of $k_\mathrm{d}$ indicate good solvent behavior, while in theta solvents, $k_\mathrm{d}$ equals 0 or can take slightly negative values. Yamakawa[190] has established $k_\mathrm{f}$ as

$$k_\mathrm{f} \approx 1.2A_2M + N_\mathrm{A}\frac{V_\mathrm{m}}{M} \tag{4.10}$$

where $V_\mathrm{m}$ is the hydrodynamic volume of the polymer chain, and $N_\mathrm{A}$ is Avogadro's number. In the zero concentration limit, $D_0$ is related to the hydrodynamic radius ($R_\mathrm{h,0}$) by the Stokes-Einstein relation,

$$D_0 = \frac{kT}{6\pi\eta_\mathrm{s}R_\mathrm{h,0}} \tag{4.11}$$

where $k$ is the Boltzmann constant, $T$ is the temperature, and $\eta_\mathrm{s}$ is the solvent viscosity.

DLS measurements were performed at two different facilities. In the UMN facility, DLS measurements were conducted at 27 °C on a Brookhaven BI-200SM research goniometer, laser light scattering system, version 2.0, with a laser wavelength of 637 nm, and BI-9000AT autocorrelator. Scattering angles of 30°, 50°, 70°, 90°, and 110° were used corresponding to a *q*-range of $5.33\times10^{-3}$–$5.34\times10^{-2}$ nm$^{-1}$ and a typical acquisition time of 10 min per angle. The value of decay rate was obtained from the third cumulant fitting of the normalized auto correlation function, and the distribution of the size was obtained via Laplace inversion using REPES.

For the majority of the samples, DLS measurements were performed at the Institute of Macromolecular Chemistry, Prague, CZ. The measurement utilized an ALV / CGS-8F goniometer with a laser wavelength of 633 nm, and an ALV 6010 correlator. The angular range was varied from 30° to 110° in increments of 20°, corresponding to a $q$ range of $5.34\times10^{-3}$–$5.35\times10^{-2}$ nm$^{-1}$. For each angle, the measurement was performed three times, averaged over 60 s each. The value of decay rate ($\Gamma$) was obtained from the third cumulant fit (shown in Figure 4.3) determined by the inbuilt ALV software, and the size distribution was obtained via Laplace inversion using REPES (shown in Figure 4.4). Measurements at 27 °C for PBzMA-160 were made at both UMN and CZ facilities for independent sets of samples with equivalent concentrations. The values of $D_0$ obtained were generally within 5% from the two independent measurements, emphasizing that the collection time of 10 mins versus 1 min does not significantly affect the experimental values. Similarly, data analysis was also performed using $\Gamma$ obtained from REPES. The experimental parameters of interest ($D_0$ and $R_{h,0}$) also varied insignificantly within the uncertainty.

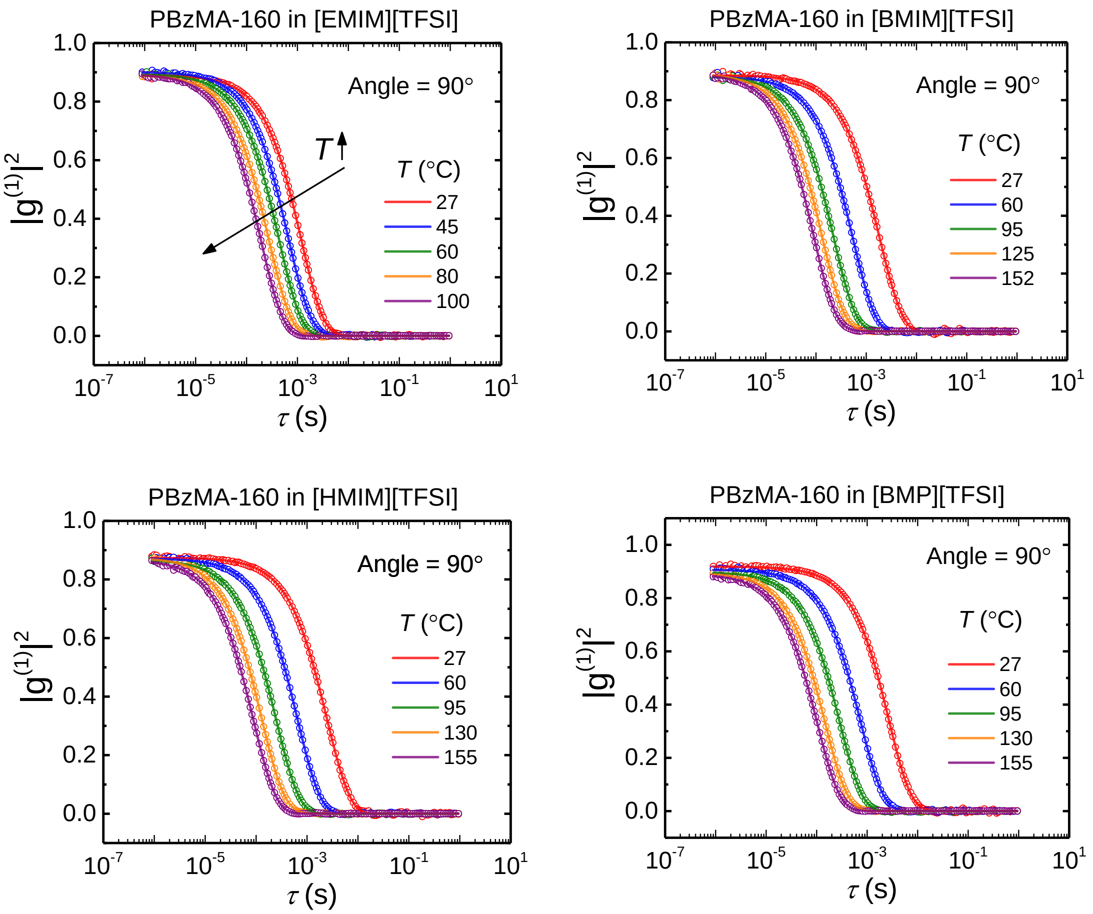

**Figure 4.3:** Cumulant fits (3rd order, eqn 4.6) for the highest concentration (~21 mg/mL) of PBzMA-160 in ILs measured at 90° angle at 5 different temperatures.

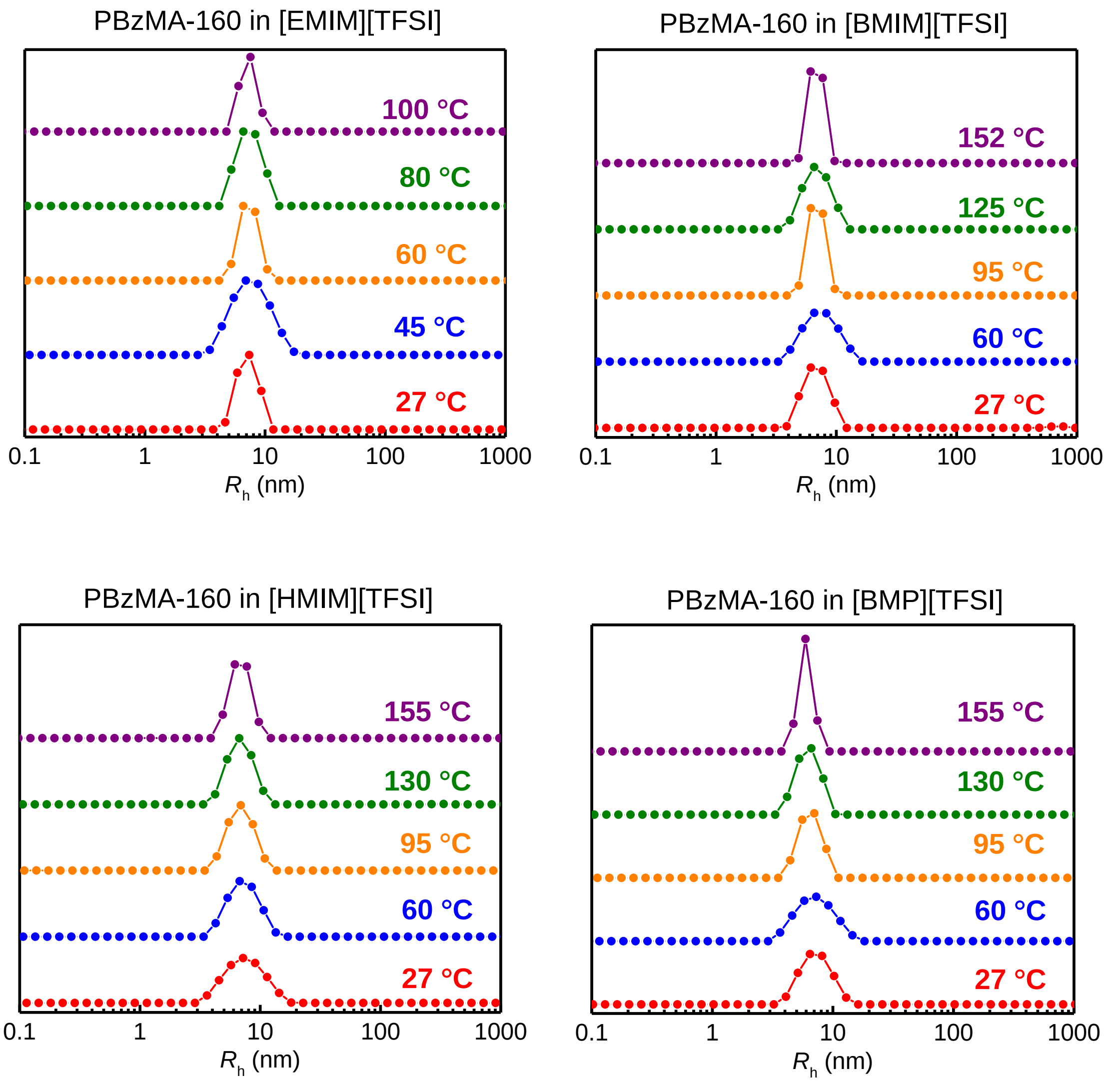

**Figure 4.4:** Intensity weighted distribution of hydrodynamic radii for the highest concentration of PBzMA-160 (~ 21 mg/mL) in ILs at five different temperatures obtained using REPES at 90° angle.

### 4.2.4 Cloud point measurements

A new batch of PBzMA ($M_w$ =70.1 kg/mol, $Đ$ = 1.06) was synthesized by identical procedures described above by Dr. Cecilia Hall. PBzMA and ILs solutions were flame-sealed in glass ampoules under vacuum and placed in a heating stage at a controlled temperature. The sample was heated at a rate of 1 °C/min and a laser beam of wavelength 633 nm was directed to the sample, with a path length of approximately 7 mm. The transmitted intensity was recorded as a function of temperature, and cloud point was defined as the temperature at which the transmittance drops to < 80% of the original homogenous solution. The cloud point temperature was recorded for an independent sample (1 wt% PBzMA in [BMIM][TFSI]) upon heating and cooling at the same rate. A relatively small hysteresis between desolvation and resolvation was observed (shown in Appendix B), with higher $T_{\mathrm{cp}}$ obtained upon cooling. Kobayashi et al. reported a similar observation with PBzMA in solvate ionic liquids. They attributed the hysteresis to slow mobility of polymer chains that dominated resolvation instead of the solvent molecules diffusing into the polymer-rich phase.[69]

For PBzMA in [BMIM][TFSI], the concentration range of 0.5 to 20 wt% was used to determine the concentration dependence of $T_{\mathrm{cp}}$. Cloud point measurements were also performed for the highest concentration of each of the molecular weight and IL pair to decide the working temperature range for SLS and DLS studies.

## 4.3 Results and Discussion

### 4.3.1 Phase behavior

As seen in Figure 4.5a, cloud point temperatures are obtained upon heating, an observation consistent with the LCST phase behavior of PBzMA in ILs.[73] According to the Flory-Huggins theory, the critical concentration ($\phi_{\mathrm{c}}$) is generally shifted to low concentrations of the polymer and decreases with increasing molecular weight ($\phi_c \approx 1/\sqrt{N}$

,where $N$ is the degree of polymerization in the units of solvent molar volume).[54] Using the former relationship, $\phi_c$ is estimated to be 4 wt% for PBzMA (71 kg/mol, $N$ = 393). However, as seen in Figure 4.5b, the observed cloud point temperature decreases consistently up to 20 wt%, emphasizing that the actual $\phi_c$ is possibly far from the calculated $\phi_c$ (4 wt%) for PBzMA in [BMIM][TFSI]. Watanabe and coworkers have also conducted cloud point measurements for an equivalent molecular weight of PBzMA in glyme-based ILs (equimolar mixtures of triglyme (G3) or tetraglyme (G4) and LiTFSI resulting in Li(G3)TFSI and Li(G4)TFSI, respectively) and observed a trend consistent with our results as shown in Figure 4.5b.[174] However, in all these cases, the critical concentrations are predicted using Flory-Huggins theory that does not anticipate LCST behavior.

Although full phase diagrams are not commonly established for polymers in ILs, some detailed work has been done for polyethers in imidazolium-based ILs that also exhibit an LCST behavior in ILs. Unlike the PBzMA system, $\phi_c$ lies at lower polymer concentrations ($\phi_c$ ~4 wt% for 22 kg/mol) for poly(ethyl glycidyl ether) (PEGE) in [EMIM][TFSI]. [67] Furthermore, this characteristic persists irrespective of the molecular weight of PEGE. In contrast, poly(ethylene oxide) in [EMIM][$BF_4$] and [BMIM][$BF_4$] exhibit unusually high $\phi_c$ (50–80 wt%), similar to our observation for PBzMA in [BMIM][TFSI].[65,66] The origin of higher critical composition is not fully resolved in PEO system but has been speculated to result due to the formation of dense polymer phases predicted by de Gennes.[191] Recent theoretical work by Lipson and White has provided two major explanations for occurrence of polymer rich critical compositions in the PEO/ [EMIM][$BF_4$] system.[192] First, the self-organization of IL molecules decreases their contribution to the ideal entropy of mixing, as opposed to the case if the solvent molecules were evenly distributed. Second, the IL component has a significantly stronger cohesive energy density compared to the polymers, which shifts the excess entropy of mixing to higher polymer composition. These arguments could partially explain the shift to higher polymer concentrations in our system as well. However, these explanations do not hold for the PEGE system, where the IL also has stronger cohesive energy density and the potential for self-organization. Therefore, the occurrence of higher critical compositions in these systems is yet to be understood in detail.

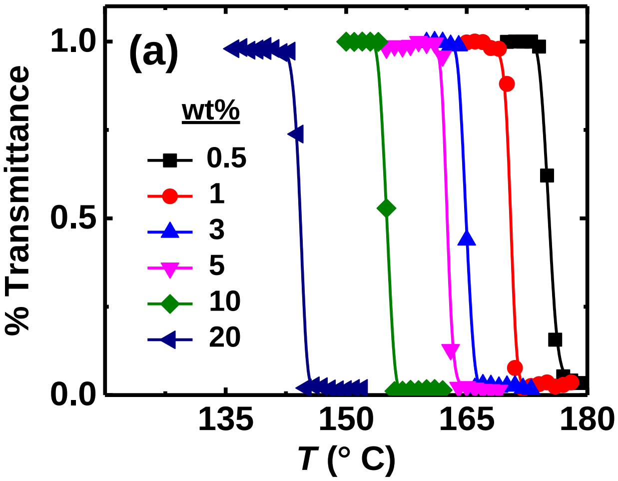

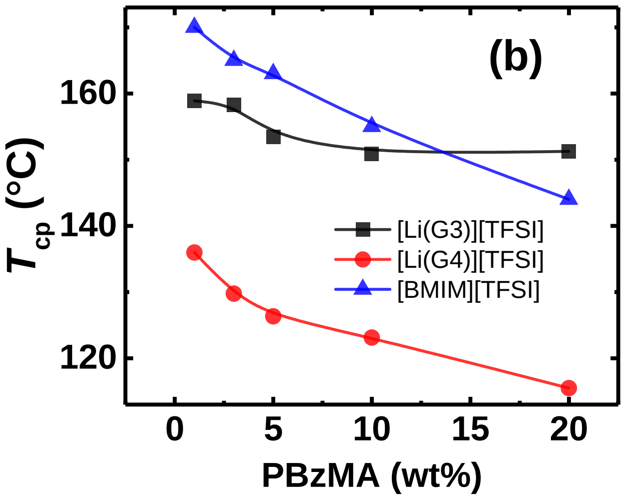

**Figure 4.5:** Cloud point measurements for PBzMA in ILs. (a) Transmittance versus temperature data for PBzMA (71 kg/mol) in [BMIM][TFSI] at a heating rate of 1 °C/min. (b) Cloud point temperature decreases continuously with increasing polymer concentration for PBzMA (71 kg/mol) in [BMIM][TFSI]. Watanabe and coworkers[69] measured cloud points for equivalent molecular weight PBzMA ($M_w$ = 70 kg/mol, $Đ$ = 1.19) in glyme-based ILs (shown in red and black), and observed a similar trend. In all cases, the critical composition possibly lies far from the expected $\phi_c$ of 4 wt%.

Cloud point measurements for the highest concentration (~ 21 mg/mL) of PBzMA-160 in 4 different ILs are shown in Figure 4.6. The values of $T_{cp}$ are 106 °C, 157 °C, 172 °C, and 226 °C for PBzMA-160 in [EMIM][TFSI], [BMIM][TFSI], [BMP][TFSI], and [HMIM][TFSI], respectively. Our observed trend in $T_{cp}$ is consistent with prior reports found in the literature.[73] The values of $T_{cp}$ obtained from cloud point measurements are used as guides to decide the temperature range for SLS and DLS studies. The highest temperatures used are approximately ($T_{cp}$ – 5) °C evaluated as 100 °C and 152 °C for [EMIM][TFSI] and [BMIM][TFSI], respectively. For [BMP][TFSI] and [HMIM][TFSI] systems, the $T_{cp}$ is higher than the experimental temperature limit. Therefore, 155 °C is used as the maximum temperature (the limit of the light scattering instrument).

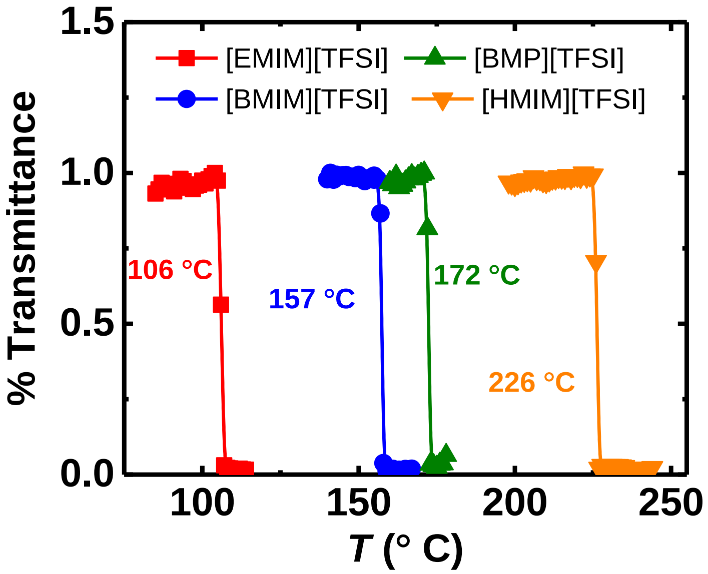

**Figure 4.6**: Transmittance measurements for the highest concentrations (~21mg/mL) of PBzMA-160 in ILs measured at a heating rate of 1 °C/min.

### 4.3.2 Static properties

*Determining* d*n*/d*c*

d*n*/d*c* was determined from the slope of refractive index as a function of concentration for PBzMA-40 in all ILs as shown in Figure 4.7. The values of d*n*/d*c* for PBzMA in ILs at three different temperatures are shown in Figure 4.8 and listed in Table 4.4. The error reported is obtained from the linear fits of refractive index versus *c* plots. All the systems show negligible temperature dependence for d*n*/d*c* within the error, except for PBzMA in [BMIM][TFSI], which has a slight dependence on *T*, $d(dn/dc)/dT = -1.1 \times 10^{-4}$ (mL/g °C). It is quite common to observe a very weak dependence of d*n*/d*c* on *T* (typically on the order of $10^{-4}$ mL/g °C) as reported in the literature.[72,157,193] For SLS measurements above 60 °C, an average d*n*/d*c* value (measured at 3 temperatures) was used. On the other hand, for PBzMA in [BMIM][TFSI], the d*n*/d*c* at higher temperatures were calculated from the linear extrapolation.

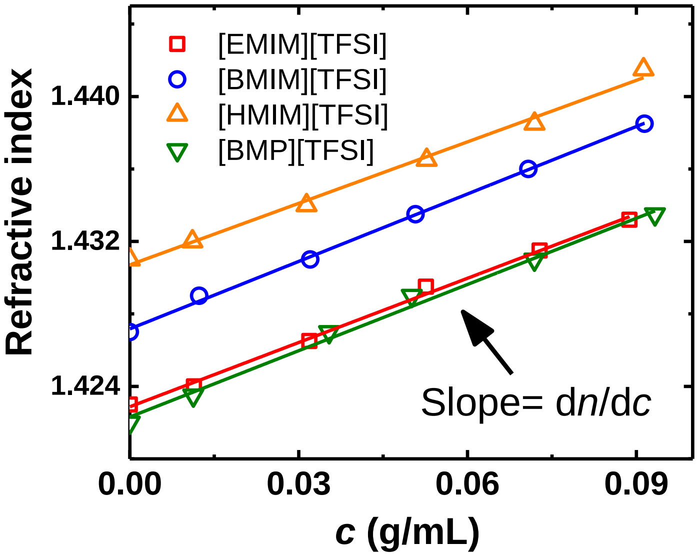

**Figure 4.7:** The refractive index of PBzMA-40 in ILs as a function of concentration at 27 °C, where the slope yields d*n*/d*c*.

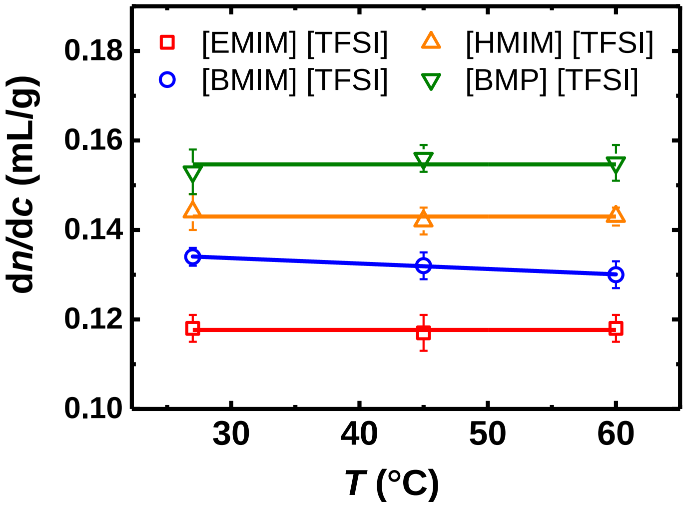

**Figure 4.8:** Dependence of d*n*/d*c* on temperature for PBzMA-40 in different ILs. The symbols and lines are vertically shifted for clarity.

**Table 4.4:** Dependence of d$n$/d$c$ on temperature

| **Solvent** | **d$n$/d$c$ (mL/g)** | | |
|---|---|---|---|
| | 27 °C | 45 °C | 60 °C |
| [EMIM][TFSI] | 0.118 ± 0.003 | 0.117 ± 0.004 | 0.118 ± 0.003 |
| [BMIM][TFSI] | 0.124 ± 0.002 | 0.122 ± 0.003 | 0.120 ± 0.003 |
| [HMIM][TFSI] | 0.124 ± 0.004 | 0.122 ± 0.003 | 0.123 ± 0.002 |
| [BMP][TFSI] | 0.123 ± 0.005 | 0.126 ± 0.003 | 0.125 ± 0.004 |

*Zimm plots*

A sample Zimm plot is shown in Figure 4.9 for PBzMA-160 in [EMIM][TFSI] and all other plots are shown in Appendix B. The scattering is independent of $q$. Thus, all the molecular weights of PBzMA used in this study can be considered to be in the Rayleigh regime ($qR_g << 1$). For each concentration, $Kc/R_{\theta,avg}$ is obtained by averaging $Kc/R_\theta$ at all angles and plotting against the concentration, as shown in Figure 4.10. By fitting these plots to eqn 4.3, $A_2$ and $M_w$ were determined at each temperature for PBzMA-160.

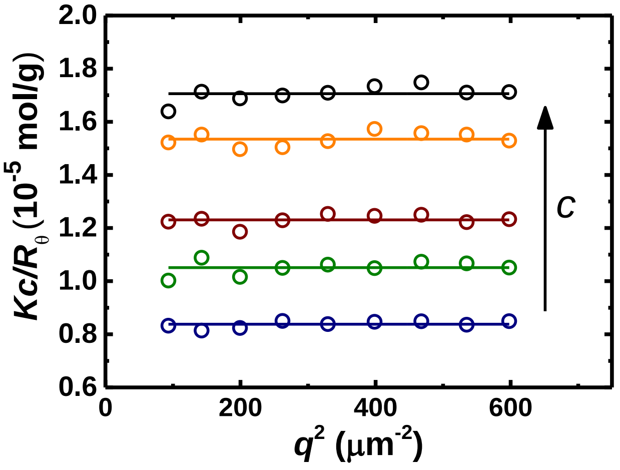

**Figure 4.9:** Representative Zimm plot for PBzMA-160 in [EMIM][TFSI] at 27 °C for 5 concentrations in the range 4–21 mg/mL. The data collected over an angular range of 40° and 120° in 10° increments were independent of angle.

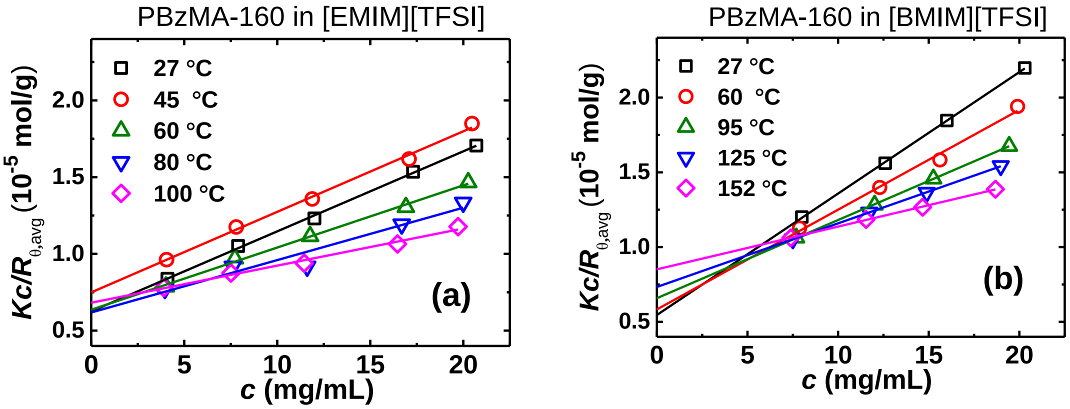

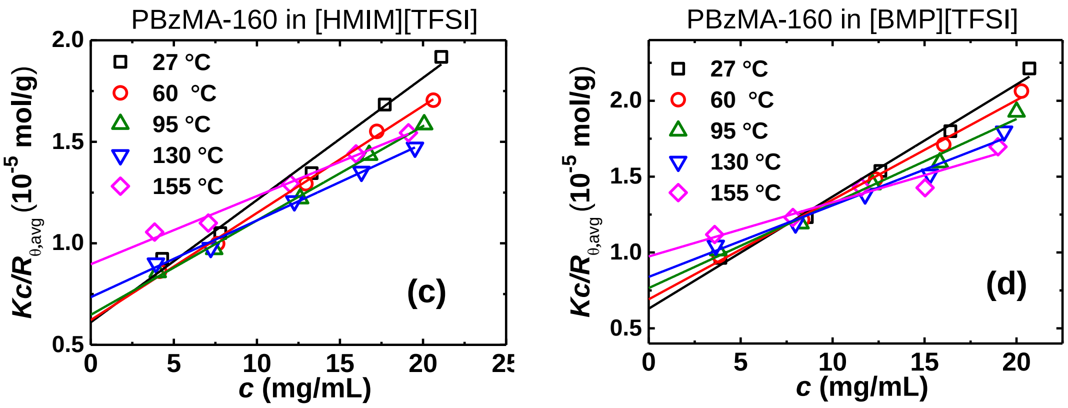

**Figure 4.10:** $Kc/R_{\theta,avg}$ as a function of $c$ for PBzMA-160 in ILs at various temperatures. The values of $A_2$ are determined from slopes of the fits (eqn 4.3) and the intercept gives $1/M_{w.}$

*Evaluating second virial coefficient*

For PBzMA-160 in all ILs, the second virial coefficient, $A_2$, dependence on temperature is shown in Figure 4.11 and the values are summarized in Table 4.8. $A_2$ decreases with increasing $T$, as anticipated for an LCST system. However, $A_2$ remains significantly positive at temperatures close to the phase separation temperature, $T_{cp}$. The temperature at which $A_2 = 0$ (theta temperature, $T_\Theta$) is never reached in this case. This is particularly surprising for PBzMA in [EMIM][TFSI] and [BMIM][TFSI] systems, as the highest temperature used are approximately $T_{cp}$– 5 °C, where $A_2 < 0$ is anticipated. The consistently positive values of $A_2$ throughout the temperature range imply that all these ILs are good solvents. According to Flory Huggins theory, the second-virial coefficient is related to the interaction parameter, $\chi$,

$$A_2 = \left(\frac{1}{2} - \chi\right)\frac{\overline{V_2}^2}{\overline{V_1}}\frac{1}{M^2} \tag{4.12}$$

where $\overline{V_2}$ is the partial molar volume of the polymer, and $\overline{V_1}$ is the partial molar volume of the solvent. Since $\chi$ has an inverse dependence on $T$, $A_2$ is proportional to $T^{-1}$. Therefore, $A_2$ is also plotted as a function of inverse $T$, which shows that the experimentally obtained $A_2$ values are far from the $A_2 = 0$ line. The major implication of this observation is that $T_\Theta$ is well above $T_{cp}$, a unique characteristic that is also observed for hydroxypropylmethylcellulose in water.[194] For this particular system, it has been speculated that the solutions include some form of aggregates that restrict the simple interpretation of $A_2$. However, for the PBzMA/IL system, DLS measurements at various concentrations (~ 4 – 21 mg/mL) and temperatures (27 °C – 100 °C) show no strong evidence of aggregation as seen in Figure 4.4, particularly for PBzMA-160 in [EMIM][TFSI] and [BMIM][TFSI], where the highest temperature is close to $T_{cp}$.

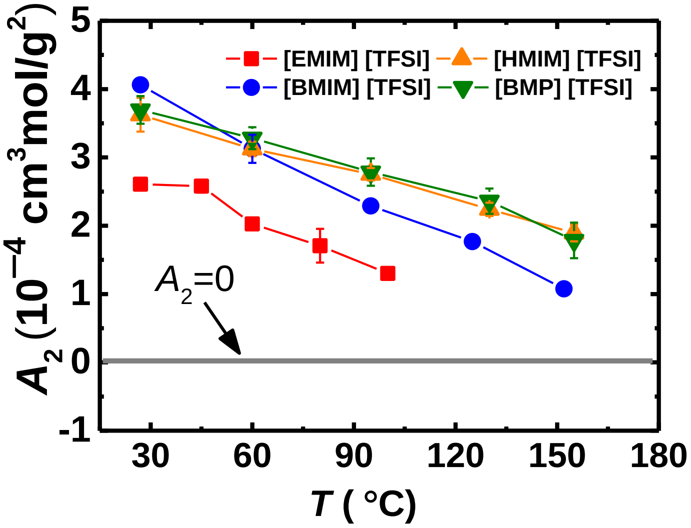

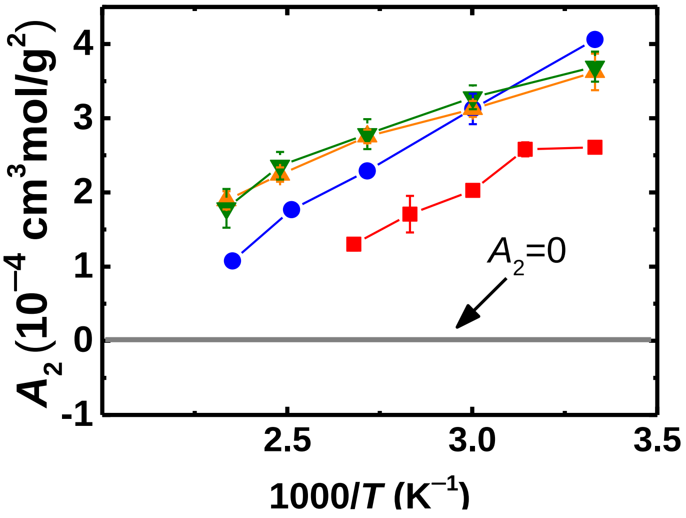

**Figure 4.11:** $A_2$ obtained from Zimm plots shown as a function of $T$ and inverse $T$. $A_2$ decreases with increasing $T$ as anticipated for LCST systems. However, $A_2$ shows weak dependence on $T$ as the values of $A_2$ remain significantly positive even at $T$ close to $T_{cp}$. The estimated theta temperatures seem far from the experimental temperature range used in the study. Solid lines are intended as guides to the eye.

*Evaluating interaction parameters*

Using eqn 4.12 and the experimental values of $A_2$, the effective interaction parameter, $\chi_{eff}$, can be evaluated at each temperature. The $\chi_{eff}$ can be expressed as a function of temperature as $\chi_{eff} = A + B/T$, where $A$ represents the entropic contribution and $B$ includes the enthalpic contribution. In terms of Flory-Huggins theory, the excess entropy of mixing is equal to $-kA\phi_p(1-\phi_p)$, and enthalpy of mixing is equal to $kB\phi_p(1-\phi_p)$. The partial molar volume of the IL was used as the reference volume, calculated using the density of the ILs at each temperature given in Table 4.2. The density of PBzMA was assumed to vary insignificantly with temperature and hence, a constant value of 1.18 g/mL was used to estimate the partial molar volume of the polymer.[195] The dependence of $\chi_{eff}$ on temperature is shown in Figure 4.12, where $\chi_{eff} < 0.5$ for all cases. The values of $A$ and $B$ can be evaluated from the intercepts and the slopes of the linear fits, respectively (listed in Table 4.5 and plotted in Figure 4.13, with the errors obtained from the linear fits). It should be emphasized that the values of $\chi_{\mathrm{eff}}$, *A*, and *B* should be viewed with caution. The eqn 4.12 does not incorporate any composition dependence of $\chi_{\mathrm{eff}}$,[196] therefore, the values of *A* and *B* are not quantitatively reliable. Furthermore, the values of these parameters are dependent on the reference volume used. For example, if a fixed reference volume of 100 cm$^3$ is used for all solvents to calculate $\chi_{\mathrm{eff}}$ , the parameters *A* and *B* change significantly (shown in Table 4.6).

However, prior reports have compared the values of *A* and *B* to discuss the entropic and enthalpic driving forces of the system.[72,76] For example, Hoarfrost et al. showed that for PnBMA in [EMIM][TFSI]/[BMIM][TFSI],[72] *A* increased with the incorporation of BMIM cation (75 wt% to 100 wt%), and concluded that the entropy of mixing decreases with higher BMIM content. On the other hand, *B* decreased with increasing BMIM content, which lowers the enthalpy of mixing.

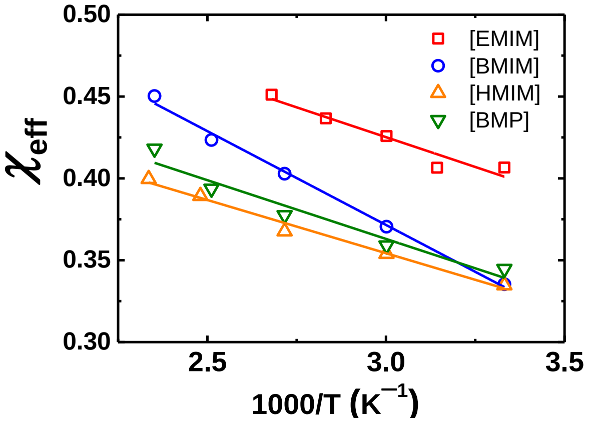

**Figure 4.12:** Temperature dependence of effective interaction parameter, $\chi_{\mathrm{eff}}$, for PBzMA-160 in ILs. Solid lines are fit to $\chi_{\mathrm{eff}} = A+B/T$, where *A* and *B* are fitting constants.

**Table 4.5:** Entropic and enthalpic contributions of $\chi_{\mathrm{eff}}$

| Solvent | $A$ | $B$(K$^{-1}$) |
|---|---|---|
| [EMIM][TFSI] | 0.64 ± 0.04 | –73 ± 12 |
| [BMIM][TFSI] | 0.72 ±0.01 | –115 ± 5 |
| [HMIM][TFSI] | 0.55 ±0.01 | –65 ± 4 |
| [BMP][TFSI] | 0.58 ±0.03 | –72 ± 10 |

**Table 4.6:** Entropic and enthalpic contributions of $\chi_{\mathrm{eff},}$ obtained using a reference molar volume of 100 cm$^3$

| Solvent | $A$ | $B$(K$^{-1}$) |
|---|---|---|
| [EMIM][TFSI] | 0.56 ± 0.01 | –30 ± 5 |
| [BMIM][TFSI] | 0.58 ± 0.00 | –41 ± 2 |
| [HMIM][TFSI] | 0.52 ± 0.00 | –23 ± 2 |
| [BMP][TFSI] | 0.58 ± 0.01 | –26 ± 3 |

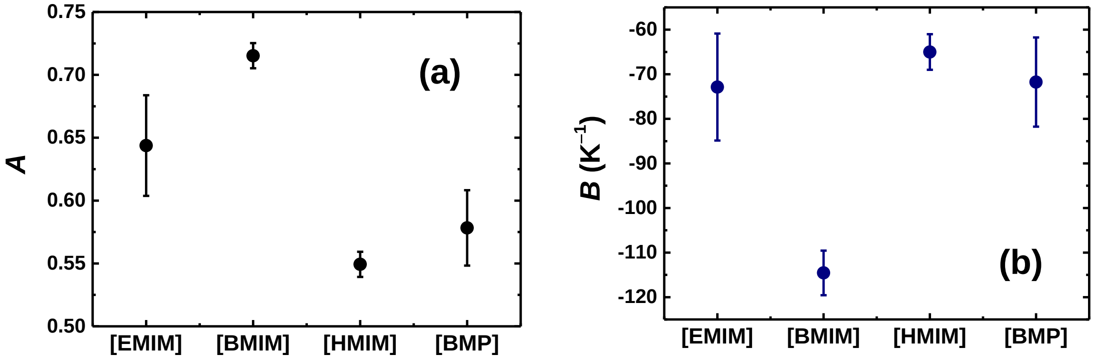

**Figure 4.13:** (a) Entropic and (b) Enthalpic components of $\chi_{\mathrm{eff}}$ varying with the cation identity of the IL for PBzMA-160 in ILs. The values are determined from the fits in Figure 4.12.

From Figure 4.13 and Table 4.5, it can be seen that the values of $B$ is negative for all cases, implying that some kind of specific attractive interaction exist between the polymer and the solvent. This information combined with the positive values of $A$ indicates that it exhibits LCST phase behavior. Prior works by Watanabe and coworkers have discussed that the benzyl groups in the polymer interact with the IL cation via cation-$\pi$ interactions, forming localized cage structures.[74,76,88] This interaction could be the primary driving force for the negative enthalpy of mixing and decrease in entropy of mixing. A relatively recent study proposed that PBzMA solvation in IL is further ordered by the intra-polymer interactions among the benzyl side groups.[174]

From Figure 4.13, it can be observed that the value of $A$ increases from EMIM to BMIM, indicating that the entropy of mixing decreases. This observation is in agreement with prior reports, where the incorporation of longer alkyl tails in the IL cations decreased the mixing entropy due to oriented solvation.[72] However, this trend does not hold for the case when HMIM cation is used. In fact, the value of $A$ decreases. On the enthalpic side, the magnitude of $B$ also exhibits a similar trend, where $|B|$ increases from EMIM to BMIM, but decreases for HMIM. Interestingly, the magnitude of $A$ and $B$ are very similar for the EMIM and BMP cations. Therefore, no specific trend can be concluded from these parameters. Hirosawa et al. used SANS model fits to determine the parameters $A$ and $B$ for a 40 kg/mol PBzMA in [EMIM][TFSI]. They report a value of $A$= 0.73 and $B = -84\ \mathrm{K}^{-1}$, which are close to the experimental values obtained from our work.[76] However, one must be very careful in comparing the values of $\chi_{\mathrm{eff}}$ values and the fitting parameters obtained from different experiments.

At a first glance, eqn 4.12 depicts that $A_2$ is dependent on the polymer molecular weight. However, since $\overline{V}_2 \sim N \sim M$, the $M$ dependence cancels outs. Therefore, the Flory-Huggins theory actually predicts that $A_2$ is not a function of $M$. In reality, however, $A_2$ is found to vary as $A_2 \sim M_w^a$, where $a$ is ≈ –0.2 for polymers in good solvents, as expected by scaling theory [99,190,197] and reported in experimental findings.[121,198–200] The $A_2$ values were also determined for lower molecular weight PBzMA at 27 °C using Zimm plots (shown in Appendix B) and the resulting values are shown in Figure 4.14 for all systems and molecular weights. Interestingly, $A_2$ exhibits a stronger dependence on $M_w$ than anticipated, with $a$ values as –0.35, –0.38, –0.48, and –0.32 for PBzMA in [EMIM][TFSI], [BMIM][TFSI], [HMIM][TFSI], and [BMP][TFSI], respectively.

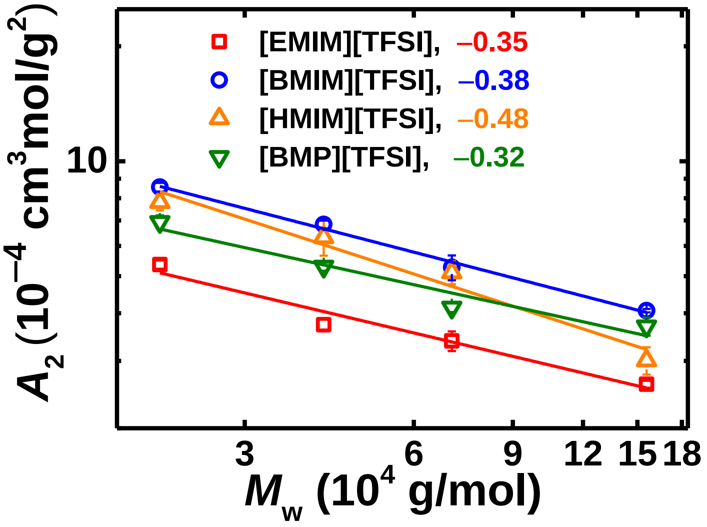

**Figure 4.14:** $A_2$ plotted as a function of $M_w$ for PBzMA in ILs. $A_2$ decreases with increasing $M_w$ as anticipated. $A_2 \sim M_w^a$, where $a$ is –0.35, –0.38, –0.48, and –0.32 for PBzMA in [EMIM][TFSI], [BMIM][TFSI], [HMIM][TFSI], and [BMP][TFSI], respectively. However, the dependence of $A_2$ on $M_w$ is surprisingly stronger than observed for polymers in good solvent systems, where $a$ ≈ –0.2.

The molecular weights obtained from the Zimm plots are plotted as a function of temperature in Figure 4.15a for PBzMA-160. The average $M_w$ values collected for all systems at all temperatures agree within 20% of $M_w$ obtained from SEC (shown as a gray line). However, at higher temperatures, the deviation seems larger for [HMIM][TFSI] and [BMP][TFSI] systems. A possible explanation for this discrepancy is the inaccuracy in d*n*/d*c* values obtained through extrapolation at higher temperature. By fixing the value of $M_w$ (obtained at 27 °C), we back-calculated the d*n*/d*c* values at the highest temperature for the four systems studied. The obtained d*n*/d*c* (shown in Table 4.7) were within 2 – 20% of the d*n*/d*c* values used in the Zimm plots. This deviation is likely within the uncertainty that would be obtained if d*n*/d*c* were to be measured at elevated temperatures (since high temperature d*n*/d*c* measurements are less reliable, as discussed in the previous section).

**Table 4.7:** d*n*/d*c* values back-calculated by fixing $M_w$

| **Solvent** | ***T*** **(°C)** | **d*n*/d*c* estimated**[a] | **d*n*/d*c* calculated**[b] | **% difference** |
|---|---|---|---|---|
| [EMIM][TFSI] | 100 | 0.118 | 0.116 | 2 |
| [BMIM][TFSI] | 152 | 0.124 | 0.114 | 8 |
| [HMIM][TFSI] | 155 | 0.124 | 0.106 | 16 |
| [BMP][TFSI] | 155 | 0.123 | 0.099 | 22 |

[a] Estimated from extrapolation shown in Figure 4.8, and used in Zimm plots

[b] Back calculated by fixing the value of $M_w$ obtained from Zimm plots at 27 °C

Figure 4.15b shows the $M_w$ obtained for the lower three molecular weights of PBzMA that reasonably agree within 20% for PBzMA-40 and PBzMA-70. However, for PBzMA-20, the $M_w$ values obtained from the Zimm plots (shown in symbols) are consistently lower (20-30%) than $M_w$ obtained from the SEC analysis (shown as a gray line). On the contrary, the $M_w$ values obtained from Zimm plots for all four solvents are in excellent agreement with each other (within 10%).

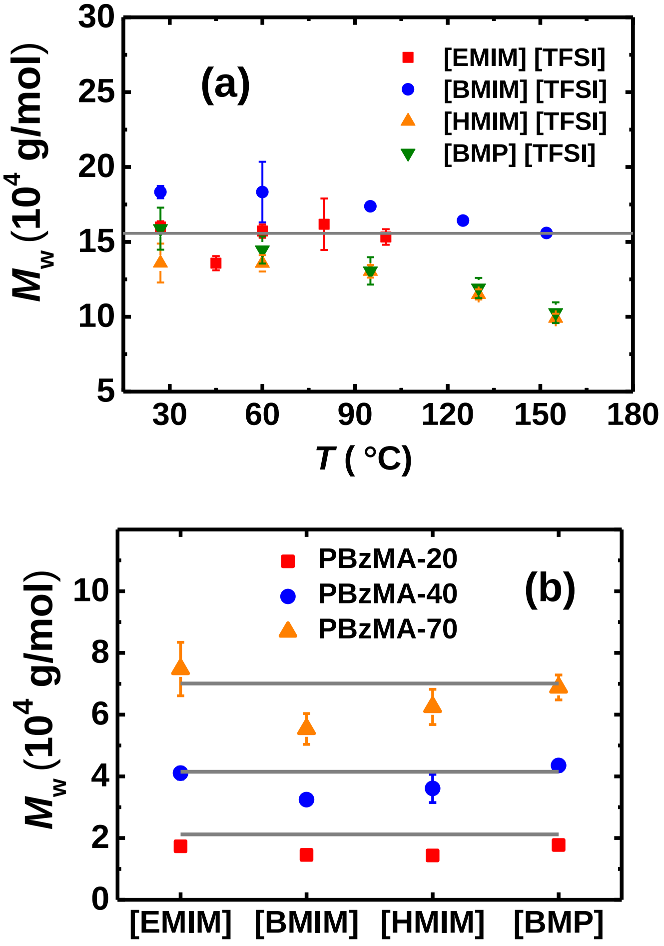

**Figure 4.15:** $M_w$ obtained from Zimm plots (a) $M_w$ plotted as a function of $T$ for PBzMA-160 in all ILs. The average $M_w$ values agree within 20% of $M_w$ obtained from SEC (shown in gray line). (b) The values of $M_w$ obtained from Zimm plots for PBzMA-20 (red symbols), PBzMA-40 (blue symbols), and PBzMA-70 (orange symbols) in different ILs. The gray lines are the values of $M_w$ obtained from SEC.

### 4.3.3 Dynamic properties

The average decay rates, Γ, were obtained from cumulant fitting (eqn 4.6) of the correlation functions obtained at five scattering angles for the lowest (27 °C) and the highest temperature (~$T_{\mathrm{cp}}$–5 °C) of the measurement. The diffusion coefficient was determined from the slope of Γ plotted versus $q^2$, as shown in Figure 4.16 for PBzMA-160 in all ILs. Plots of Γ versus $q^2$ were linear for all cases. For all the other temperatures, the measurements were performed only at 90° scattering angle, where $D_{\mathrm{m}}$ was evaluated using eqn 4.7.

**PBzMA-160 in [EMIM][TFSI]**

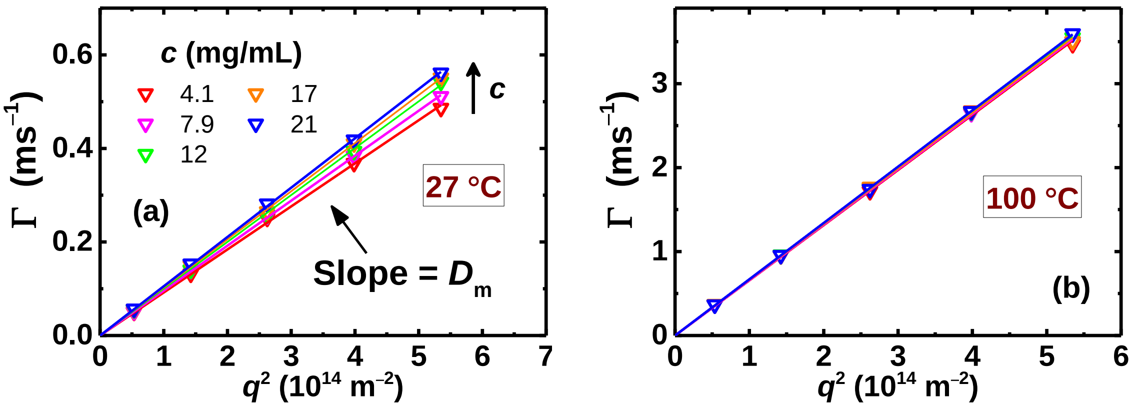

**PBzMA-160 in [BMIM][TFSI]**

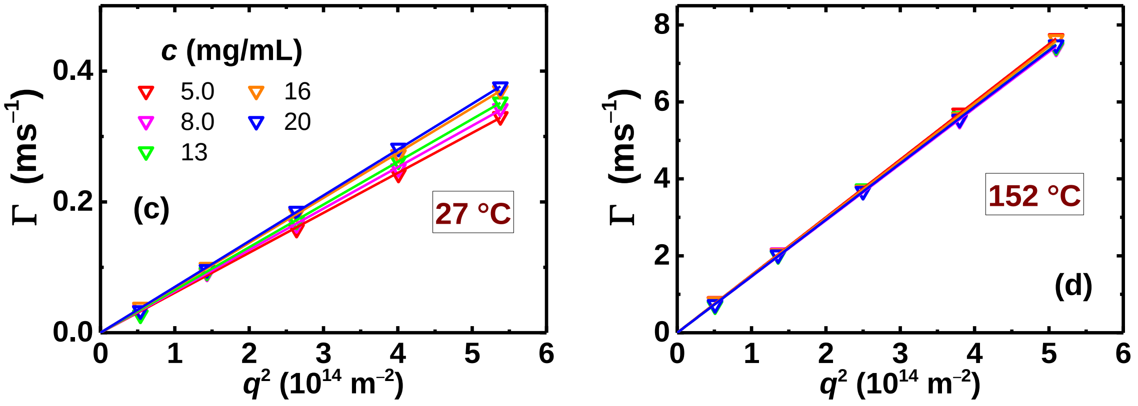

PBzMA-160 in [HMIM][TFSI]

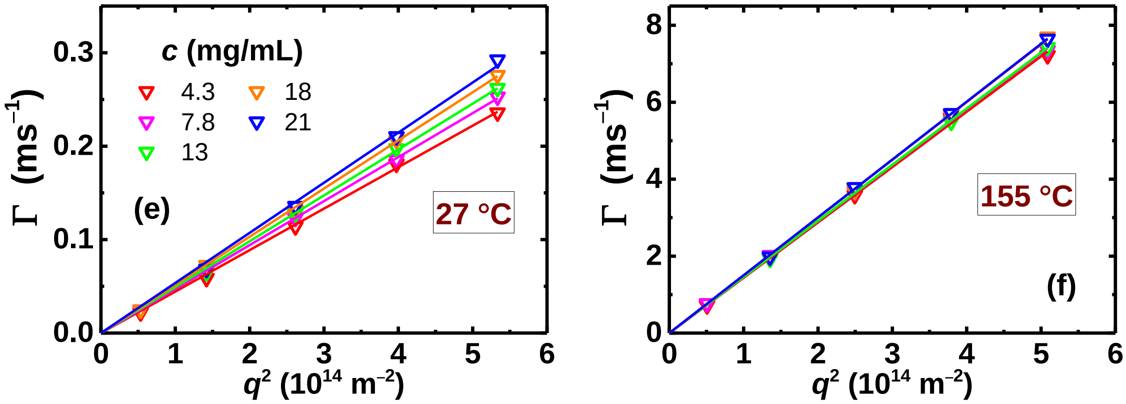

PBzMA-160 in [BMP][TFSI]

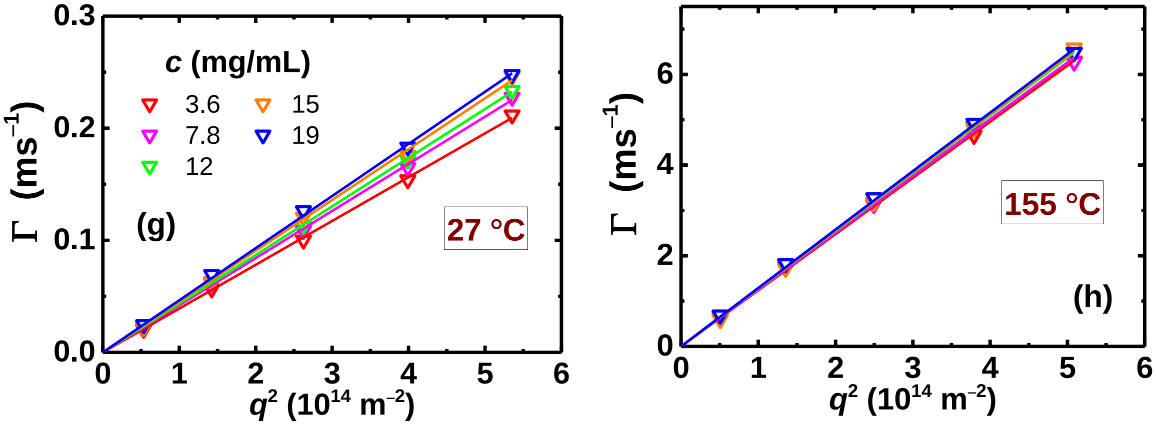

**Figure 4.16:** Plots of Γ vs. $q^2$ for PBzMA-160 in ILs at 27 °C and the highest temperature used for each system. Γ varies linearly with $q^2$ and the slope yields $D_m$.

The average mutual diffusion coefficients obtained from the slope of Γ versus $q^2$ plots are plotted in Figure 4.17 as a function of concentration for all PBzMA-160 systems at the lowest and the highest temperature. For PBzMA-160 in [EMIM][TFSI], the slope remains positive at the highest temperature. An important implication of this result is that $k_d > 0$ at $T_{cp}$ –5 °C, consistent with the good solvent behavior of the second virial coefficient ($A_2 > 0$) obtained from the Zimm plots. For PBzMA in [BMIM][TFSI], $k_d$ is essentially zero, indicative of theta-like behavior at $T_{cp}$ –5 °C. For [HMIM][TFSI] and [BMP][TFSI] systems, $T$ = 155 °C is far from the observed $T_{cp}$, and thus, the positive values of $k_d$ are not surprising. Overall, data from DLS further corroborates the good solvent behavior of PBzMA in most of the ILs. The values of $D_0$ and $k_d$ are summarized in Table 4.8 at all temperatures.

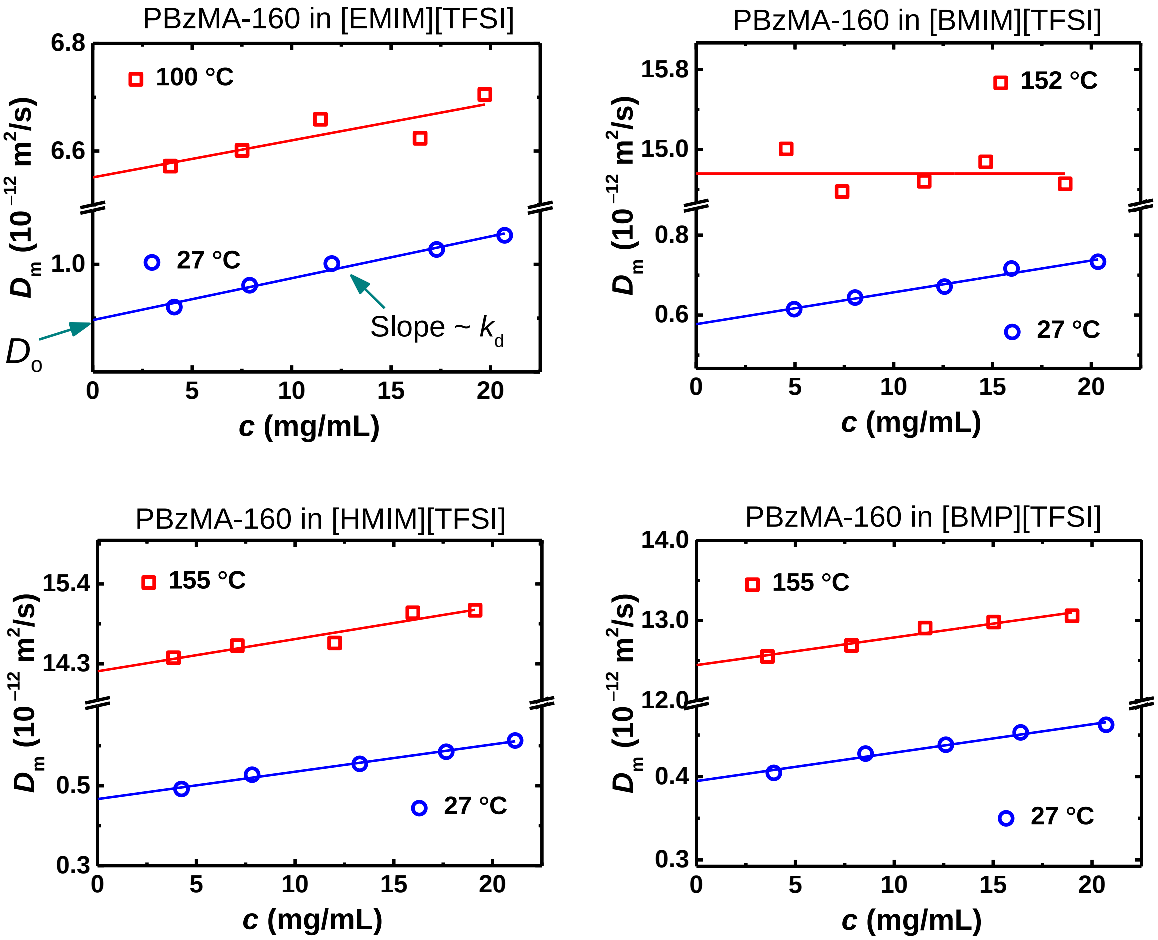

**Figure 4.17:** $D_m$ vs. $c$ for PBzMA-160 in [EMIM][TFSI], [BMIM][TFSI], [HMIM][TFSI], and [BMP][TFSI]. $D_m$ varies linearly with $c$, where the solid line represents fits to eqn 4.8. The slope and intercept gives $k_d$ and $D_o$, respectively.

The frictional virial coefficient, $k_f$, is estimated using the measured experimental values of $A_2$ and $k_d$ in eqn 4.9 (assuming $V_p$ is negligible). $k_f$ is also calculated using Yamakawa's theoretical prediction (shown in eqn 4.10).[190] Here, the hydrodynamic volume is obtained by the relation, $V_m = (4/3)\pi R_h{}^3$, where $R_h$ is obtained from the DLS measurements discussed later. From Table 4.8, it can be seen that the magnitude of calculated $k_f$ is in reasonable agreement with that estimated from the theory.

**Table 4.8:** Structural, dynamic, and thermodynamic parameters of PBzMA-160 in ionic liquids

| **$T$ (°C)** | **$R_{h,0}$ (nm)** | **$D_0$ ($10^{-12}$ m$^2$/s)** | **$k_d$ (mL/g)** | **$A_2$ ($10^{-4}$ cm$^3$mol /g$^2$)** | **$k_f$ Expt (mL/g)** | **$k_f$ Theory (mL/g)** | **$k_{f, expt}$/ $k_{f, theory}$** |
|---|---|---|---|---|---|---|---|
| **PBzMA-160 in [EMIM][TFSI]** | | | | | | | |
| 27 | 8.3 | 0.90 | 8.7 | 2.61 | 73 | 58 | 1.3 |
| 45 | 8.0 | 1.73 | 5.2 | 2.58 | 75 | 57 | 1.3 |
| 60 | 7.9 | 2.68 | 5.4 | 2.03 | 58 | 46 | 1.3 |
| 80 | 7.1 | 4.40 | 4.2 | 1.71 | 49 | 38 | 1.3 |
| 100 | 5.9 | 6.55 | 1.0 | 1.30 | 39 | 28 | 1.4 |
| **PBzMA-160 in [BMIM][TFSI]** | | | | | | | |
| 27 | 8.3 | 0.58 | 10 | 4.06 | 116 | 85 | 1.4 |
| 60 | 8.1 | 2.06 | 8.8 | 3.13 | 89 | 67 | 1.3 |
| 95 | 7.9 | 4.95 | 9.2 | 2.29 | 62 | 51 | 1.2 |
| 125 | 7.4 | 9.00 | 5.4 | 1.77 | 50 | 40 | 1.3 |
| 152 | 6.5 | 14.9 | 0 | 1.08 | 34 | 25 | 1.4 |

|  |  |  |  |  |  |  |  |
|---|---|---|---|---|---|---|---|
| **PBzMA-160 in [HMIM][TFSI]** |  |  |  |  |  |  |  |
| 27 | 8.4 | 0.42 | 12 | 3.62 | 101 | 77 | 1.3 |
| 60 | 8.7 | 1.56 | 13 | 3.12 | 84 | 69 | 1.2 |
| 95 | 8.1 | 4.32 | 10 | 2.75 | 76 | 60 | 1.3 |
| 130 | 7.5 | 9.12 | 6.1 | 2.24 | 64 | 49 | 1.3 |
| 155 | 7.1 | 14.2 | 3.1 | 1.89 | 56 | 41 | 1.4 |
| **PBzMA-160 in [BMP][TFSI]** |  |  |  |  |  |  |  |
| 27 | 8.5 | 0.38 | 12 | 3.70 | 103 | 79 | 1.3 |
| 60 | 8.4 | 1.40 | 13 | 3.28 | 89 | 71 | 1.3 |
| 95 | 7.7 | 3.73 | 11 | 2.79 | 76 | 59 | 1.3 |
| 130 | 6.4 | 7.74 | 7.0 | 2.36 | 66 | 48 | 1.4 |
| 155 | 6.3 | 12.3 | 2.8 | 1.79 | 53 | 37 | 1.4 |

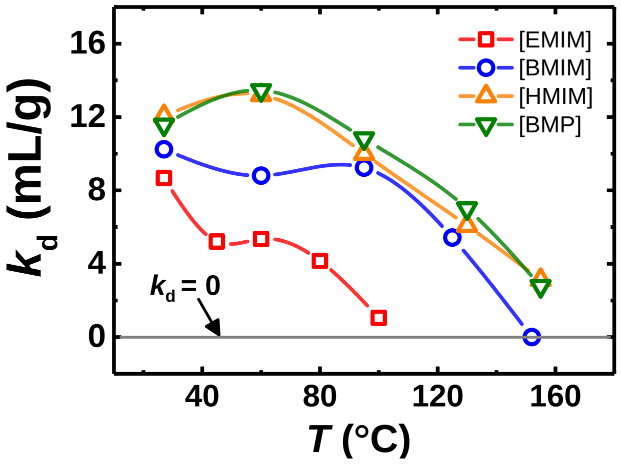

**Figure 4.18:** Temperature dependence of diffusion virial coefficient for PBzMA-160 in ILs. The solid lines are guides to the eye.

Based on our cloud point measurements and prior reports, the miscibility of PBzMA-160 decreases in the following order HMIM > BMP> BMIM > EMIM. In the case of imidazolium-based cations, a similar conclusion is inferable from the $A_2$ and $k_\mathrm{d}$ values over the temperature range of 27 °C – 100 °C (listed in Table 4.8, and shown in Figure 4.11 and Figure 4.18). In particular, the values of $A_2$ are considerably lower for PBzMA-160 in [EMIM][TFSI] compared to other ILs. This observation is further supported by the $k_\mathrm{d}$ values shown in Figure 4.18. Overall, the combined results from cloud point, SLS, and DLS measurements support a consistent picture of better solvation of PBzMA with increasing alkyl chain length of the imidazolium cation. For the case of PBzMA-160 in [BMP][TFSI], the $A_2$ and $k_\mathrm{d}$ values are larger than those obtained in [EMIM][TFSI] and [BMIM][TFSI], which is in agreement with the cloud point measurement. However, between BMP and HMIM, no significant variation in $A_2$ and $k_\mathrm{d}$ was observed. This suggests that the solvation properties [BMP][TFSI] is very similar to [HMIM][TFSI], an observation that is particularly surprising as the cloud point temperature is about 40 °C higher in [HMIM][TFSI].

The concentration dependence of $D_\mathrm{m}$ was also measured for the three lower molecular weights of PBzMA in all ILs at 27 °C (shown in Figure 4.19). The values of $k_\mathrm{d}$ and $D_0$ evaluated from the slopes and intercepts of the linear fits of $D_\mathrm{m}$ vs. $c$ plots, respectively, are listed in Table 4.9. As seen in Figure 4.20, $k_\mathrm{d}$ remains positive for PBzMA-40 and PBzMA-70, but are negative for all the cases of PBzMA-20. The negative values of $k_\mathrm{d}$ for PBzMA-20 is not surprising as the $A_2M$ term contribution is smaller for lower molecular weight polymers in the given relation, $k_\mathrm{d} = 2A_2M - k_\mathrm{f} - V_\mathrm{p}$.

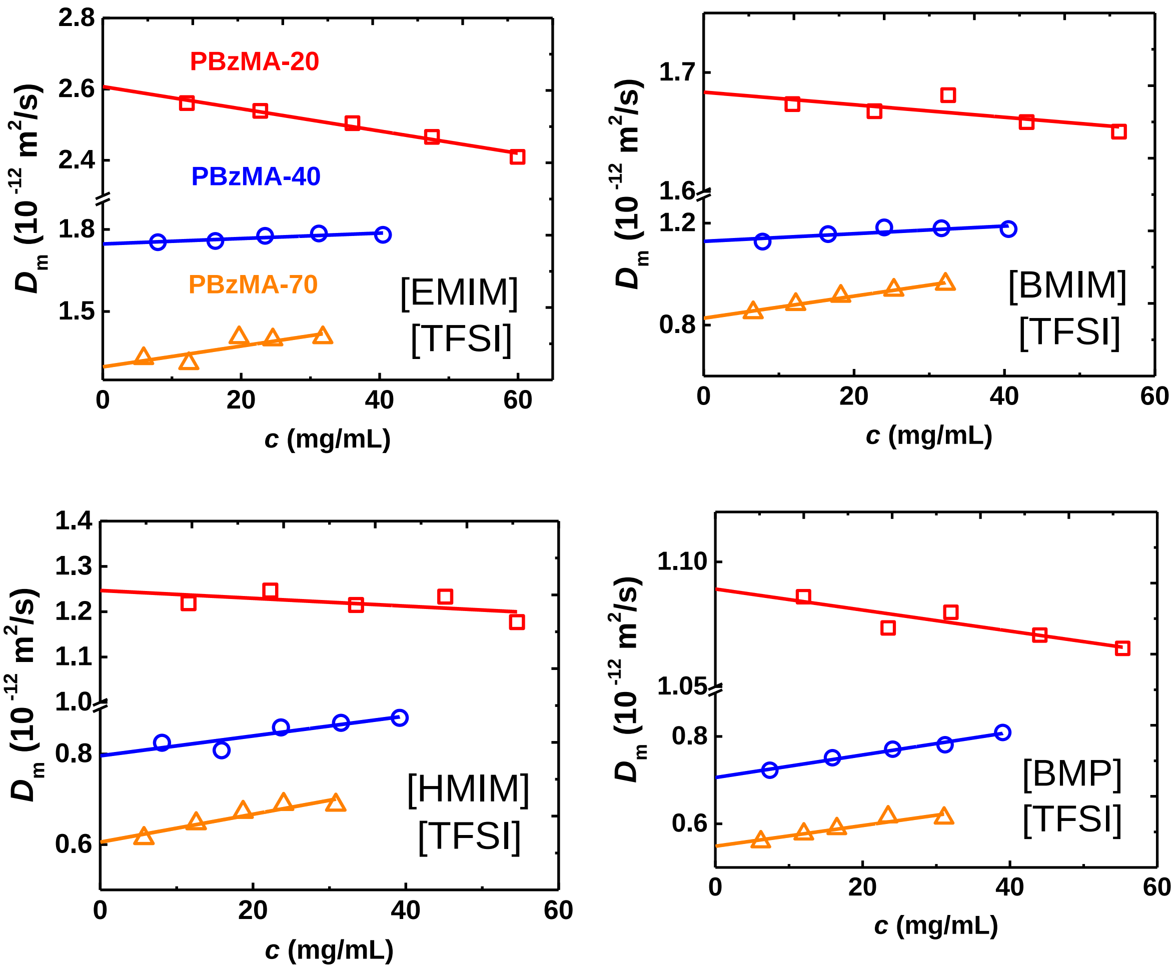

**Figure 4.19:** $D_m$ vs. $c$ for PBzMA-20 (red), PBzMA-40 (blue), and PBzMA-70 (orange) in all ILs.

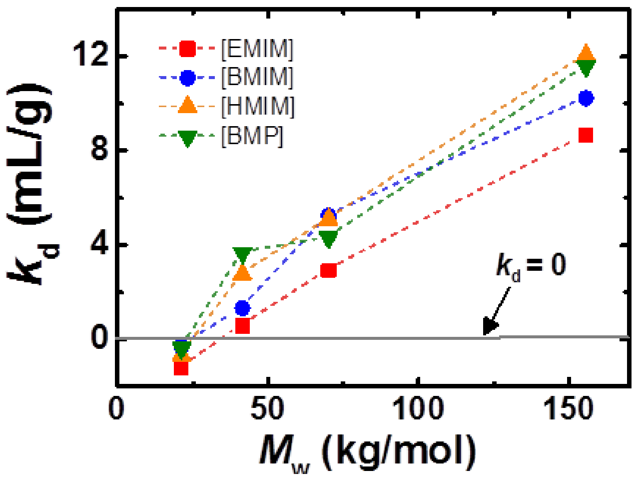

**Figure 4.20:** Dependence of $k_d$ on $M_w$ for all molecular weights of PBzMA in ILs

**Table 4.9:** $D_0$ and $k_d$ values for PBzMA in ILs at 27 °C

| **Solvent** | **$D_0$ ($10^{-13}$ m$^2$/s)** | | |
|---|---|---|---|
| | **20 k** | **40 k** | **70 k** |
| [EMIM][TFSI] | 26 | 17.5 | 13.0 |
| [BMIM][TFSI] | 16.8 | 11.2 | 8.22 |
| [HMIM][TFSI] | 12.5 | 7.96 | 6.05 |
| [BMP][TFSI] | 10.9 | 7.06 | 5.49 |
| | **$k_d$ (mL/g)** | | |
| | **20 k** | **40 k** | **70 k** |
| [EMIM][TFSI] | –1.2 | 0.6 | 2.9 |
| [BMIM][TFSI] | –0.3 | 1.3 | 5.2 |
| [HMIM][TFSI] | –0.7 | 2.8 | 5.1 |
| [BMP][TFSI] | –0.4 | 3.7 | 4.3 |

### 4.3.4 Structural properties

The infinite dilution hydrodynamic radii ($R_{\mathrm{h},0}$) were calculated from the Stokes-Einstein relation (eqn 4.11), where the solvent viscosity($\eta_{\mathrm{s}}$) was calculated using Vogel-Fulcher-Tamman (VFT) equation[178,180] given as

$$\eta_{\mathrm{s}} = \eta_0 \exp\left(\frac{B}{T - T_0}\right) \tag{4.13}$$

where $\eta_0$, $B$, $T_0$ are fitting constants listed in Table 4.10.

**Table 4.10:** Fitting parameters of eqn 4.13

| IL | $n_0$ (mPas) | $B$ (K) | $T_0$ (K) |
|---|---|---|---|
| [EMIM][TFSI][183] | 0.40 | 509 | 182 |
| [BMIM][TFSI][183] | 0.25 | 625 | 180 |
| [HMIM][TFSI][183] | 0.16 | 757 | 173 |
| [BMP][TFSI][184] | 0.29 | 651 | 181 |

Figure 4.21 shows the temperature dependence of $R_{\mathrm{h},0}$ for PBzMA-160 in all ILs and the absolute values are summarized in Table 4.11. For PBzMA-160 in [EMIM][TFSI], [BMIM][TFSI], [HMIM][TFSI], and [BMP][TFSI], $R_{\mathrm{h},0}$ decreases by approximately 30, 21, 15, 26% over the temperature range investigated, respectively. This behavior is in agreement with other LCST systems, where solvent quality worsens with increasing temperature, reducing the size of the polymer chain.

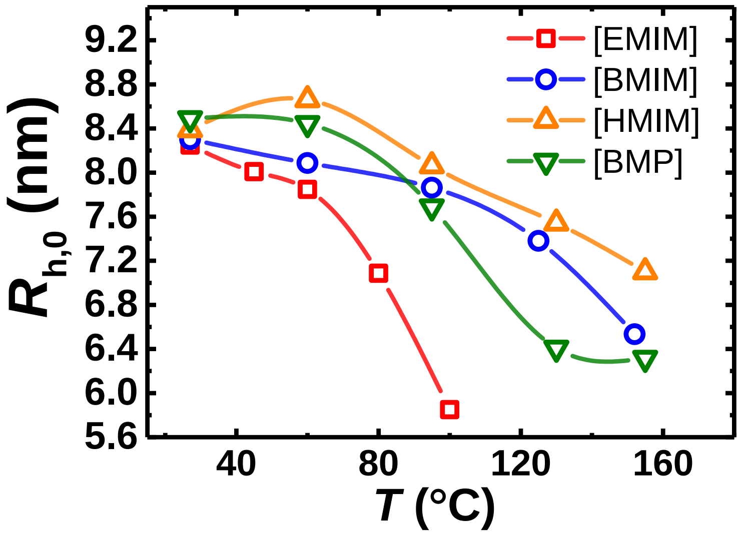

**Figure 4.21:** Temperature dependence of infinite dilution hydrodynamic radii for PBzMA-160 in ILs. The solid lines are guides to the eye.

The molecular weight dependence of both $D_0$ and $R_{h,0}$ are shown in Figure 4.22, and correspond to

$$\begin{aligned} R_{h,0} &= bM_w^{\nu} \\ D_0 &\sim M_w^{-\nu} \end{aligned} \tag{4.14}$$

**Table 4.11:** Hydrodynamic radii and scaling exponents in different ILs at 27 °C

| **Solvent** | **$R_{h,0}$ (nm)** | | | | **$R_{h,0} = b\,M_w^{\nu}$** | |
|---|---|---|---|---|---|---|
| | **20 k** | **40 k** | **70 k** | **160 k** | **$\nu$** | **$b$ (nm)** |
| [EMIM][TFSI] | 2.8 | 4.2 | 5.7 | 8.3 | 0.54 | 0.014 |
| [BMIM][TFSI] | 2.9 | 4.3 | 5.9 | 8.3 | 0.53 | 0.014 |
| [HMIM][TFSI] | 2.9 | 4.5 | 5.9 | 8.4 | 0.53 | 0.016 |
| [BMP][TFSI] | 3.0 | 4.5 | 5.9 | 8.5 | 0.53 | 0.016 |

where $\nu$ is the Flory exponent, and $b$ is the pre-factor. For flexible polymer coils, the hydrodynamic radius is related to the radius of gyration as $\rho = R_{g,0} / R_{h,0}$, where $\rho$ is approximately 1.5.[161] Due to this proportionality, $R_{g,0}$ and $R_{h,0}$ follow the same dependence on $M_w$ ($R_g \sim R_h \sim M^{\nu}$).[201] On the other hand, $D_0$ exhibits an inverse dependence. The experimental values of $\nu$ along with the individual hydrodynamic radii at 27 °C are listed in Table 4.11. The exponents lie between 0.52–0.54, indicating that all ILs are moderately good solvents for PBzMA. As previously discussed in Chapters 2 and 3, it is common to observe the value of $\nu$ between 0.5 and 0.6 due to a broad crossover between Gaussian and swollen chain behavior.[151,167] It is also possible that the values of $\nu$ would be higher if the dependence of $R_g$ on $M_w$ were determined instead. The equilibrium property, $R_g$, reflects solvent quality more directly than the dynamic property, $R_h$. As pointed out by des Cloizeaux[202] and further verified by Han and Akcazu[159], for $R_h \sim M^{\nu'}$ and $R_g \sim M^{\nu}$, $\nu' < \nu$ despite the theoretical prediction that $\nu' = \nu$.

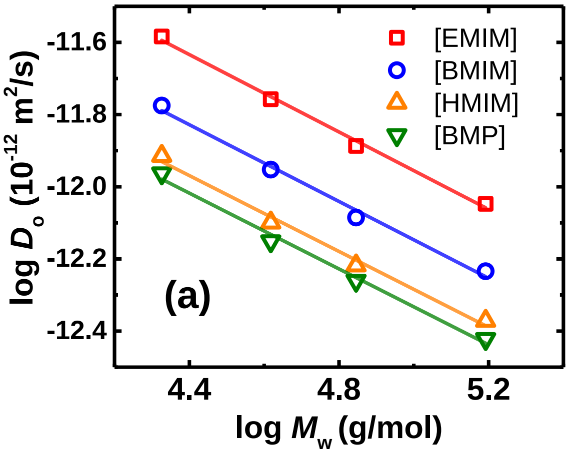

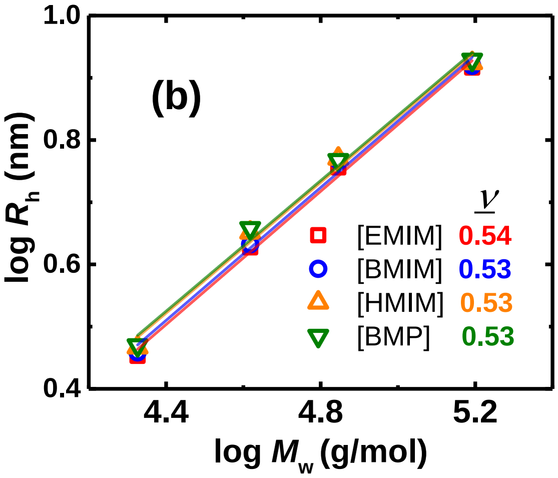

**Figure 4.22:** Infinite dilution dynamic properties of PBzMA in ILs at 27 °C. (a) log $D_0$ varies linearly with log $M_w$, where the slope yields $-\nu$. (b) $R_{h,0}$ versus $M_w$ also gives $\nu$, where $\nu$ is between 0.52 to 0.54 for all solvents. Thus, the ILs are marginally good solvents for PBzMA at 27 °C .

### 4.3.5 Summary

The static and dynamic properties of a range of molecular weights ($2\times10^4$ – $1.6\times10^5$ g/mol) of PBzMA were assessed in four different ionic liquids using light scattering. The relevant structural, dynamic, and thermodynamic parameters have been examined as a function of concentration, temperature, and molecular weight. The primary conclusions are as follows

1. Turbidimetry measurements reveal that the critical concentration is potentially shifted towards more polymer-rich composition, as opposed to lower concentrations of polymer as predicted by the original Flory Huggins theory. The phase separation temperatures increase with increasing imidazolium-cation chain length and changing the cation from imidazolium to pyrrolidinium, consistent with prior reports.

2. Using static light scattering, the second-virial coefficients were obtained for PBzMA-160 in the temperature range from 27 °C to 155 °C. $A_2$ is found to be consistently positive for all the cases. This observation is particularly surprising for PBzMA-160 in [EMIM][TFSI] and [BMIM][TFSI] as the measurements were performed close to their phase separation temperatures, where $A_2 < 0$ is anticipated. The major implication of this result is that the theta temperature ($A_2$ =0) lies above the $T_{\mathrm{cp}}$, an unusual behavior that has also been reported for HPMC in water.
3. $A_2$ was also evaluated for other molecular weights of PBzMA in all four ILs. It is found that $A_2$ exhibits a stronger dependence on $M_{\mathrm{w}}$ ($A_2 \sim M_{\mathrm{w}}^{-0.3-0.5)}$ in all cases, compared to commonly observed dependence of $A_2 \sim M_{\mathrm{w}}^{-0.2}$ for polymers in good solvents.
4. The mutual diffusion coefficients of PBzMA-160 in ILs were measured as a function of concentration at several temperatures (27 °C – 155 °C) using dynamic light scattering. The $k_d$ values obtained from the slopes of $D_{\mathrm{m}}$ vs. $c$ remain positive for almost all the cases, which further supports the positive values of $A_2$ obtained from the SLS measurements.
5. The frictional coefficients ($k_{\mathrm{f}}$) calculated from the experimental $A_2$ and $k_{\mathrm{d}}$ values are in reasonable agreement with the $k_{\mathrm{f}}$ values obtained from the theoretical predictions.
6. $R_{\mathrm{h},0}$ decreases approximately 15 – 30% with increasing $T$ for PBzMA-160 as anticipated for an LCST system, where the solvent quality worsens with increasing $T$.

7. Flory exponents obtained from the dependence of both $D_0$ and $R_{h,0}$ on $M_w$ lie between 0.52 –0.54, indicating the ILs are marginally good solvents for PBzMA at 27 °C.

## Acknowledgement

This work was supported by the National Science Foundation (DMR-1707578). We would like to thank Dr. Petr Stepanek for generously allowing us to access his high temperature light scattering instrument at the Institute of Macromolecular Chemistry, Prague, CZ. We gratefully acknowledge Dr. Peter Cernoch and Zulfiya Cernochova for their technical assistance with the light scattering measurements. We also thank Dr. Cecilia Hall for kindly providing the polymers. Helpful discussions with Dr. Svetlana Morozova are appreciated.

# Chapter 5 – Summary and Outlook

## 5.1 Thesis summary

The goal of this thesis was to expand the current understanding on solvation behavior of polymers in ILs. In this work, the solution properties of two fundamentally and technologically relevant polymers, PEO and PBzMA, were studied in varying ionic liquids, primarily using scattering techniques. As PEO is nearly isorefractive with the ILs of interest, it is very difficult to measure coil dimensions using light scattering. Therefore, we utilized small-angle neutron scattering instead, using *d*-PEO for enhanced contrast. We synthesized a wide range of accessible molecular weights (10 to 250 kg/mol) of *d*-PEO and studied their coil dimensions in [BMIM][$BF_4$]. We found an excluded volume exponent of 0.55 at 80 ºC, which strongly suggested that PEO adopts a slightly swollen, flexible coil conformation in [BMIM][$BF_4$]. Our results clarified the uncertainty surrounding PEO coil dimensions in this ionic liquid, as computer simulations at various levels of complexity have led to conflicting results, and prior experimental results also did not present a completely consistent picture. To the best of our knowledge, our work was the first report to establish the molecular weight dependence of $R_g$ for polymers and ionic liquid systems. More recently, our work has successfully guided the development of new simulation models that accurately predicted PEO chain conformation for modest chain lengths, obtaining $\nu \approx 0.56$.[203]

We extended our initial work to examine the change in coil dimensions upon varying the cation and anion structure of the ILs, and also probing the influences of temperature and added salt. For all the ILs studied at 80 °C, $0.58 \leq \nu \leq 0.60$, indicating good solvent behavior compared to *d*-PEO in [BMIM][$BF_4$] investigated previously ($\nu$ = 0.55). We reported that greater expansion of *d*-PEO coils was observed in ILs with cations with longer alkyl chains ([HMIM][$BF_4$]) and with less basic anions ([BMIM][TFSI] and [BMIM][$PF_6$]); interestingly, variation of the anion has a stronger effect. We also demonstrated that $R_{g,0}$ of *d*-PEO has a moderate dependence on temperature, and no significant variation of $R_{g,0}$ was observed in ternary mixtures containing up to 10 wt% LiTFSI.

The thermodynamic, dynamic, and structural properties of a range of molecular weights of PBzMA ($10^4$–$10^5$ kg/mol) were assessed in three different imidazolium-based ILs and one pyrrolidinium-based IL. The concentration dependence of cloud point temperatures indicated a shift in the critical composition to the polymer-rich region, a behavior that is unusual for polymer solutions. Using static light scattering, the temperature and molecular weight dependence of the second-virial coefficient were established. A stronger dependence of $A_2$ on $M_w$ ($A_2 \sim M_w^a$, $a \approx -0.3$ to $-0.5$) was observed in all ILs, compared to previous reports of polymers in good solvents ($a \approx -0.2$). $A_2$ is found to be consistently positive throughout the investigated temperature range (27 °C to 155 °C). This observation is particularly surprising for PBzMA-160 in [EMIM][TFSI] and [BMIM][TFSI], as the measurements were performed close to their phase separation temperatures, where $A_2 < 0$ is anticipated. The mutual diffusion coefficients of PBzMA-160 in ILs were measured as a function of concentration at several temperatures (27 °C – 155 °C) using dynamic light scattering. The $k_d$ values obtained from the slopes of $D_m$ vs. $c$ remain positive for almost all the cases, which further corroborates the positive values of $A_2$ obtained from the SLS measurements. The

$k_f$ values calculated from the experimental $A_2$ and $k_d$ values are in reasonable agreement with the $k_f$ values obtained from the theoretical predictions. On the structural side, $R_{h,0}$ decreases by approximately 15 – 30% with increasing $T$ for PBzMA-160 as anticipated for an LCST system, where the solvent quality worsens with increasing $T$. Flory exponents obtained from the dependence of both $D_0$ and $R_{h,0}$ on $M_w$ lie between 0.52–0.54, indicating that the ILs are marginally good solvents for PBzMA at 27 °C.

## 5.2 Outlook

Studies related to understanding the solvation behavior of polymer in ILs are still in their early stages. There are many combinations of polymers and ILs that exist, offering a wide range of solvation properties that can be probed in these systems. Therefore, many future directions exist in this field, with a few of them listed below.

1. Despite some theoretical[192,204–206]and experimental[207] investigations, the unusual phase behavior of PEO in [EMIM][$BF_4$] and [BMIM][$BF_4$] is not fully understood to date. One theoretical study has provided two main reasons for such behavior.[192] First, the structural organization of ILs lowers the entropy of mixing, and second, the stronger cohesive energy density of ILs shifts the phase diagram polymer-rich region. However, this theory doesn’t apply to a PEO derivative, PEGE in IL, which has critical concentrations located at lower polymer concentrations.[67] Therefore, further theoretical developments and experimental work is required to fully resolve the occurrence of high critical compositions for polymers and ILs systems.
2. The solvation of PBzMA in IL is also incompletely understood. The consistently positive value of $A_2$ close to phase separation temperatures is surprising, and thus

needs more detailed investigation. Some additional work could entail determining the spinodal temperatures, and the concentration dependence of the interaction parameters using SANS. Other useful direction would be to construct a full phase diagram to determine the critical points ($\phi_c$ and $T_c$) and their molecular weight dependence. The theta temperatures can be assessed from the extrapolation of $T_c$ to infinite molecular weight.

3. This thesis work can also be expanded to many other polymers and ILs with varying polymer architectures. An interesting system is PNIPAm in [EMIM][TFSI],[61] which exhibits UCST behavior in contrast to the LCST behavior of PBzMA and PEO in ILs. Furthermore, PNIPAm system is viable in light scattering due to considerable contrast between the polymer and IL. Another system that could be studied is a PBzMA derivative, poly(2-phenylethyl methacrylate) (PPhEtMA) in [EMIM][TFSI],[76] which also offers contrast in light scattering. The phase separation for this system is approximately 60 °C lower than PBzMA, which allows the opportunity to study solvation properties at relatively accessible temperatures (25 – 50 °C).

4. Our work investigated the static and dynamic properties of polymers in ILs using scattering techniques. Future studies can investigate the rheological properties of these systems. There is an increasing amount of work put into characterizing the viscoelastic behavior of biopolymers[103,104,208,209] and a few other synthetic polymers in ILs.[105,106,207,210,211] However, there are many interesting systems discussed in Chapter 1 that can be explored from the perspective of rheology.

5. Prior work (discussed in Chapter 1) including this thesis, has focused on evaluating solvation behavior of polymer solutions in the limit of infinite dilution. In the future,

it would be interesting to probe the semi-dilute and concentrated regimes. A combination of techniques such as SANS and rheology are particularly useful to assess solution properties in concentrated regimes.

6. The ionic nature of ionic liquids make them unique compared to traditional molecular solvents. The investigation of the solution behavior of polyelectrolyte in ionic liquids is also a topic of great interest. A relatively recent work has been conducted for two negatively charged polyelectrolytes, DNA and polystyrene sulfonate, in ILs.[89] However, many other polyelectrolyte systems and their solution properties are yet to be mapped out in detail.

# Bibliography

(1) MacFarlane, D. R.; Kar, M.; Pringle, J. M. *Fundamentals of Ionic Liquids*; Wiley: Weinheim, Germany, 2017.

(2) Mallakpour, S.; Dinari, M. *Ionic Liquids as Green Solvents: Progress and Prospects*; Springer Netherlands: Dordrecht, 2012.

(3) Marsh, K.; Boxall, J.; Lichtenthaler, R. Room temperature ionic liquids and their mixtures−a review. *Fluid Phase Equilib.* **2004**, *219*, 93–98.

(4) Berthod, A.; Ruiz-Ángel, M. J.; Carda-Broch, S. Ionic liquids in separation techniques. *J. Chromatogr. A* **2008**, *1184*, 6–18.

(5) Welton, T. Room-temperature ionic liquids. Solvents for synthesis and catalysis. *Chem. Rev.* **1999**, *99*, 2071−2083.

(6) Rogers, R. D.; Seddon, K. R. Perspective article: Ionic liquids solvents of the future? *Science* **2003**, *302*, 792.

(7) Cassol, C. C.; Ebeling, G.; Ferrera, B.; Dupont, J. A simple and practical method for the preparation and purity determination of halide-free imidazolium ionic liquids. *Adv. Synth. Catal.* **2006**, *348*, 243–248.

(8) Scammells, P. J.; Scott, J. L.; Singer, R. D. Ionic liquids: the neglected issues. *Aust. J. Chem.* **2005**, *58*, 155.

(9) Wasserscheid, P.; Welton, T. *Ionic Liquids in Synthesis*; Wiley-VCH, 2002; Vol.

7.

(10) Schröder, U.; Wadhawan, J. D.; Compton, R. G.; Marken, F.; Suarez, P. A. Z.; Consorti, C. S.; de Souza, R. F.; Dupont, J. Water-induced accelerated ion diffusion: voltammetric studies in 1-methyl-3-[2,6-(s)-dimethylocten-2-yl]imidazolium tetrafluoroborate, 1-butyl-3-methylimidazolium tetrafluoroborate and hexafluorophosphate ionic liquids. *New J. Chem.* **2000**, *24*, 1009–1015.

(11) Shin, J. Ionic liquids to the rescue? Overcoming the ionic conductivity limitations of polymer electrolytes. *Electrochem. commun.* **2003**, *5*, 1016–1020.

(12) Tokuda, H.; Tsuzuki, S.; Susan, M. A. B. H.; Hayamizu, K.; Watanabe, M. How ionic are room-temperature ionic liquids? An indicator of the physicochemical properties. *J. Phys. Chem. B* **2006**, *110*, 19593–19600.

(13) Zhao, D.; Liao, Y.; Zhang, Z. Toxicity of ionic liquids. *Clean Soil Air Water* **2007**, *35*, 42–48.

(14) Thuy Pham, T. P.; Cho, C.-W.; Yun, Y.-S. Environmental fate and toxicity of ionic liquids: a review. *Water Res.* **2010**, *44*, 352–372.

(15) Ueki, T.; Watanabe, M. Polymer in ionic liquids: Dawn of neoteric solvents and innovative materials. *Bull. Chem. Soc. Jpn.* **2012**, *85*, 33–50.

(16) Ueki, T.; Watanabe, M. Macromolecules in ionic liquids: progress, challenges, and opportunities. *Macromolecules* **2008**, *41*, 3739–3749.

(17) Crowhurst, L.; Mawdsley, P. R.; Perez-Arlandis, J. M.; Salter, P. A.; Welton, T.

Solvent-solute interactions in ionic liquids. *Phys. Chem. Chem. Phys.* **2003**, *5*, 2790–2794.

(18) Xie, H.; Li, S.; Zhang, S. Ionic liquids as novel solvents for the dissolution and blending of wool keratin fibers. *Green Chem.* **2005**, *7*, 606–608.

(19) Liu, Q.; Janssen, M. H. A.; Van Rantwijk, F.; Sheldon, R. A. Room-temperature ionic liquids that dissolve carbohydrates in high concentrations. *Green Chem.* **2005**, *7*, 39–42.

(20) Zhang, J.; Wu, J.; Yu, J.; Zhang, X.; He, J.; Zhang, J. Application of ionic liquids for dissolving cellulose and fabricating cellulose-based materials: state of the art and future trends. *Mater. Chem. Front.* **2017**, *1*, 1273–1290.

(21) Zhao, B.; Greiner, L.; Leitner, W. Cellulose solubilities in carboxylate-based ionic liquids. *RSC Adv.* **2012**, *2*, 2476–2479.

(22) Kubisa, P. Ionic liquids as solvents for polymerization processes-progress and challenges. *Prog. Polym. Sci.* **2009**, *34*, 1333–1347.

(23) Kubisa, P. Application of ionic liquids as solvents for polymerization processes. *Prog. Polym. Sci.* **2004**, *29*, 3–12.

(24) Shen, Y.; Tang, H.; Ding, S. Catalyst separation in atom transfer radical polymerization. *Prog. Polym. Sci.* **2004**, *29*, 1053–1078.

(25) Harrisson, S.; Mackenzie, S. R.; Haddleton, D. M. Unprecedented solvent-induced acceleration of free-radical propagation of methyl methacrylate in ionic liquids.

*Chem. Commun.* **2002**, *23*, 2850–2851.

(26) Ye, Y. S.; Rick, J.; Hwang, B. J. Ionic liquid polymer electrolytes. *J. Mater. Chem. A* **2013**, *1*, 2719–2743.

(27) Sato, T.; Masuda, G.; Takagi, K. Electrochemical properties of novel ionic liquids for electric double layer capacitor applications. *Electrochim. Acta* **2004**, *49*, 3603–3611.

(28) Choi, J. H.; Xie, W.; Gu, Y.; Frisbie, C. D.; Lodge, T. P. Single ion conducting, polymerized ionic liquid triblock copolymer films: high capacitance electrolyte gates for n-type transistors. *ACS Appl. Mater. Interfaces* **2015**, *7*, 7294–7302.

(29) Mecerreyes, D. Polymeric ionic liquids: Broadening the properties and applications of polyelectrolytes. *Prog. Polym. Sci.* **2011**, *36*, 1629–1648.

(30) Gu, Y.; Lodge, T. P. Synthesis and gas separation performance of triblock copolymer ion gels with a polymerized ionic liquid mid-block. *Macromolecules* **2011**, *44*, 1732–1736.

(31) Chopade, S. A.; So, S.; Hillmyer, M. A.; Lodge, T. P. Anhydrous proton conducting polymer electrolyte membranes via polymerization-induced microphase separation. *ACS Appl. Mater. Interfaces* **2016**, *8*, 6200–6210.

(32) Chopade, S. A.; Au, J. G.; Li, Z.; Schmidt, P. W.; Hillmyer, M. A.; Lodge, T. P. Robust polymer electrolyte membranes with high ambient-temperature lithium-ion conductivity via polymerization-induced microphase separation. *ACS Appl. Mater.*

*Interfaces* **2017**, *9*, 14561–14565.

(33) Osada, I.; de Vries, H.; Scrosati, B.; Passerini, S. Ionic-liquid-based polymer electrolytes for battery applications. *Angew.Chem. Int. Ed.* **2016**, *55*, 500–513.

(34) Ketabi, S.; Lian, K. Thermal and structural characterizations of PEO-EMIHSO$_4$ polymer electrolytes. *Solid State Ionics* **2012**, *227*, 86–90.

(35) Jeddi, K.; Qazvini, N. T.; Cangialosi, D.; Chen, P. Correlation between segmental dynamics, glass transition, and lithium ion conduction in poly(methyl methacrylate)/ionic liquid mixture. *J. Macromol. Sci. Part B Phys.* **2013**, *52,* 590–603.

(36) Xue, Z.; He, D.; Xie, X. Poly(ethylene oxide)-based electrolytes for lithium-ion batteries. *J. Mater. Chem. A* **2015**, *3*, 19218–19253.

(37) Sutto, T. E. The electrochemical behavior of trialkylimidazolium imide based ionic liquids and their polymer gel electrolytes. *J. Electrochem. Soc.* **2007**, *154*, 130–135.

(38) Lewandowski, A.; Świderska, A. New composite solid electrolytes based on a polymer and ionic liquids. *Solid State Ionics* **2004**, *169,* 21–24.

(39) Shin, J.-H.; Henderson, W. A.; Passerini, S. PEO-based polymer electrolytes with ionic liquids and their use in lithium metal-polymer electrolyte batteries. *J. Electrochem. Soc.* **2005**, *152*, A978–A983.

(40) Ohno, H.; Ito, K. Room-temperature molten salt polymers as a matrix for fast ion

conduction. *Chem. Lett.* **1998**, *27*, 751–752.

(41) Yuan, J.; Mecerreyes, D.; Antonietti, M. Poly(ionic liquid)s: an update. *Prog. Polym. Sci.* **2013**, *38*, 1009–1036.

(42) Wu, B.; Zhang, Z. W.; Huang, M. H.; Peng, Y. Polymerizable ionic liquids and polymeric ionic liquids: facile synthesis of ionic liquids containing ethylene oxide repeating unit: via methanesulfonate and their electrochemical properties. *RSC Adv.* **2017**, *7*, 5394–5401.

(43) Jana, S.; Parthiban, A.; Chai, C. L. L. Transparent, flexible and highly conductive ion gels from ionic liquid compatible cyclic carbonate network. *Chem. Commun.* **2010**, *46*, 1488–1490.

(44) Susan, M. A. B. H.; Kaneko, T.; Noda, A.; Watanabe, M. Ion gels prepared by in situ radical polymerization of vinyl monomers in an ionic liquid and their characterization as polymer electrolytes. *J. Am. Chem. Soc.* **2005**, *127*, 4976–4983.

(45) Noro, A.; Matsushita, Y.; Lodge, T. P. Gelation mechanism of thermoreversible supramacromolecular ion gels via hydrogen bonding. *Macromolecules* **2009**, *42*, 5802–5810.

(46) Matsumoto, K.; Endo, T. Synthesis of ion conductive networked polymers based on an ionic liquid epoxide having a quaternary ammonium salt structure. *Macromolecules* **2009**, *42*, 4580–4584.

(47) He, Y.; Lodge, T. P. Thermoreversible ion gels with tunable melting temperatures

from triblock and pentablock copolymers. *Macromolecules* **2008**, *41*, 167–174.

(48) He, Y.; Boswell, P. G.; Bühlmann, P.; Lodge, T. P. Ion gels by self-assembly of a triblock copolymer in an ionic liquid. *J. Phys. Chem. B* **2007**, *111*, 4645–4652.

(49) He, Y.; Lodge, T. P. A thermoreversible ion gel by triblock copolymer self-assembly in an ionic liquid. *Chem. Commun.* **2007**, *41*, 2732–2734.

(50) Cho, J. H.; Lee, J.; Xia, Y.; Kim, B.; He, Y.; Renn, M. J.; Lodge, T. P.; Daniel Frisbie, C. Printable ion-gel gate dielectrics for low-voltage polymer thin-film transistors on plastic. *Nat. Mater.* **2008**, *7*, 900–906.

(51) Gray, F. M.; MacCallum, J. R.; Vincent, C. A.; Giles, J. R. M. Novel polymer electrolytes based on ABA block copolymers. *Macromolecules* **1988**, *21*, 392–397.

(52) Lee, K. H.; Kang, M. S.; Zhang, S.; Gu, Y.; Lodge, T. P.; Frisbie, C. D. “Cut and stick” rubbery ion gels as high capacitance gate dielectrics. *Adv. Mater.* **2012**, *24*, 4457–4462.

(53) Snedden, P.; Cooper, A. I.; Scott, K.; Winterton, N. Cross-linked polymer-ionic liquid composite materials. *Macromolecules* **2003**, *36*, 4549–4556.

(54) Flory, P. J. *Principles of Polymer Chemistry*; Cornell University Press: New York, 1953.

(55) Tsuyumoto, M.; Einaga, Y.; Fujita, H. Phase equilibrium of the ternary system consisting of two monodisperse polystyrenes and cyclohexane. *Polym. J.* **2006**, *16*, 229–240.

(56) Fujishige, S.; Kubota, K.; Ando, I. Phase transition of aqueous solutions of poly(n-isopropylacrylamide) and poly(n-isopropylmethacrylamide). *J. Phys. Chem.* **1989**, *93*, 3311–3313.

(57) Lee, H. N.; Rosen, B. M.; Fenyvesi, G.; Sunkara, H. B. UCST and LCST phase behavior of poly(trimethylene ether) glycol in water. *J. Polym. Sci. Part A Polym. Chem.* **2012**, *50*, 4311–4315.

(58) Seuring, J.; Agarwal, S. First example of a universal and cost-effective approach: Polymers with tunable upper critical solution temperature in water and electrolyte solution. *Macromolecules* **2012**, *45*, 3910–3918.

(59) Maeda, Y.; Nakamura, T.; Ikeda, I. Hydration and phase behavior of poly(n-vinylcaprolactam) and poly(n-vinylpyrrolidone) in water. *Macromolecules* **2002**, *35*, 217–222.

(60) Ward, M. A.; Georgiou, T. K. Thermoresponsive terpolymers based on methacrylate monomers: effect of architecture and composition. *J. Polym. Sci. Part A Polym. Chem.* **2010**, *48*, 775–783.

(61) Ueki, T.; Watanabe, M. Upper critical solution temperature behavior of poly(n-isopropylacrylamide) in an ionic liquid and preparation of thermo-sensitive nonvolatile gels. *Chem. Lett.* **2006**, *35*, 964–965.

(62) Nayak, P. K.; Hathorne, A. P.; Bermudez, H. Critical solution behavior of poly(n-isopropylacrylamide) in ionic liquid–water mixtures. *Phys. Chem. Chem. Phys.* **2013**, *15*, 1806–1809.

(63) Ueki, T. Stimuli-responsive polymers in ionic liquids. *Polym. J.* **2014**, *46*, 1–10.

(64) Rodríguez, H.; Francisco, M.; Rahman, M.; Sun, N.; Rogers, R. D. Biphasic liquid mixtures of ionic liquids and polyethylene glycols. *Phys. Chem. Chem. Phys.* **2009**, *11*, 10916–10922.

(65) Lee, H.-N.; Newell, N.; Bai, Z.; Lodge, T. P. Unusual lower critical solution temperature phase behavior of poly(ethylene oxide) in ionic liquids. *Macromolecules* **2012**, *45*, 3627–3633.

(66) Lee, H.-N.; Lodge, T. P. Lower critical solution temperature (LCST) phase behavior of poly(ethylene oxide) in ionic liquids. *J. Phys. Chem. Lett.* **2010**, *1*, 1962–1966.

(67) Tsuda, R.; Kodama, K.; Ueki, T.; Kokubo, H.; Imabayashi, S.; Watanabe, M. LCST-type liquid-liquid phase separation behaviour of poly(ethylene oxide). *Chem. Commun.* **2008**, *40*, 4939–4941.

(68) Kodama, K.; Nanashima, H.; Ueki, T.; Kokubo, H.; Watanabe, M. Lower critical solution temperature phase behavior of linear polymers in imidazolium-based ionic liquids: Effects of structural modifications. *Langmuir* **2009**, *25*, 3820–3824.

(69) Kobayashi, Y.; Kitazawa, Y.; Hashimoto, K.; Ueki, T.; Kokubo, H.; Watanabe, M. Thermosensitive phase separation behavior of poly(benzyl methacrylate)/solvate ionic liquid solutions. *Langmuir* **2017**, *33*, 14105–14114.

(70) Ueki, T.; Karino, T.; Kobayashi, Y.; Shibayama, M.; Watanabe, M. Difference in

lower critical solution temperature behavior between random copolymers and a homopolymer having solvatophilic and solvatophobic structures in an ionic liquid. *J. Phys. Chem. B* **2007**, *111*, 4750–4754.

(71) Lee, H. N.; Lodge, T. P. Poly (n-butyl methacrylate) in ionic liquids with tunable lower critical solution temperature (LCST). *J. Phys. Chem.* **2010**, *115*, 1971–1977.

(72) Hoarfrost, M. L.; He, Y.; Lodge, T. P. Lower critical solution temperature phase behavior of poly(n-butyl methacrylate) in ionic liquid mixtures. *Macromolecules* **2013**, *46*, 9464–9472.

(73) Ueki, T.; Arai, A. A.; Kodama, K.; Kaino, S.; Takada, N.; Morita, T.; Nishikawa, K.; Watanabe, M. Thermodynamic study on phase transitions of poly(benzyl methacrylate) in ionic liquid solvents. *Pure Appl. Chem.* **2009**, *81*, 1829–1841.

(74) Ueki, T.; Watanabe, M. Lower critical solution temperature behavior of linear polymers in ionic liquids and the corresponding volume phase transition of polymer gels. *Langmuir* **2007**, *23*, 988–990.

(75) Ueki, T.; Karino, T.; Kobayashi, Y.; Shibayama, M.; Watanabe, M. Difference in lower critical solution temperature behavior between random copolymers and a homopolymer having solvatophilic and solvatophobic structures in an ionic liquid. *J. Phys. Chem. B* **2007**, *111*, 4750–4754.

(76) Hirosawa, K.; Fujii, K.; Ueki, T.; Kitazawa, Y.; Littrell, K. C.; Watanabe, M.; Shibayama, M. SANS study on the solvated structure and molecular interactions of a thermo-responsive polymer in a room temperature ionic liquid. *Phys. Chem.*

*Chem. Phys.* **2016**, *18*, 17881–17889.

(77) Kitazawa, Y.; Ueki, T.; Niitsuma, K.; Imaizumi, S.; Lodge, T. P.; Watanabe, M. Thermoreversible high-temperature gelation of an ionic liquid with poly(benzyl methacrylate-b-methylmethacrylate-b-benzylmethacrylate) triblock copolymer. *Soft Matter* **2012**, *8*, 8067–8074.

(78) Hoarfrost, M. L.; Lodge, T. P. Effects of solvent quality and degree of polymerization on the critical micelle temperature of poly(ethylene oxide-b-n-butyl methacrylate) in ionic liquids. *Macromolecules* **2014**, *47*, 1455–1461.

(79) Lodge, T. P. A unique platform for materials design. *Science* **2008**, *321*, 50–51.

(80) Lodge, T. P.; Ueki, T. Mechanically tunable, readily processable ion gels by self-assembly of block copolymers in ionic liquids. *Acc. Chem. Res.* **2016**, *49*, 2107–2114.

(81) Tamura, S.; Ueki, T.; Ueno, K.; Kodama, K.; Watanabe, M. Thermosensitive self-assembly of diblock copolymers with lower critical micellization temperatures in an ionic liquid. *Macromolecules* **2009**, *42*, 6239–6244.

(82) Ueki, T.; Watanabe, M.; Lodge, T. P. Doubly thermosensitive self-assembly of diblock copolymers in ionic liquids. *Macromolecules* **2009**, *42*, 1315–1320.

(83) Sharma, N.; Lakhman, R. K.; Zhou, Y.; Kasi, R. M. Physical gels of [BMIM][$BF_4$ ] by n-tert-butylacrylamide/ethylene oxide based triblock copolymer self-assembly: synthesis, thermomechanical, and conducting properties. *J. Appl. Polym.*

*Sci.* **2013**, *128*, 3982–3992.

(84) Ueki, T.; Nakamura, Y.; Lodge, T. P.; Watanabe, M. Light-controlled reversible micellization of a diblock copolymer in an ionic liquid. *Macromolecules* **2012**, *45*, 7566–7573.

(85) Ueki, T.; Nakamura, Y.; Yamaguchi, A.; Niitsuma, K.; Lodge, T. P.; Watanabe, M. UCST phase transition of azobenzene-containing random copolymer in an ionic liquid. *Macromolecules* **2011**, *44*, 6908–6914.

(86) Hall, C. C.; Lodge, T. P. Photoreversible order-disorder transition in an ionic liquid solvated block polymer. *ACS Macro Lett.* **2019**, *8*, 393–398.

(87) Asai, H.; Fujii, K.; Ueki, T.; Sawamura, S.; Nakamura, Y.; Kitazawa, Y.; Watanabe, M.; Han, Y.-S.; Kim, T.-H.; Shibayama, M. Structural study on the ucst-type phase separation of poly(n-isopropylacrylamide) in ionic liquid. *Macromolecules* **2013**, *46*, 1101–1106.

(88) Fujii, K.; Ueki, T.; Niitsuma, K.; Matsunaga, T.; Watanabe, M.; Shibayama, M. Structural aspects of the lcst phase behavior of poly(benzyl methacrylate) in room-temperature ionic liquid. *Polymer* **2011**, *52*, 1589–1595.

(89) Chen, Y.; Zhang, Y.; Ke, F.; Zhou, J.; Wang, H.; Liang, D. Solubility of neutral and charged polymers in ionic liquids studied by laser light scattering. *Polymer* **2011**, *52*, 481–488.

(90) Mondal, J.; Choi, E.; Yethiraj, A. Atomistic simulations of poly(ethylene oxide) in

water and an ionic liquid at room temperature. *Macromolecules* **2014**, *47*, 438–446.

(91) Choi, E.; Yethiraj, A. Conformational properties of a polymer in an ionic liquid: computer simulations and integral equation theory of a coarse-grained model. *J. Phys. Chem. B* **2015**, *119*, 9091–9097.

(92) McDaniel, J. G.; Choi, E.; Son, C.-Y.; Schmidt, J. R.; Yethiraj, A. Conformational and dynamic properties of poly(ethylene oxide) in an ionic liquid: development and implementation of a first-principles force field. *J. Phys. Chem. B* **2016**, *120*, 231–243.

(93) Triolo, A.; Russina, O.; Keiderling, U.; Kohlbrecher, J. Morphology of poly(ethylene oxide) dissolved in a room temperature ionic liquid: a small angle neutron scattering study. *J. Phys. Chem. B* **2006**, *110*, 1513–1515.

(94) Werzer, O.; Warr, G. G.; Atkin, R. Conformation of poly(ethylene oxide) dissolved in ethylammonium nitrate. *J. Phys. Chem. B* **2011**, *115*, 648–652.

(95) Chen, Z.; McDonald, S.; Fitzgerald, P. A.; Warr, G. G.; Atkin, R. Structural effect of glyme–Li+ salt solvate ionic liquids on the conformation of poly(ethylene oxide). *Phys. Chem. Chem. Phys.* **2016**, *18*, 14894–14903.

(96) Stefanovic, R.; Chen, Z.; Fitzgerald, P. A.; Warr, G. G.; Atkin, R.; Page, A. J.; Webber, G. B. Effect of halides on the solvation of poly(ethylene oxide ) in the ionic liquid propylammonium nitrate. *J. Colloid Interface Sci.* **2019**, *534*, 649–654.

(97) Chen, Z.; FitzGerald, P. A.; Warr, G. G.; Atkin, R. Conformation of poly(ethylene oxide) dissolved in the solvate ionic liquid [Li(G4)]TFSI. *Phys. Chem. Chem. Phys.* **2015**, *17*, 14872–14878.

(98) Chen, Z.; Mcdonald, S.; Fitzgerald, P.; Warr, G. G.; Atkin, R. Small angle neutron scattering study of the conformation of poly(ethylene oxide ) dissolved in deep eutectic solvents. *J. Colloid Interface Sci.* **2017**, *506*, 486–492.

(99) de Gennes, P.-G. *Scaling Concepts in Polymer Physics*; Cornell University Press: New York, 1979.

(100) Liu, F.; Lv, Y.; Liu, J.; Yan, Z. C.; Zhang, B.; Zhang, J.; He, J.; Liu, C. Y. Crystallization and rheology of poly(ethylene oxide) in imidazolium ionic liquids. *Macromolecules* **2016**, *49*, 6106–6115.

(101) Haward, S. J.; Sharma, V.; Butts, C. P.; McKinley, G. H.; Rahatekar, S. S. Shear and extensional rheology of cellulose/ionic liquid solutions. *Biomacromolecules* **2012**, *13*, 1688–1699.

(102) Mehrdad, A.; Niknam, Z. Investigation on the interactions of poly(ethylene oxide) and ionic liquid 1-butyl-3-methyl-imidazolium bromide by viscosity and spectroscopy. *J. Chem. Eng. Data* **2016**, *61*, 1700–1709.

(103) Zhu, X.; Chen, X.; Wang, X.; Saba, H.; Zhang, Y.; Wang, H. Understanding the interactions in acrylic copolymer/1-butyl-3-methylimidazolium chloride from solution rheology. *Polym. Adv. Technol.* **2013**, *24*, 90–96.

(104) Zhu, X.; Chen, X.; Saba, H.; Zhang, Y.; Wang, H. Linear viscoelasticity of poly(acrylonitrile-co-itaconic acid)/1-butyl-3-methylimidazolium chloride extended from dilute to concentrated solutions. *Eur. Polym. J.* **2012**, *48*, 597–603.

(105) Smith, J. A.; Webber, G. B.; Warr, G. G.; Zimmer, A.; Atkin, R.; Werzer, O. Shear dependent viscosity of poly(ethylene oxide) in two protic ionic liquids. *J. Colloid Interface Sci.* **2014**, *430*, 56–60.

(106) Mehrdad, A.; Shekaari, H.; Niknam, Z. Effect of ionic liquid on the intrinsic viscosity of polyvinyl pyrrolidone in aqueous solutions. *Fluid Phase Equilib.* **2013**, *353*, 69–75.

(107) Gericke, M.; Schlufter, K.; Liebert, T.; Heinze, T.; Budtova, T. Rheological properties of cellulose/ionic liquid solutions : from dilute to concentrated states. *Biomacromolecules* **2009**, No. 10, 1188–1194.

(108) Winterton, N. Solubilization of polymers by ionic liquids. *J. Mater. Chem.* **2006**, *16*, 4281–4293.

(109) Wang, Z.-G. 50th anniversary perspective : polymer conformation—a pedagogical review. *Macromolecules* **2017**, *50*, 9073−9114.

(110) Xu, Z.; Hadjichristidis, N.; Fetters, L. J.; Mays, J. W. Structure/chain-flexibility relationships of polymers. In *Physical Properties of Polymers*; Springer Berlin Heidelberg, 1995; pp 1–50.

(111) Lodge, T. P.; Hiemenz, P. C. *Polymer Chemistry*, 2nd ed.; CRC Press, 2007.

(112) Flory, P. J. The configuration of real polymer chains. *J. Chem. Phys.* **1949**, *17*.

(113) Flory, P. J. *Statistical Mechanics of Chain Molecules*; Interscience Publishers, 1969.

(114) Freed, K. F. Concentration and excluded volume dependence of coherent scattering functions for polymers: chain conformational space renormalization group. *J. Chem. Phys.* **1983**, *79*, 6357–6371.

(115) Pfeuty, P.; Velasco, R. M.; de Gennes, P. G. Conformation properties of one isolated polyelectrolyte chain in d dimensions. *J. Phys. Lettres* **2007**, *38*, 5–7.

(116) Terao, K.; Nakamura, Y.; Norisuye, T. Solution properties of polymacromonomers consisting of polystyrene. 2. Chain dimensions and stiffness in cyclohexane and toluene. *Macromolecules* **1999**, *32*, 711–716.

(117) Sperling, L. H. Characterization of polymer conformation and morphology through small-angle neutron scattering—a literature review. *Polym. Eng. Sci.* **1984**, *24*, 1–21.

(118) Dondos, A.; Benoit, H. The influence of solvents on unperturbed dimensions of polymer in solution. *Macromolecules* **1971**, *4*, 279–283.

(119) Yamakawa, H. Concentration dependence of polymer chain configurations in solution. *J. Chem. Phys.* **1961**, *34*, 1360–1372.

(120) Hoeve, C. A. J. Unperturbed chain dimensions of polymeric chains. *J. Chem. Phys.* **1960**, *32*, 888–893.

(121) Devanand, K.; Selser, J. C. Asymptotic behavior and long-range interactions in aqueous solutions of poly(ethylene oxide). *Macromolecules* **1991**, *24*, 5943–5947.

(122) Miyaki, Y.; Einaga, Y.; Fujita, H. Excluded-volume effects in dilute polymer solutions.7. Very high molecular weight polystyrene in benzene and cyclohexane. *Macromolecules* **1978**, *11*, 1180–1186.

(123) Choi, J. W.; Cheruvally, G.; Kim, Y. H.; Kim, J. K.; Manuel, J.; Raghavan, P.; Ahn, J. H.; Kim, K. W.; Ahn, H. J.; Choi, D. S. Poly(ethylene oxide)-based polymer electrolyte incorporating room-temperature ionic liquid for lithium batteries. *Solid State Ionics* **2007**, *178*, 1235–1241.

(124) Phys, J. C.; Costa, L. T.; Sun, B.; Jeschull, F.; Brandell, D. Polymer-ionic liquid ternary systems for Li- battery electrolytes : molecular dynamics studies of litfsi in a emim-tfsi and peo blend. **2017**, *024904*.

(125) Shin, J.-H.; Henderson, W. A.; Passerini, S. PEO-based polymer electrolytes with ionic liquids and their use in lithium metal-polymer electrolyte batteries. *J. Electrochem. Soc.* **2005**, *152*, A978–A983.

(126) de Vries, H.; Jeong, S.; Passerini, S. Ternary polymer electrolytes incorporating pyrrolidinium-imide ionic liquids. *RSC Adv.* **2015**, *5*, 13598–13606.

(127) Zhang, S.; Lee, K. H.; Frisbie, C. D.; Lodge, T. P. Ionic conductivity, capacitance, and viscoelastic properties of block copolymer-based ion gels. *Macromolecules* **2011**, *44*, 940–949.

(128) Gu, Y.; Zhang, S.; Martinetti, L.; Lee, K. H.; McIntosh, L. D.; Frisbie, C. D.; Lodge, T. P. High toughness, high conductivity ion gels by sequential triblock copolymer self-assembly and chemical cross-linking. *J. Am. Chem. Soc.* **2013**, *135*, 9652–9655.

(129) Lodge, T.P. Characterization of polymer materials by scattering techniques, with applications to block copolymers. *Microchim. Acta* **1994**, *116*, 1–31.

(130) Montalbán, M. G.; Bolívar, C. L.; Díaz Baños, F. G.; Víllora, G. Effect of temperature, anion, and alkyl chain length on the density and refractive index of 1-alkyl-3-methylimidazolium-based ionic liquids. *J. Chem. Eng. Data* **2015**, *60*, 1986–1996.

(131) Mark, J. E. *Physical Properties of Polymers Handbook*; Springer New York, 2007.

(132) Wignall, G. D.; Melnichenko, Y. B. Recent applications of small-angle neutron scattering in strongly interacting soft condensed matter. *Reports Prog. Phys.* **2005**, *68*, 1761.

(133) Stefanovic, R.; Chen, Z.; FitzGerald, P. A.; Warr, G. G.; Atkin, R.; Page, A. J.; Webber, G. B. Effect of halides on the solvation of poly(ethylene oxide) in the ionic liquid propylammonium nitrate. *J. Colloid Interface Sci.* **2019**, *534*, 649–654.

(134) Szwarc, M. *Living Polymers and Mechanisms of Anionic Polymerization*; Advances in Polymer Science; Springer Berlin Heidelberg, 2014.

(135) Eisenbach, C. D.; Peuscher, M.; Wegner, G.; Weiss, M. Synthesis of

poly(ethylene-d4 oxide ) with unimodal and narrow molecular weight distribution. **1983**, *184*, 2313–2323.

(136) Eisenbach, C. D.; Peuscher, M. Some aspects on the anionic preparation and solution properties of poly(ethylene oxide). *Makromol. Chem., Rapid Commun.* **1980**, *12*, 105–112.

(137) Boileau, S.; Deffieux, A.; Lassalle, D.; Menezes, F.; Vidal, B. Reactivities of anionic species for the ring opening of ethylene oxide. *Tetrahedron Lett.* **1978**, *19*, 1767–1770.

(138) Herzberger, J.; Niederer, K.; Pohlit, H.; Seiwert, J.; Worm, M.; Wurm, F. R.; Frey, H. Polymerization of ethylene oxide, propylene oxide, and other alkylene oxides: Synthesis, novel polymer architectures, and bioconjugation. *Chem. Rev.* **2016**, *116*, 2170–2243.

(139) Hillmyer, M. A.; Bates, F. S. Synthesis and characterization of model polyalkane-poly(ethylene oxide) block copolymers. *Macromolecules* **1996**, *29*, 6994–7002.

(140) Morawetz, H. *Modern Methods of Polymer Characterization*; John Wiley & Sons, Inc., 1992.

(141) Fetters, L. J.; Lohse, D. J.; Richter, D.; Witten, T. A.; Zirkel, A. Connection between polymer molecular weight, density, chain dimensions, and melt viscoelastic properties. *Macromolecules* **1994**, *27*, 4639–4647.

(142) Hammouda, B. SANS from polymers—review of the recent literature. *Polym. Rev.*

**2010**, *50*, 14–39.

(143) Glinka, C. J.; Barker, J. G.; Hammouda, B.; Krueger, S.; Moyert, J. J.; Orts, W. J. The 30 m small-angle neutron scattering instruments at the national institute of standards and technology. *J. Appl. Cryst* **1998**, *31*, 430–445.

(144) Kline, S. R. Reduction and analysis of SANS and USANS data using IGOR-Pro. *J. Appl. Crystallogr.* **2006**, *39*, 895–900.

(145) Debye, P. Light scattering in solutions. *J. Appl. Phys.* **1944**, *15*, 338–342.

(146) Matsushita, Y.; Shimizu, K.; Noda, I.; Chang, T.; Han, C. C. Chain conformation of block copolymers in dilute solutions measured by small-angle neutron scattering. *Polymer* **1992**, *33*, 2412–2415.

(147) Matsushita, Y.; Noda, I.; Nagasawa, M.; Lodge, T. P.; Amis, E. J.; Han, C. C. Expansion factor of a part of a polymer chain in a good solvent measured by small-angle neutron scattering. *Macromolecules* **1984**, *17*, 1785–1789.

(148) Triolo, A.; Russina, O.; Bleif, H.-J.; Di Cola, E. Nanoscale segregation in room temperature ionic liquids. *J. Phys. Chem. B* **2007**, *111*, 4641–4644.

(149) Russina, O.; Triolo,A.; Gontrani, L.; Caminti, R. Mesoscopic structural heterogeneities in room-temperature ionic liquids. *J. Phys. Chem. Lett.* **2012**, *3*, 27−33.

(150) Russina, O.; Triolo, A. Chapter 4 - Ionic liquids and neutron scattering. In *Neutron Scattering - Applications in Biology, Chemistry, and Materials Science*;

Fernandez-Alonso, F., Price, D. L., Eds.; Experimental Methods in the Physical Sciences; Academic Press, 2017; Vol. 49, pp 213–278.

(151) Krigbaum, W. R.; Flory, P. J. Statistical mechanics of dilute polymer solutions. iv. variation of the osmotic second coefficient with molecular weight. *J. Am. Chem. Soc.* **1953**, *75*, 1775–1784.

(152) Vandermiers, C.; Damman, P.; Dosiere, M. Static and quasielastic light scattering from solutions of poly (ethylene oxide) in methanol. *Polymer* **1998**, *39*, 5627–5631.

(153) Kawaguchi, S.; Imai, G.; Suzuki, J.; Miyahara, A.; Kitano, T.; Ito, K. Aqueous solution properties of oligo- and poly(ethylene oxide) by static light scattering and intrinsic viscosity. *Polymer* **1997**, *38*, 2885–2891.

(154) Mark, J. E. *Polymer Data Handbook*, 2nd ed.; Oxford University Press, 2009.

(155) Whitehouse, B. A. Gel permeation chromatograph calibration. Intrinsic viscosity-polydispersity effect. *Macromolecules* **1971**, *4*, 463–466.

(156) Wagner, H. The mark-houwink-sakurada equation for the viscosity of linear polyethylene. *J.Phys.Chem* **1985**, *14*, 611–617.

(157) Chiang, R.; Carolina, N. The temperature dependence of the specific refractive index increment of polyethylene in various solvents. *J. Polym. Sci. Part C* **1965**, *304*, 295–304.

(158) Ullman, R. Intrinsic viscosity and diffusion of solutions. **1981**, *14*, 746–755.

(159) Akcasu, A. Z.; Han, C. C. Molecular weight and temperature dependence of polymer dimensions in solution. *Macromolecules* **1979**, *12*, 276–280.

(160) Swislow, G.; Sun, S.-T.; Nishio, I.; Tanaka, T. Coil-globule phase transition in a single polystyrene chain in cyclohexane. *Phys. Rev. Lett.* **1980**, *44*, 796–798.

(161) Wu, C.; Wang, X. Globule-to-coil transition of a single homopolymer chain in solution. *Phys. Rev. Lett.* **1998**, *80*, 4092–4094.

(162) Joost, M.; Kunze, M.; Jeong, S.; Schönhoff, M.; Winter, M.; Passerini, S. Ionic mobility in ternary polymer electrolytes for lithium-ion batteries. *Electrochim. Acta* **2012**, *86*, 330–338.

(163) Triolo, A.; Celso, F. Lo; Arrighi, V.; Strunz, P.; Lechner, R. E.; Mastragostino, M.; Passerini, S.; Annis, B. K.; Triolo, R. Structural and dynamical characterization of melt PEO–salt mixtures. *Physica A* **2002**, *304*, 308–313.

(164) Annis, B. K.; Kim, M. H.; Wignall, G. D.; Borodin, O.; Smith, G. D. A study of the influence of Li+ on the chain conformations of poly(ethylene oxide) in the melt by small-angle neutron scattering and molecular dynamics simulations. *Macromolecules* **2000**, *33*, 7544–7548.

(165) Kharel, A.; Lodge, T. P. Coil dimensions of poly(ethylene oxide) in an ionic liquid by small-angle neutron scattering. *Macromolecules* **2017**, *50*, 8739–8744.

(166) Irwin, M. T.; Hickey, R. J.; Xie, S.; Bates, F. S.; Lodge, T. P. Lithium salt-induced microstructure and ordering in diblock copolymer/homopolymer blends.

*Macromolecules* **2016**, *49*, 4839–4849.

(167) Flory, P. J.; Krigbaum, W. Statistical mechanics of dilute polymer solutions. II. *J. Chem. Phys.* **1950**, *18*, 1086.

(168) Chen, Z.; McDonald, S.; FitzGerald, P.; Warr, G. G.; Atkin, R. Small angle neutron scattering study of the conformation of poly(ethylene oxide) dissolved in deep eutectic solvents. *J. Colloid Interface Sci.* **2017**, *506*, 486–492.

(169) Kodama, K.; Tsuda, R.; Niitsuma, K.; Tamura, T.; Ueki, T.; Kokubo, H.; Watanabe, M. Structural effects of polyethers and ionic liquids in their binary mixtures on lower critical solution temperature liquid-liquid phase separation. *Polym. J.* **2011**, *43*, 242–248.

(170) Miranda, D. F. Interactions and morphology of triblock copolymer - ionic liquid mixtures and applications for gel polymer electrolytes, University of Massachusetts-Amherst, 2012.

(171) Muldoon, M. J.; Gordon, C. M.; Dunkin, I. R. Investigations of solvent–solute interactions in room temperature ionic liquids using solvatochromic dyes. *J. Chem. Soc., Perkin Trans.* **2001**, *2*, 433–435.

(172) Tsuzuki, S.; Tokuda, H.; Hayamizu, K.; Watanabe, M. Magnitude and directionality of interaction in ion pairs of ionic liquids : relationship with ionic conductivity. *J. Phys. Chem. B* **2005**, *109*, 16474–16481.

(173) Slagowski, E.; Tsai, B.; McIntyre, D. The dimensions of polystyrene near and

below the theta temperature. *Macromolecules* **1976**, *9*, 687–688.

(174) Fujii, K.; Ueki, T.; Hashimoto, K.; Kobayashi, Y.; Kitazawa, Y.; Hirosawa, K.; Matsugami, M.; Ohara, K.; Watanabe, M.; Shibayama, M. Microscopic structure of solvated poly(benzyl methacrylate) in an imidazolium-based ionic liquid: high-energy X-ray total scattering and all-atom md simulation study. *Macromolecules* **2017**, *50*, 4780–4786.

(175) Lee, H. N.; Bai, Z.; Newell, N.; Lodge, T. P. Micelle/inverse micelle self-assembly of a peo-pnipam block copolymer in ionic liquids with double thermoresponsivity. *Macromolecules* **2010**, *43*, 9522–9528.

(176) Podzimek, S. *Light Scattering, Size Exclusion Chromatography and Asymmetric Flow Field Flow Fractionation: Powerful Tools for the Characterization of Polymers, Proteins and Nanoparticles*; John Wiley & Sons: New Jersey, 2011.

(177) Richards, R. W. Dilute solution properties of poly(benzyl methacrylate). *Polymer* **1977**, *18*, 114–120.

(178) Tokuda, H.; Hayamizu, K.; Ishii, K.; Susan, M. A. B. H.; Watanabe, M. Physicochemical properties and structures of room temperature ionic liquids. 2. variation of alkyl chain length in imidazolium cation. *J. Phys. Chem. B* **2005**, *109*, 6103–6110.

(179) Tokuda, H.; Hayamizu, K.; Ishii, K.; Susan, M. A. B. H.; Watanabe, M. Physicochemical properties and structures of room temperature ionic liquids. 1. variation of anionic species. *J. Phys. Chem. B* **2004**, *108*, 16593–16600.

(180) Tokuda, H.; Ishii, K.; Susan, M. A. B. H.; Tsuzuki, S.; Hayamizu, K.; Watanabe, M. Physicochemical properties and structures of room-temperature ionic liquids. 3. variation of cationic structures. *J. Phys. Chem. B* **2006**, *110*, 2833–2839.

(181) B. Chu. *Laser Light Scattering, 2nd Ed*; Academic Press: San Diego, 1991.

(182) M.B. Huglin (ed). *Light Scattering from Polymer Solutions*; Academic Press: New York, 1972.

(183) Montalbán, M. G.; Bolívar, C. L.; Díaz Baños, F. G.; Víllora, G. Effect of temperature, anion, and alkyl chain length on the density and refractive index of 1-alkyl-3-methylimidazolium-based ionic liquids. *J. Chem. Eng. Data* **2015**, *60*, 1986–1996.

(184) Seoane, R. G.; Corderí, S.; Gómez, E.; Calvar, N.; González, E. J.; MacEdo, E. A.; Domínguez, Á. Temperature dependence and structural influence on the thermophysical properties of eleven commercial ionic liquids. *Ind. Eng. Chem. Res.* **2012**, *51*, 2492–2504.

(185) Berne, B. J.; Pecora, R. *Dynamic Light Scattering*; Wiley: New York, 1976.

(186) Schmitz, K. S. *Dynamic Light Scattering by Macromolecules*; Academic Press: San Diego, 1990.

(187) Jakeš, J. Regularized positive exponential sum (REPES) program - a way of inverting laplace transform data obtained by dynamic light scattering. *Collect. Czechoslov. Chem. Commun.* **1995**, *60*, 1781–1797.

(188) Bhatt, M.; Jamieson, A. M.; Petschek, R. G. Static and dynamic scaling relationships in the light scattering properties of polystyrenes in good solvents. *Macromolecules* **1989**, *22*, 1374–1380.

(189) Bhatt, M.; Jamieson, A. M. Dynamic light scattering studies of polystyrene in tetrahydrofuran at intermediate scattering vectors. *Macromolecules* **1988**, *21*, 3015–3022.

(190) Yamakawa, H. *Modern Theory of Polymer Solutions*; Harper and Row: New York, 1971.

(191) de Gennes, P. G. Special features of water soluble polymers. *Pure Appl. Chem.* **1992**, *64*, 1585–1588.

(192) White, R. P.; Lipson, J. E. G. Origins of unusual phase behavior in polymer/ionic liquid solutions. *Macromolecules* **2013**, *46*, 5714–5723.

(193) Horska, J.; Stejskal, J.; Kratochvfl, P. Refractive index increments of polyethylene. **1979**, *24*, 1845–1855.

(194) Lodge, T. P.; Maxwell, A. L.; Lott, J. R.; Schmidt, P. W.; McAllister, J. W.; Morozova, S.; Bates, F. S.; Li, Y.; Sammler, R. L. Gelation, phase separation, and fibril formation in aqueous hydroxypropylmethylcellulose solutions. *Biomacromolecules* **2018**, *19*, 816–824.

(195) Mandal, T. K.; Kuo, J. F.; Woo, E. M. Miscibility and spherulite growth kinetics in the poly(ethylene oxide)/poly(benzyl methacrylate) system. *J. Polym. Sci. Part B*

*Polym. Phys.* **2000**, *38*, 562–572.

(196) Scholte, T. H. G. Determination of thermodynamic parameters of polymer-solvent systems by light scattering. **1970**, *6*, 1063–1074.

(197) des Cloizeaux, G. J. *Polymers in Solution*; Clarendon Press: Oxford, 1990.

(198) Sung, J. H.; Lee, D. C.; Park, H. J. Conformational characteristics of poly(ethylene oxide) (PEO) in methanol. *Polymer* **2007**, *48*, 4205–4212.

(199) Fetters, L. J.; Hadjichristidis, N.; Lindner, J. S.; Mays, J. W. Molecular weight dependence of hydrodynamic and thermodynamic properties for well-defined linear polymers in solution. *J. Phys. Chem. Ref. Data* **1994**, *23*, 619–640.

(200) Kinugasa, S.; Nakahara, H.; Kawahara, J. I.; Koga, Y.; Takaya, H. Static light scattering from poly(ethylene oxide) in methanol. *J. Polym. Sci. Part B Polym. Phys.* **1996**, *34*, 583–586.

(201) de Gennes, P. G. Dynamics of entangled polymer solutions. II. Inclusion of hydrodynamic interactions. *Macromolecules* **1976**, *9*, 594–598.

(202) Weill, G.; des Cloizeaux, J. Dynamics of polymers in dilute solutions: an explanation of anomalous indices by cross-over effects. *J. Phys.* **1979**, *40*, 99–105.

(203) Son, C. Y.; Mcdaniel, J. G.; Cui, Q.; Yethiraj, A. Conformational and dynamic properties of poly(ethylene oxide ) in BMIM+ $BF_4$ −: a microsecond computer simulation study using ab initio force fields. *Macromolecules* **2018**, *51*, 5336–5345.

(204) Nakamura, I. Spinodal decomposition of a polymer and ionic liquid mixture: effects of electrostatic interactions and hydrogen bonds on phase instability. *Macromolecules* **2016**, *49*, 690–699.

(205) Choi, E.; Yethiraj, A. Entropic mechanism for the lower critical solution temperature of poly(ethylene oxide) in a room temperature ionic liquid. *ACS Macro Lett.* **2015**, *4*, 799–803.

(206) Jung, H.; Yethiraj, A. A simulation method for the phase diagram of complex fluid mixtures. *J. Chem. Phys.* **2018**, *148*.

(207) Xiao, Z.; Larson, R. G.; Chen, Y.; Zhou, C.; Niu, Y.; Li, G. Unusual phase separation and rheological behavior of poly(ethylene oxide)/ionic liquid mixtures with specific interactions. *Soft Matter* **2016**, *12*, 7613–7623.

(208) Rudaz, C.; Budtova, T. Rheological and hydrodynamic properties of cellulose acetate/ionic liquid solutions. *Carbohydr. Polym.* **2013**, *92*, 1966–1971.

(209) Xinjun Zhu,1,2 Hina Saba,1 Yumei Zhang, 1 Huaping Wang. The viscoelastic behavior of concentrated polyacrylonitrile/1-butyl-3-methylimidazolium chloride from solution to gel. *Polym. Eng. Sci.* **2014**, *54*, 598–606.

(210) Liu, Z.; Wang, W.; Stadler, F. J.; Yan, Z.-C. Rheology of concentrated polymer/ionic liquid solutions: an anomalous plasticizing effect and a universality in nonlinear shear rheology. *Polymers* **2019**, *11*, 877.

(211) Luo, H.; Xiao, Z.; Chen, Y.; Niu, Y.; Li, G. Phase separation kinetics and

rheological behavior of poly(ethylene oxide)/ionic liquid mixtures with large dynamic asymmetry. *Polymer* **2017**, *123*, 290–300.

# Appendix A

## *d*-PEO in [BMIM][TFSI]

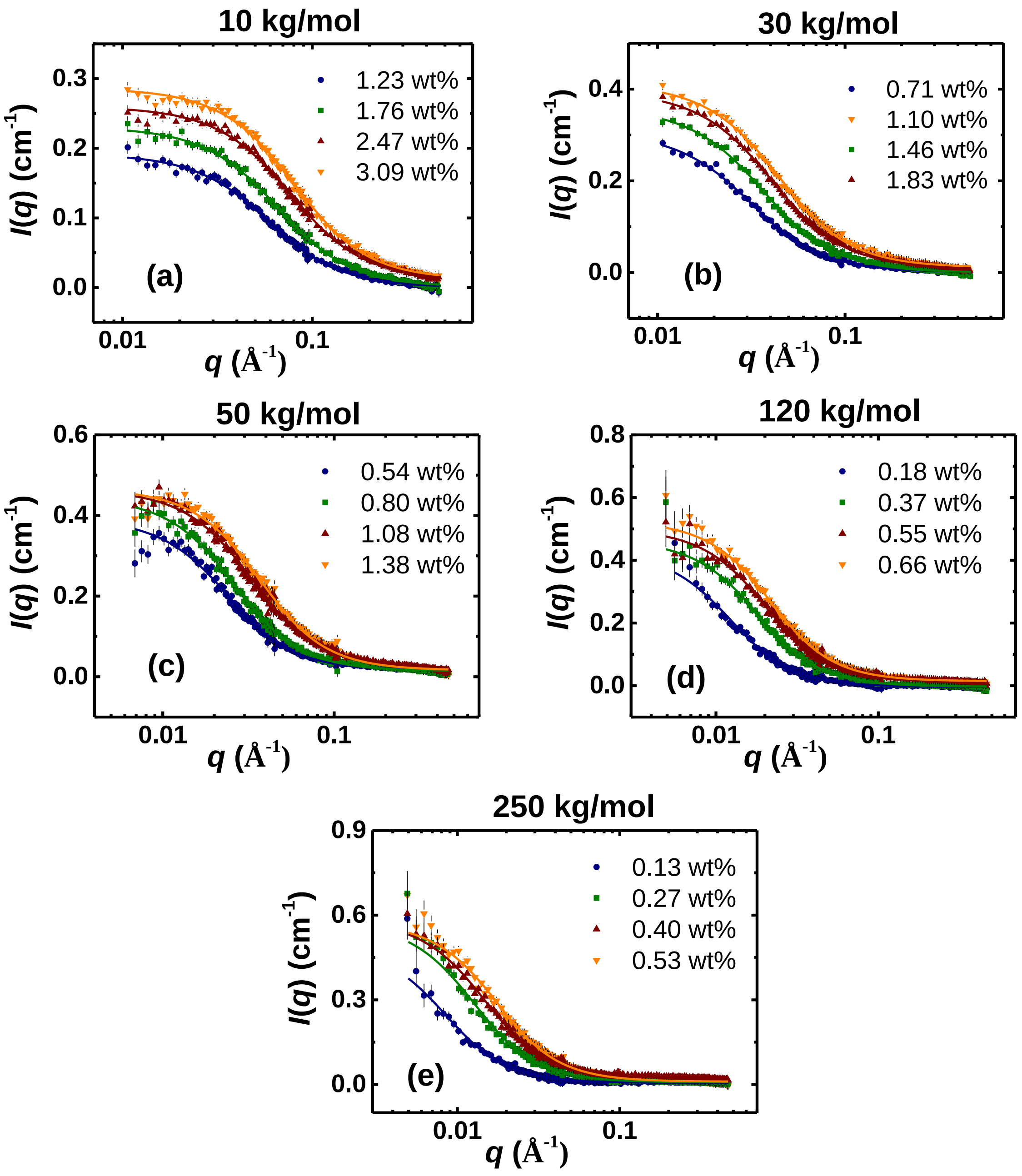

**Figure A1:** Background subtracted SANS scattering profiles (symbols) for all molecular weights of d-PEO in [BMIM][TFSI] at 80 °C with the corresponding Debye function fits represented by solid curves.

# *d*-PEO in [BMIM][PF$_6$]

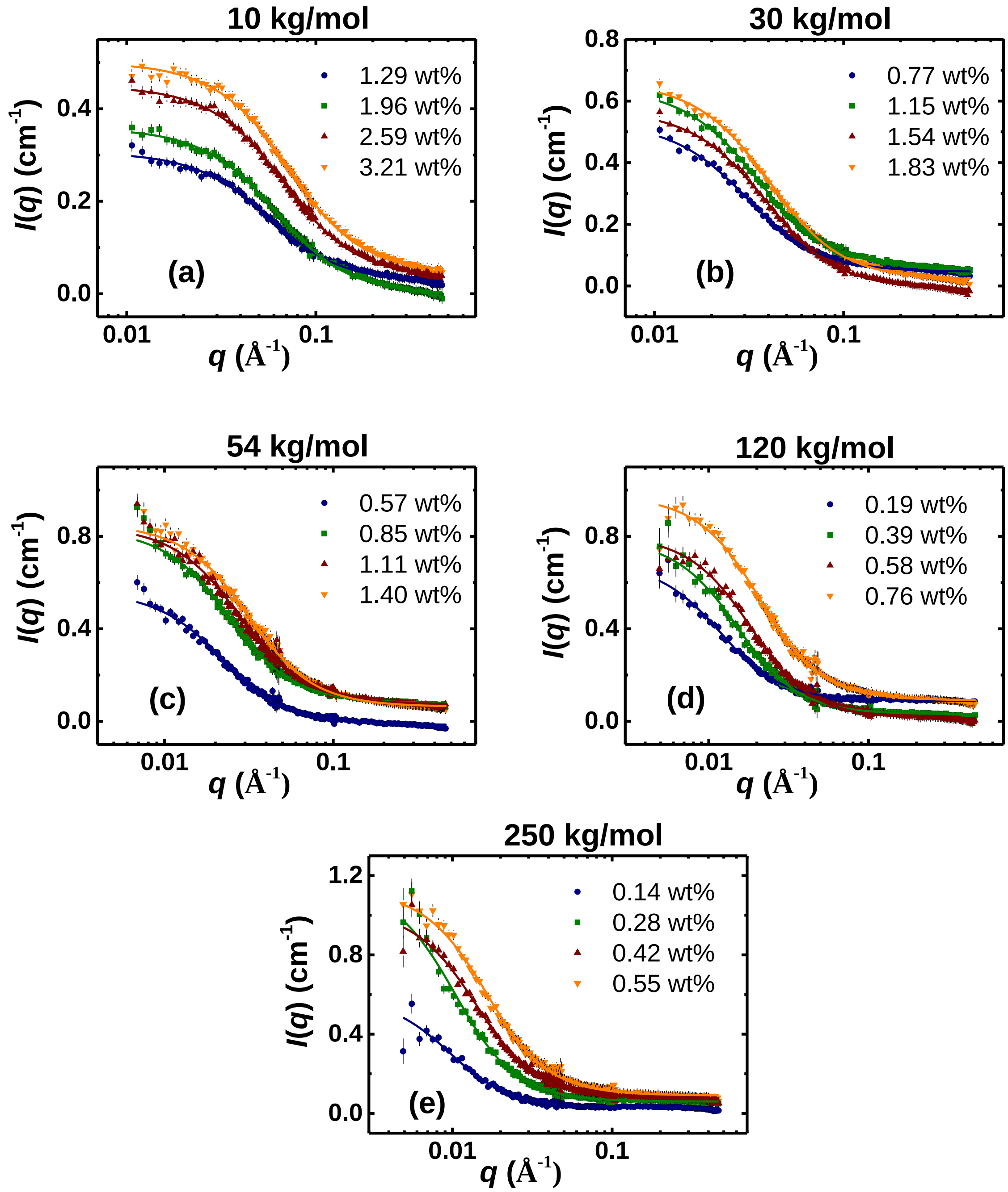

**Figure A2:** Background subtracted SANS scattering profiles (symbols) for all molecular weights of *d*-PEO in [BMIM][PF$_6$] at 80 °C with the corresponding Debye function fits represented by solid curves.

# *d*-PEO in [HMIM][BF$_4$]

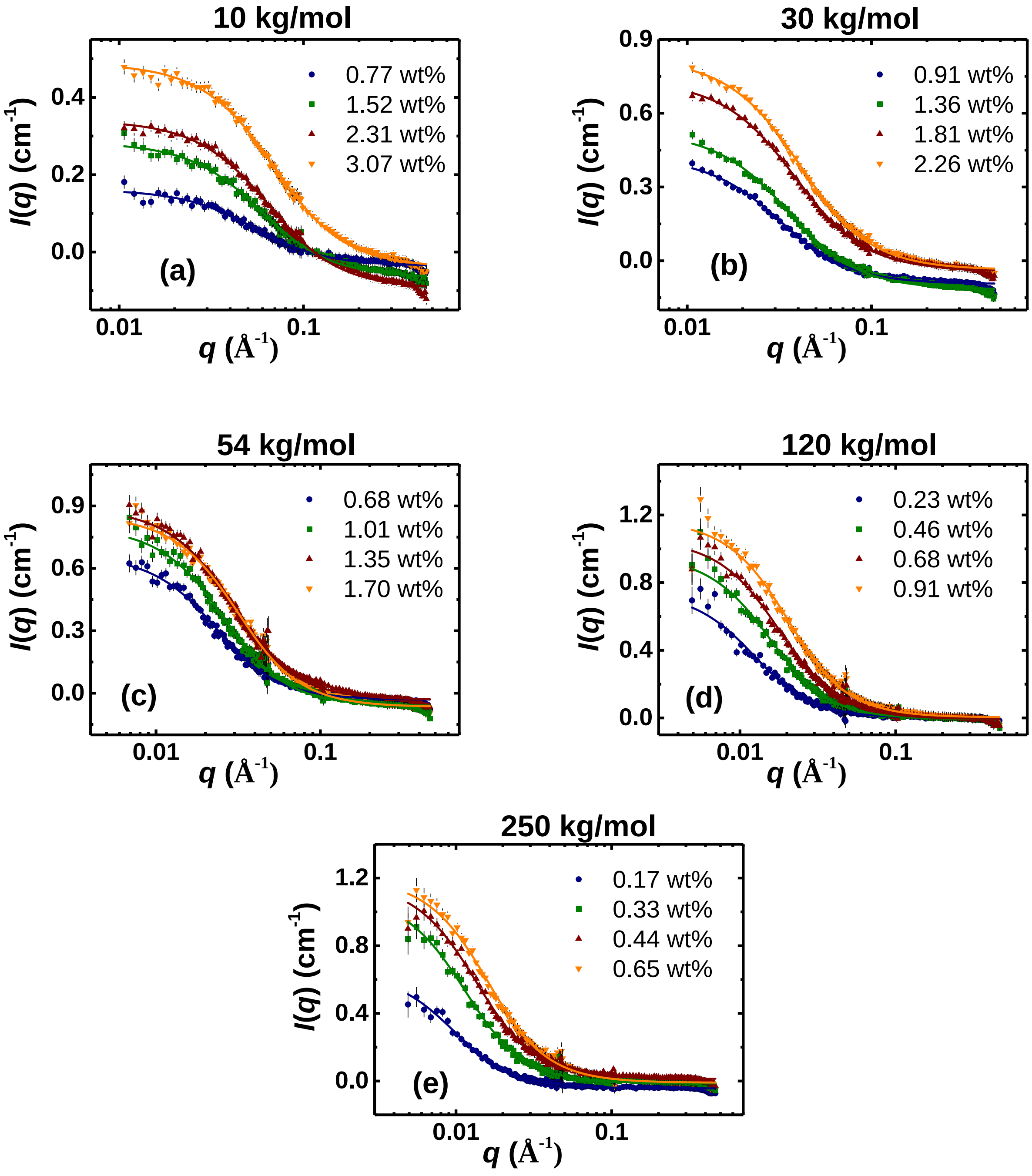

**Figure A3:** Background subtracted SANS scattering profiles (symbols) for all molecular weights of *d*-PEO in [HMIM][BF$_4$] at 80 °C with the corresponding Debye function fits represented by solid curves.

# *d*-PEO-30 in LiTFSI/[BMIM][TFSI]

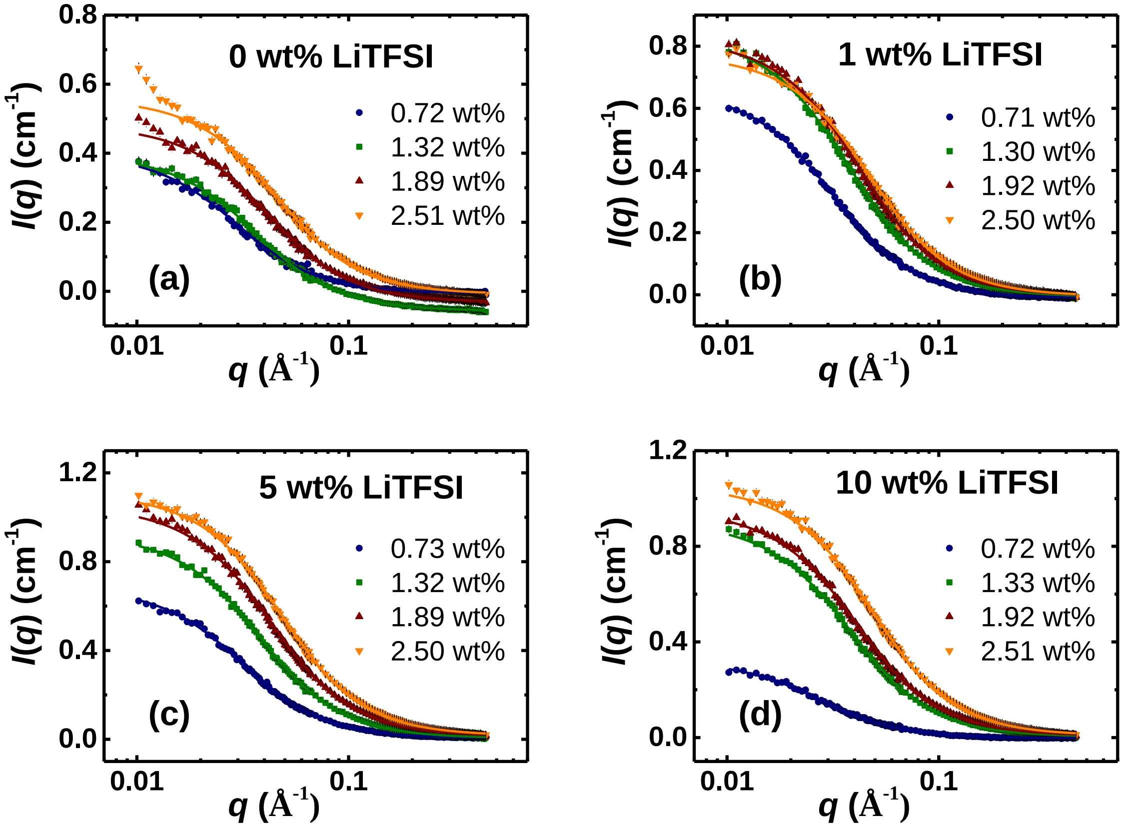

**Figure A4:** Background subtracted SANS scattering profiles (symbols) for *d*-PEO-30 in LiTFSI/[BMIM][TFSI] at 80 °C, with concentrations of LiTFSI (wt%) of 0, 1, 5, and 10, presented in parts a, b, c, and d, respectively. The corresponding Debye function fits are represented by solid curves.

# *d*-PEO-54 in [EMIM][BF$_4$]

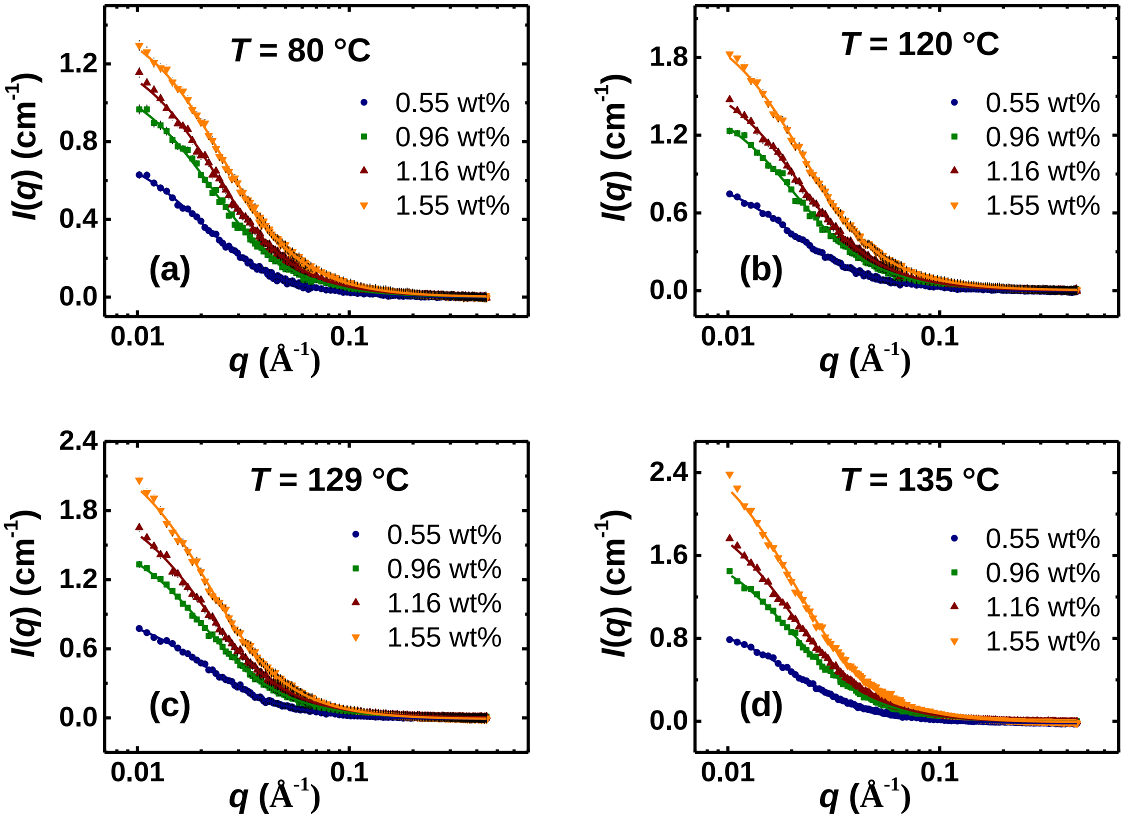

**Figure A5:** Background subtracted SANS scattering profiles (symbols) for *d*-PEO-54 in [EMIM][BF$_4$] at temperatures 80 °C, 120 °C, 129 °C, and 135 °C presented in parts a, b, c, and d, respectively. The corresponding Debye function fits are represented by solid curves.

**Table A1:**List of Debye function fitting parameters for background subtracted SANS scattering profiles of *d*-PEO in [BMIM][TFSI]

| $M_w$ (kg/mol) | $c$ (wt%) | $A$ | $B$ | $R_g$ (Å) |
|---|---|---|---|---|
| 10 | 1.23 | 0.19 | 0.00 | 27.2 |
| | 1.76 | 0.23 | 0.00 | 24.4 |
| | 2.47 | 0.25 | 0.01 | 20.9 |
| | 3.09 | 0.27 | 0.01 | 19.9 |
| 30 | 0.71 | 0.30 | 0.00 | 51.3 |
| | 1.10 | 0.36 | 0.00 | 44.1 |
| | 1.46 | 0.39 | 0.01 | 39.4 |
| | 1.83 | 0.40 | 0.01 | 36.4 |
| 54 | 0.54 | 0.38 | 0.02 | 67.4 |
| | 0.80 | 0.43 | 0.01 | 61.2 |
| | 1.08 | 0.44 | 0.02 | 48.5 |
| | 1.38 | 0.45 | 0.02 | 43.4 |
| 120 | 0.18 | 0.43 | 0.00 | 132 |
| | 0.37 | 0.47 | 0.00 | 89.1 |
| | 0.55 | 0.49 | 0.01 | 79.9 |
| | 0.66 | 0.51 | 0.01 | 74.0 |
| 250 | 0.13 | 0.49 | 0.01 | 192 |
| | 0.27 | 0.57 | 0.01 | 128 |
| | 0.40 | 0.56 | 0.02 | 110 |
| | 0.53 | 0.57 | 0.01 | 91.8 |

**Table A2** : List of Debye function fitting parameters for background subtracted SANS scattering profiles of *d*-PEO in [BMIM][PF$_6$]

| $M_w$ (kg/mol) | $c$ (wt%) | $A$ | $B$ | $R_g$ (Å) |
|---|---|---|---|---|
| 10 | 1.29 | 0.28 | 0.02 | 28.4 |
| | 1.96 | 0.36 | 0.00 | 26.1 |
| | 2.59 | 0.42 | 0.03 | 23.6 |
| | 3.21 | 0.46 | 0.04 | 22.3 |
| 30 | 0.77 | 0.49 | 0.05 | 52.6 |
| | 1.15 | 0.59 | 0.05 | 46.2 |
| | 1.54 | 0.58 | -0.01 | 41.7 |
| | 1.83 | 0.64 | 0.02 | 39.8 |
| 54 | 0.57 | 0.58 | -0.02 | 73.4 |
| | 0.85 | 0.75 | 0.08 | 66.2 |
| | 1.11 | 0.77 | 0.07 | 57.8 |
| | 1.40 | 0.79 | 0.06 | 50.9 |
| 120 | 0.19 | 0.60 | 0.09 | 137 |
| | 0.39 | 0.76 | 0.03 | 106 |
| | 0.58 | 0.79 | 0.01 | 87.5 |
| | 0.76 | 0.88 | 0.09 | 77.0 |
| 250 | 0.14 | 0.57 | 0.03 | 168 |
| | 0.28 | 1.10 | 0.06 | 155 |
| | 0.42 | 0.96 | 0.08 | 115 |
| | 0.55 | 1.04 | 0.09 | 99 |

**Table A3:** List of Debye function fitting parameters for background subtracted SANS scattering profiles of *d*-PEO in [HMIM][$BF_4$]

| $M_w$ (kg/mol) | $c$ (wt%) | $A$ | $B$ | $R_g$ (Å) |
|---|---|---|---|---|
| 10 | 0.77 | 0.20 | –0.04 | 29.7 |
| | 1.52 | 0.35 | –0.07 | 27.4 |
| | 2.31 | 0.44 | –0.10 | 24.8 |
| | 3.07 | 0.53 | –0.04 | 23.2 |
| 30 | 0.91 | 0.52 | –0.09 | 50.5 |
| | 1.36 | 0.64 | –0.12 | 45.5 |
| | 1.81 | 0.77 | –0.04 | 41.9 |
| | 2.26 | 0.86 | –0.04 | 39.4 |
| 54 | 0.68 | 0.70 | –0.03 | 69.4 |
| | 1.01 | 0.86 | –0.06 | 62.3 |
| | 1.35 | 0.92 | –0.03 | 54.9 |
| | 1.70 | 0.92 | –0.07 | 51.2 |
| 120 | 0.23 | 0.75 | 0.00 | 131 |
| | 0.46 | 0.97 | –0.01 | 104 |
| | 0.68 | 1.06 | –0.01 | 90.3 |
| | 0.91 | 1.17 | 0.00 | 79.5 |
| 250 | 0.17 | 0.69 | –0.04 | 167 |
| | 0.33 | 1.12 | –0.01 | 142 |
| | 0.44 | 1.17 | 0.01 | 120 |
| | 0.65 | 1.21 | –0.01 | 101 |

**Table A4:** List of Debye function fitting parameters for background subtracted SANS scattering profiles of *d*-PEO-30 in LiTFSI/[BMIM][TFSI]

| **LiTFSI (wt%)** | ***c* (wt%)** | ***A*** | ***B*** | **$R_g$ (Å)** |
|---|---|---|---|---|
| 0 | 0.72 | 0.41 | –0.01 | 54.5 |
| | 1.32 | 0.45 | –0.06 | 43.9 |
| | 1.89 | 0.51 | –0.03 | 38.6 |
| | 2.51 | 0.57 | –0.01 | 34.9 |
| 1 | 0.71 | 0.67 | –0.01 | 50.9 |
| | 1.30 | 0.84 | –0.01 | 42.6 |
| | 1.92 | 0.83 | 0.00 | 37.9 |
| | 2.50 | 0.78 | 0.00 | 33.8 |
| 5 | 0.73 | 0.68 | 0.00 | 51.1 |
| | 1.32 | 0.92 | 0.00 | 42.3 |
| | 1.89 | 1.04 | 0.01 | 37.4 |
| | 2.50 | 1.09 | 0.02 | 33.1 |
| 10 | 0.72 | 0.32 | 0.00 | 58.5 |
| | 1.33 | 0.90 | 0.00 | 42.2 |
| | 1.92 | 0.94 | 0.01 | 39.2 |
| | 2.51 | 1.04 | 0.01 | 32.9 |

**Table A5:** List of Debye function fitting parameters for background subtracted SANS scattering profiles of *d*-PEO-54 in [EMIM][$BF_4$]

| ***T*** **( °C)** | ***c*** **(wt%)** | ***A*** | ***B*** | $R_g$ **(Å)** |
|---|---|---|---|---|
| 80 | 0.55 | 0.79 | 0.00 | 81.8 |
| | 0.96 | 1.17 | 0.00 | 73.9 |
| | 1.16 | 1.31 | 0.00 | 70.4 |
| | 1.55 | 1.46 | 0.00 | 64.5 |
| 120 | 0.55 | 0.93 | –0.01 | 81.2 |
| | 0.96 | 1.53 | 0.00 | 78.8 |
| | 1.16 | 1.75 | 0.00 | 76.4 |
| | 1.55 | 2.14 | 0.00 | 72.6 |
| 129 | 0.55 | 0.96 | –0.01 | 79.4 |
| | 0.96 | 1.65 | 0.00 | 79.7 |
| | 1.16 | 1.94 | 0.00 | 78.2 |
| | 1.55 | 2.41 | –0.01 | 76.0 |
| 135 | 0.55 | 1.01 | –0.02 | 81.2 |
| | 0.96 | 1.78 | –0.01 | 81.8 |
| | 1.16 | 2.17 | –0.01 | 82.5 |
| | 1.55 | 2.76 | –0.01 | 79.9 |

# Appendix B

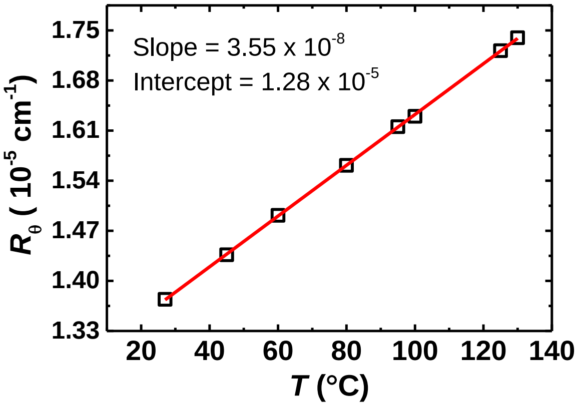

**Figure A6:** Rayleigh ratio of toluene vs. *T* obtained at a wavelength of 633 nm. The linear fit is used to obtain $R_\theta$ by extrapolation for *T* > 135 °C.

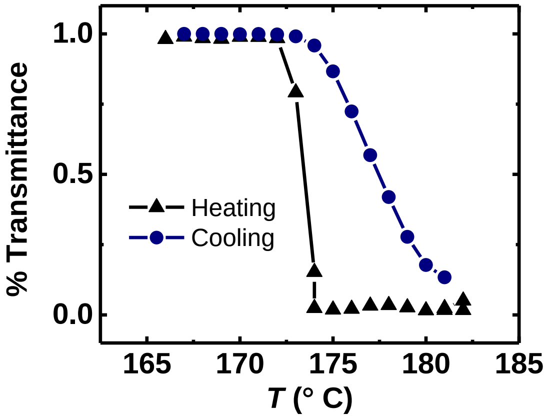

**Figure A7:** Heating and cooling curves of a 1 wt% PBzMA-70 in [BMIM][TFSI] measured at a rate of 1 °C/min, exhibiting a hysteresis upon heating and cooling.

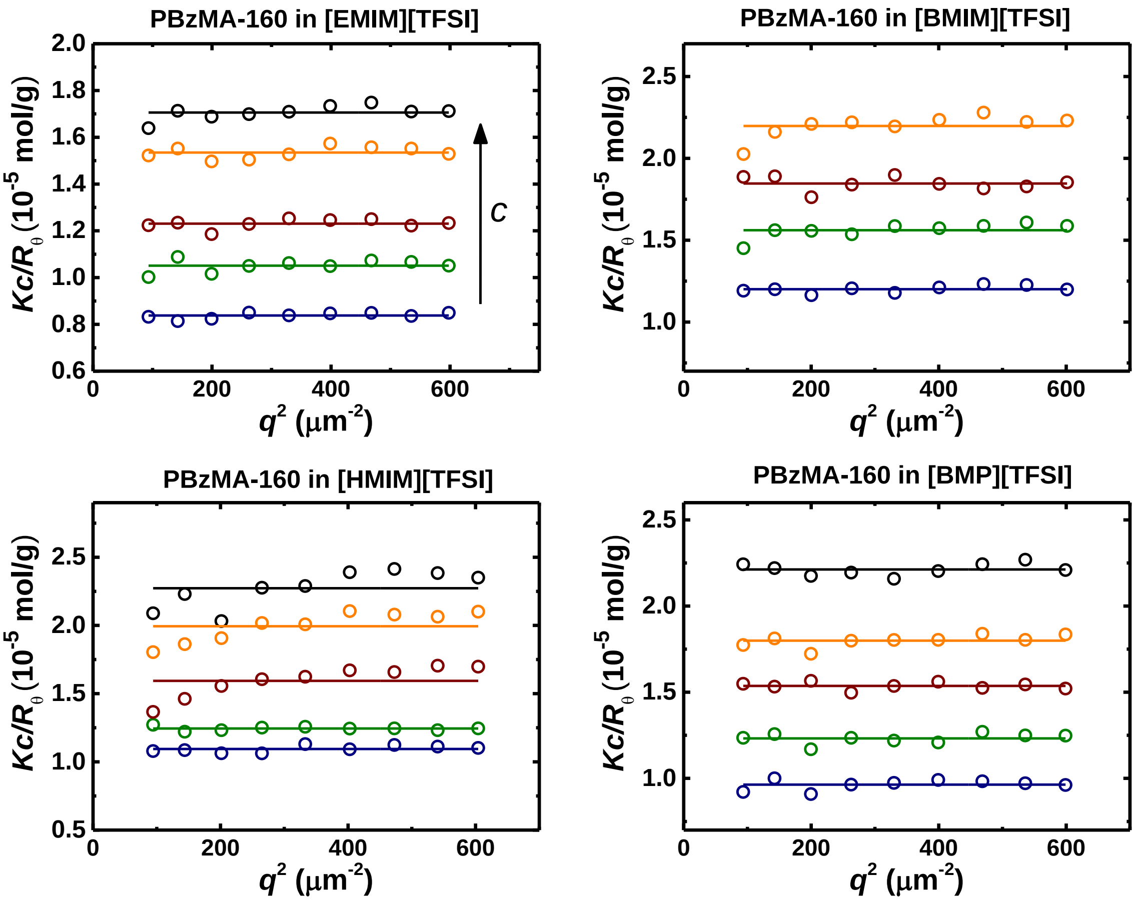

**Figure A8:** Zimm plots of PBzMA-160 in ILs at 27 °C for concentrations in the range 4–21 mg/mL. The data collected over an angular range of 40° and 120° in 10° increments were independent of angle.

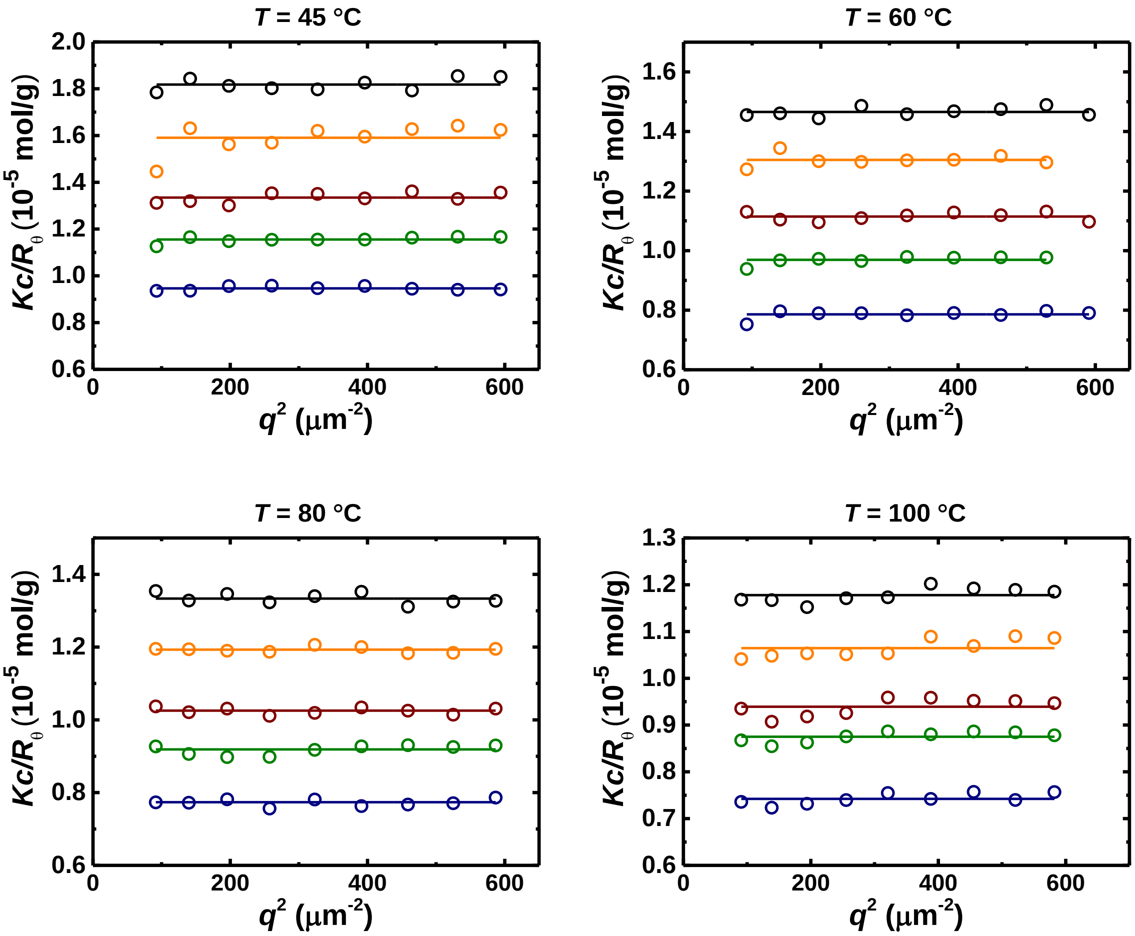

**Figure A9:** Zimm plots of PBzMA-160 in [EMIM][TFSI] at various temperatures.

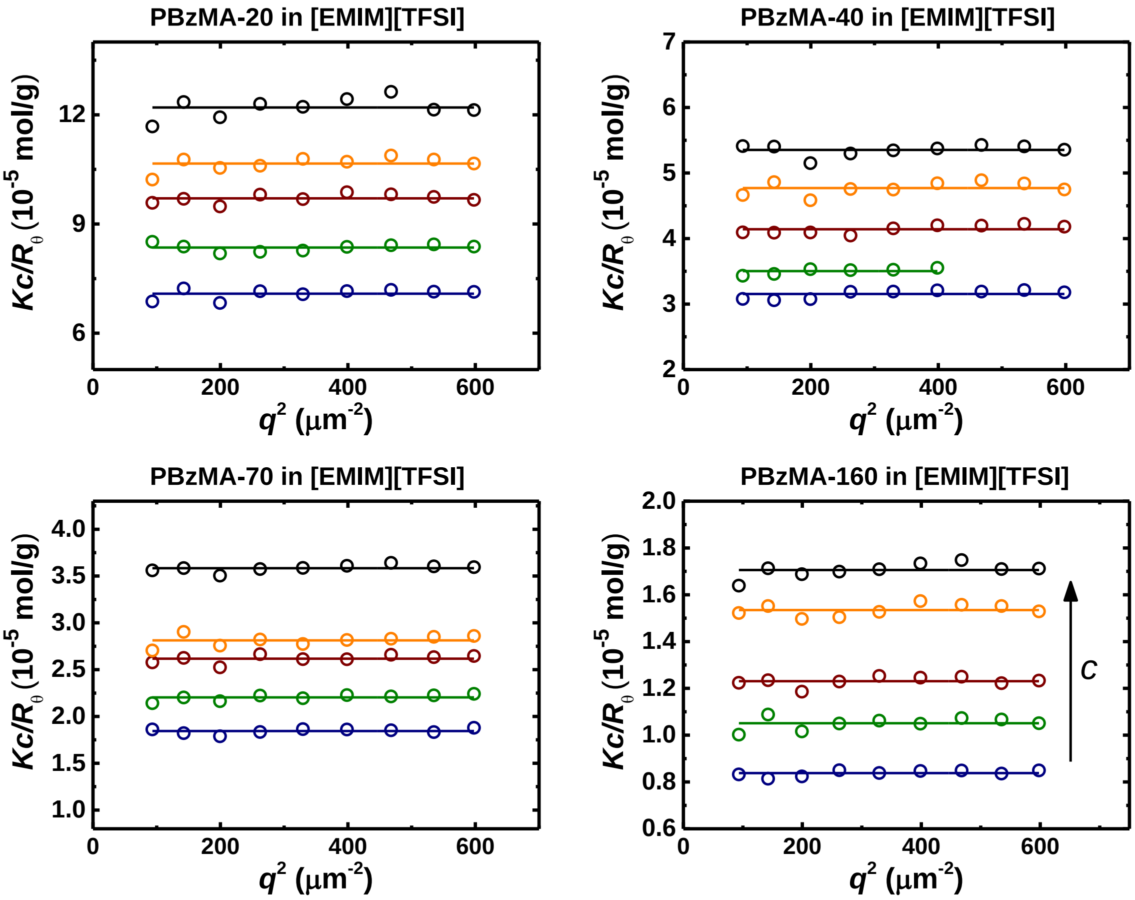

**Figure A10:** Zimm plots of various molecular weights of PBzMA in [EMIM][TFSI] .

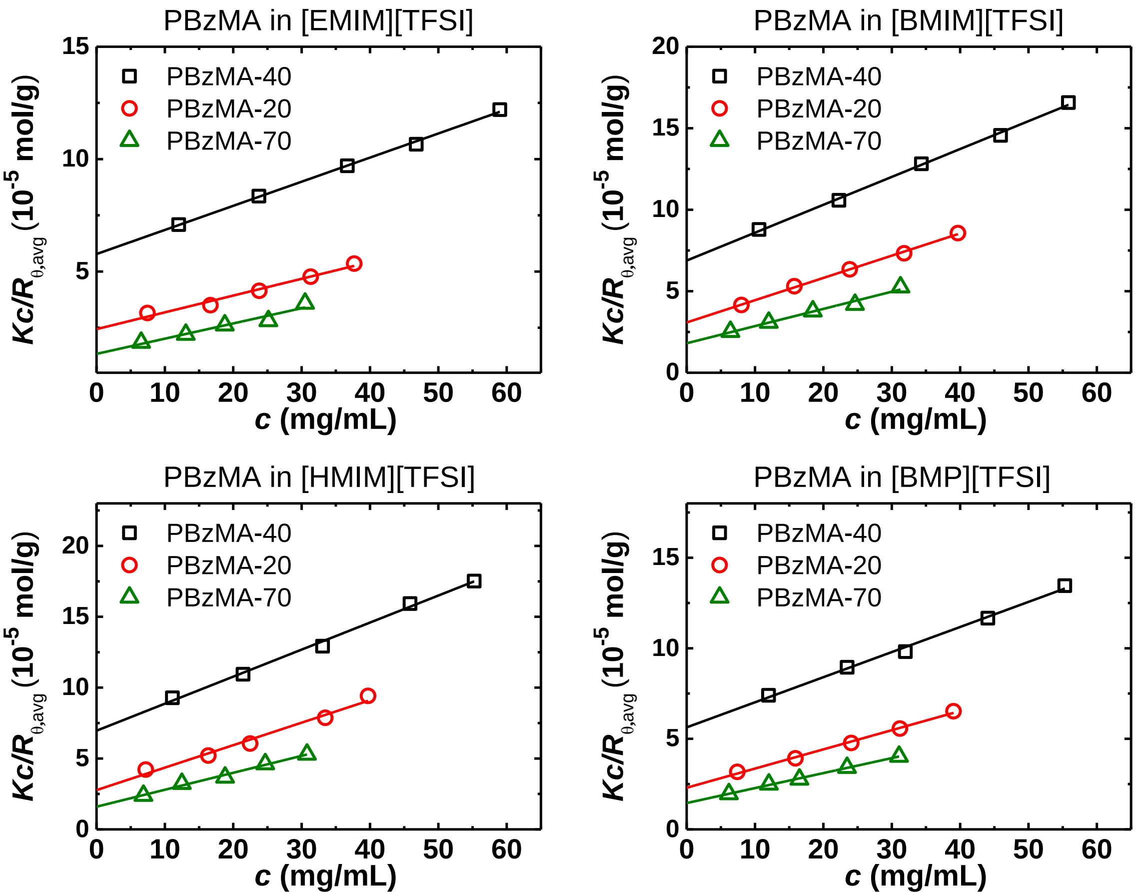

**Figure A11:** $Kc/R_{\theta,\mathrm{avg}}$ as a function of $c$ for PBzMA in ILs at 27 °C .